DYNAMICS OF PHASE TRANSITIONS IN SOME FERROELECTRIC AND OTHER LIQUID CRYSTALS

A THESIS

SUBMITTED IN FULFILMENT OF THE REQUIREMENT FOR

THE DEGREE OF

DOCTOR OF PHILLOSOPHY

BY

AYON BHATTACHARJEE

TO

THE NORTH EASTERN HILL UNIVERSITY

SHILLONG - 793 022

INDIA

APRIL - 2002

Dedicated To...

Ma

&

Baba

NORTH EASTERN HILL UNIVERSITY
SHILLONG
(April, 2002)

I Ayon Bhattacharjee, hereby declare that the subject matter of this thesis is the record of work done by me, that the contents of this thesis did not form basis of the award of any previous degree to me or to the best of my knowledge to anybody else, and that the thesis has not been submitted by me for any research degree in any other University/Institute.

This is being submitted to the North Eastern Hill University, Shillong for the degree of Doctor of Philosophy in Physics.

Ayon Bhattacharjee

(Ayon Bhattacharjee)
(Candidate)

9.4.02

(Prof. M.K Parida)
(Head)
Professor & Head,
Department of Physics,
North Eastern Hill University,
Shillong-793022.

1.4.2002

(Prof. A.L. Verma)
(Supervisor)

Acknowledgement

The opportunity to work under the supervision and guidance of Prof. A. L. Verma is a privilege for which I will always be indebted to fate. I wish to express my heartfelt gratitude for his inspiring and invaluable guidance, ceaseless patience, continual support, boundless affection and care. I am grateful that even with his extremely busy schedule, I could get uninterrupted attention for the successful completion of this work.

I extend most sincere thanks and gratitude to Dr. P. R. Alapati for his constant help in introducing me to the subject of Liquid Crystals and to Prof. D. T. Khathing for his support.

My heartfelt thanks to Mr. Hranghmingthanga for his constant help and camaraderie, to Dr. Taposh Chakraborty for his advice in data analysis and to Mr. A. K. Rathore for his technical assistance.

I take this opportunity to thank all my friends in NEHU, of whom Mr. R. Roy deserves a special mention. I would also like to thank Mr. B. Gogoi and Dr. A. K. Thakur from NERIST for their cooperation.

I am very grateful to NEHU for giving me the opportunity to undertake and complete this work successfully. I acknowledge with gratitude the financial assistance from the Department of Science and Technology (DST) New Delhi during the period of this programme.

It gives me immense pleasure to place on record the debt I owe to my parents for their ungrudging patience, support and continuous encouragement.

Above all, I thank God who has always been with me.

Ayon Bhattacharjee

CONTENTS

SYNOPSIS

"***Liquid crystals***" defined as a thermodynamically stable phase characterized by anisotropy of properties without the existence of a three dimensional lattice, are a class of fascinating compounds, discovered as early as 1888 by an Austrian botanist Reinitzer. Later, Lehmann identified liquid crystalline phases in derivatives of cholesteryl compounds and named them as intermediate phases or "mesophases". The liquid crystals possess both the isotropic properties of liquids and the crystalline properties of solids, and occur between the fully ordered solid phase and fully disordered liquid phase. The recent discoveries of ferroelectric liquid crystals, re-entrant phenomena following the bilayer arrangement in individual compounds as well as in mixtures, the hexatic smectic B phase differing from the classical crystal smectic B phase, discotic liquid crystals, polymer dispersed liquid crystals, and of late banana shaped molecules and liquid crystal dimers, and their display characteristics have added more glamour and importance to liquid crystals research. Today the developments of liquid crystal display devices have provided some very important and practical applications of liquid crystals in diverse areas.

There are several experimental techniques such as X-ray diffractometry, dilatometric analysis, nuclear magnetic resonance (NMR), electron spin resonance (ESR) / electron paramagnetic resonance (EPR), Fourier Transform infrared spectroscopy (FTIR) and Raman spectroscopy, etc., which can be used to study the phase transitions in the liquid crystalline systems and the associated changes in the different physical / chemical properties. So far as Raman spectroscopy is concerned,

variation of certain physical quantities affects the polarizability tensor, which result in changes in measurable parameters of certain vibrational modes of the Raman spectrum of the system. Therefore, Raman spectroscopy is considered to be one of the most important techniques for studying the phase transitions in liquid crystals. Further, an added advantage of Raman spectroscopy is that it provides information at both microscopic as well as macroscopic levels of the system. Time-resolved FTIR spectroscopy, in addition to being bond specific like Raman spectroscopy, also enables to collect data at specific time delays during the switching of ferroelectric liquid crystals to stable states thereby providing information on segmental mobility.

In the present thesis, both Raman and time-resolved FTIR spectroscopy have been extensively used. Raman spectroscopic technique has been employed to study the phase transitions and the associated molecular dynamics in two homologues of the N(p-n-alkyloxy benzylidene) p-n alkylanilines homologous series, (nO.m), 5O.5 and 5O.6. The nO.m series of compounds is an interesting series of Schiff base liquid crystalline compounds, in which the intermediate members 5O.5 and 5O.6 are quite intersesting compounds from the basic research point of view as they exhibit several smectic mesophases in addition to the nematic phase. In fact, 5O.6 exhibits six phases, which is the maximum number of phases reported so far in a single compound. Also, 5O.5 and 5O.6 systems exhibit the exotic smectic F phase which is extremely rare in the nO.m series. Again, one can observe a large tilt angle variation of the smectic C phase in 5O.5 where the tilt angle varies from 0^{o} to 23^{o} within a temperature range of 4 °C. Some compounds of the nO.m series are found to exhibit a first order nematic- smectic A transition whereas other compounds of this series exhibit second order transition with a

tricritical point. Due to so many peculiarities, these two compounds were selected for our studies.

Time-resolved FTIR spectroscopy was another technique used by us, which was applied in understanding the switching behaviour of an antiferroelectric liquid crystal, 4-(1-methylheptyloxy carbonyl) phenyl 4-(4'-octyloxy benzoylxy) benzoate, named as Chisso 2061, in surface stabilized ferroelectric liquid crystal (SSFLC) cells. Ferroelectric liquid crystals having spontaneous polarization exhibit a very fast response (~ 1 μs) with large changes in refractive index ($\Delta n \sim 0.1$) and are very important for fast electro-optical devices. Currently, this group of liquid crystals is used in a wide variety of fast electro-optic devices like flat panel displays and printhead arrays. The antiferroelectric liquid crystal, when confined in a suitable SSFLC cell, gives an electric field induced ferroelectric liquid crystalline state. The molecules in this state can be switched from one state to another by applying an appropriate electric field.

Chapter 1 gives a brief introduction to liquid crystals. The various classes of liquid crystalline compounds along with their important properties have been dealt in some details in this chapter. A description of the different liquid crystalline phases based on their structural characteristics and observed textures under polarizing microscope are given. Some theoretical aspects of liquid crystals like the various order parameters have been briefly discussed. A section has also been dedicated to explain the importance and significance, with respect to contemporary research and applications, on the study of nO.m homologous series and the chiral antiferroelectric liquid crystals. The origin of ferroelectricity has been explained in brief. Some

earlier works on liquid crystals have also been described with an emphasis on the spectroscopic techniques, especially time-resolved FTIR spectroscopy in case of ferroelectric liquid crystals.

Chapter 2 can broadly be divided into two sections. The first part deals with the theory of the experimental techniques used. Here basic principles and the theoretical background of Raman and time-resolved FTIR spectroscopy has been described. The second part of this chapter is dedicated to the explanation of the actual experimental techniques used in the present study. This portion includes sections on synthesis of the liquid crystalline compounds, their characterization and brief discussion on the phase transition sequence of the nO.m compounds. The construction details of high temperature cells fabricated by us for recording the Raman spectra of the liquid crystals in bulk and in free-standing thin films have been described. The sample preparation and the commercial cells used to record the spectra are also discussed. Another section of this chapter deals with the instrumentation used for Raman and asynchronous time-resolved Fourier transform infrared spectroscopies.

In chapter 3, experiments on the bulk samples of liquid crystalline compound 5O.5 are carried out using Raman spectroscopy with the objective of understanding the molecular dynamics at the different phase transitions. By carefully studying the temperature dependent Raman spectra, changes in the spectral parameters at various phase transitions were analyzed. Our results indicate that the crystal—G phase transition in 5O.5 is a first order transition between two well defined three

dimensional structures. At the transition, the alkyl chains attain a higher degree of orientational and vibrational freedom whereas the core portion remains almost rigid. The lateral gap among the pseudo- hexagonal clusters enable the alkyl chains to move freely, putting strain on the core part of the molecule resulting in softening of the -ϕ-N= bond. The G—S_F transition is characterized by a subtle increase in the peak positions and the linewidths indicating higher freedom of molecules in the S_F phase. Almost constant integrated intensity suggests that there is only a loss of intermolecular ordering at this transition. The S_F—S_C phase transition shows sharp changes in all the spectral parameters indicating the first order nature of this transition. There is also a high degree of positional and orientational freedom of the molecules in the S_C phase. The S_A—N phase transition is a second order transition marked by gradual changes in peak positions, linewidths and integrated intensities. Some pre-transitional effects are also observed which are attributed to the formation of cybotactic clusters.

The studies in chapter 4 can be divided into three parts. Firstly, comparative studies of the Raman spectra of 5O.5 and 5O.6 in bulk forms are discussed. Secondly, comparative analysis of Raman spectra of 5O.6 in bulk, solution and thin film forms are described. Finally, changes in spectral parameters at the S_F—S_B phase transition are correlated with the molecular dynamics at this transition. From these studies following conclusions have been drawn. Comparative analysis of Raman spectra of 5O.5 and 5O.6 compounds suggest that the strain on the various segments increases with increase in end chain length of the molecule (i.e., the alkyl chain) as is evident from the shift of the peak positions to lower wavenumber in case

of the higher homologue 5O.6. In the solution state, though the strain on the molecule due to the lattice is reduced, there is a tendency towards the straightening of the molecule resulting in the increase in strength of all bonds except for the C=N bond which weakens. In the thin film form, the molecules are aligned perpendicular to the layers in a random bipolar orientation without affecting the core much.

In chapter 5 experiments conducted on the electric field induced ferroelectric (S_{C^*}) phase of a chiral, anti-ferroelectric liquid crystal at different temperatures using time-resolved Fourier transform infrared (FTIR) spectroscopy are discussed. The sample was confined in a surface stabilized ferroelectric liquid crystal (SSFLC) cell and switched between the surface stabilized states in the microsecond range using an external ac electric field. An important conclusion from the FTIR studies reported in of this chapter is that, contrary to existing beliefs there is biased orientation and hindered rotation of almost all the molecular segments around the average molecular long axis, and also hindered rotation of the whole molecule around its long molecular axis for this antiferroelectric liquid crystal. It is also observed that the different segments reorient through different angles during dynamic switching as well as under dc electric field. The benzene rings are found to be skewed with respect to each other forming a non-planar structure which results in a distorted packing of the aromatic cores in the smectic layers .

Chapter 6 gives a summary of the work carried out on the different liquid crystalline systems and reports the major conclusions drawn from each chapter. Scope for future work and potential applications have also been discussed.

Chapter 1

INTRODUCTION

1. General Introduction

"Liquid Crystal" may be defined as a thermodynamically stable phase characterized by anisotropy of properties without the existence of a three dimensional crystal lattice. For many organic materials, the transition from the solid to the liquid phase does not occur in a single step but takes place in a cascade of transitions [1]. The molecular ordering in these intermediate phases, known as '***mesophases,***' lies between that of a solid and an isotropic liquid. These ordered fluid mesophases are commonly called liquid crystals and are most often composed of elongated molecules. In these mesophases, the molecules show some degree of rotational order (and in a few cases partial translational order as well) even though the crystal lattice has been destroyed. Lack of a lattice requires that these mesophases be fluid; they are, however, *'ordered fluid phases'*. It is this simultaneous possession of liquid-like (fluidity) and solid-like (molecular order) character in a single phase that makes liquid crystals unique and gives rise to so many interesting properties as well as technological applications. A most fascinating aspect of liquid crystals is that their study, which began as basic research with purely academic interests, has led to the development of a host of devices with very versatile applications. The research area of liquid crystals is interdisciplinary and is of equal interest to physicists, chemists, mathematicians and electronic technologists for the development of high quality electro-optic devices.

Liquid crystals were discovered by an Austrian botanist, F. Reinitzer [2] in the year 1888. A year later, Lehman [3] identified liquid crystalline phases in some cholesteryl compounds and termed them as intermediate phases. Liquid crystalline phases are generally characteristic of materials composed of molecules which are highly anisotropic in shape (i.e., anisometric) [4] and are commonly exhibited by rod or disc shaped molecules. This anisometry is essential since the molecules exhibiting liquid crystalline character should not only possess some rigidity but should also be able to rotate around the long molecular axis, sweeping a cylindrical volume, thereby undermining the importance of rotational order/disorder.

A liquid crystal generally comprises of anisometric organic molecules possessing some rigidity in the structure. The general structure of a liquid crystalline compound is shown below [5].

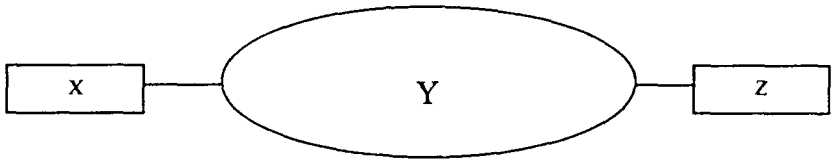

In this figure X and Z represent the zigzag tails of the liquid crystal, which may be R (R= alkyl chains), RO, CN, NO_2, Cl, etc. Y is the central rigid part called core. Y is generally composed of phenyl rings, substituted phenyl rings (Aromatic), Aro-CH=N-Aro, Aro-N=N(O)-Aro Aro-CH=N-Aro=N-Aro, Aro-COO-Aro, etc. The properties regarding the liquid crystalline nature exhibited by the two molecules possessing the same molecular formula but different atomic arrangement are subtle. For example, the compounds (1) and (2),

(1) $CH_3CH_2CH_2CH_2CH_2OAroCN$

(2) $CH_3CH_2OCH_2CH_2CH_2AroCN$

possess the same formula with identical chain lengths and rod like shapes, but differ only in the location of oxygen. The compound (1) exhibits a mesomorphic phase between 53 °C and 65 °C while compound (2) does not show any liquid crystalline properties.

1.1 CLASSIFICATION OF LIQUID CRYSTALS.

Liquid crystals can be broadly classified into two groups, viz. thermotropic and lyotropic, depending on the processes by which the intermediate phases occur. The thermotropic liquid crystals are formed while heating a solid or while cooling an isotropic liquid. The lyotropic liquid crystals are those in which the intermediate phases are exhibited under the influence of the solvents on solids or liquids and are biologically very important. However, modern texts prefer to classify liquid crystals on the basis of their molecular structures into four comprehensive groups which are:

a) Calamitic Liquid Crystals [6-10].

b) Discotic Liquid Crystals [11-15].

c) Lyotropic Liquid Crystals [16-20].

d) Defect Phases [21-25].

Based on structure and symmetry these liquid crystalline groups are further classified into different mesophases. Since the present thesis deals with the study of molecular dynamics in thermotropic mesophases as well as phase transitions, a brief description of various order parameters used to classify the liquid crystals is given in the next section.

1.1.1 ORDER PARAMETERS

When a system undergoes a phase transition, one cannot describe the two different phases by a single analytic function. Hence an extra parameter is required for describing the system in a low symmetry phase. This parameter which is used to quantify the positional or orientational order of the liquid crystalline molecules is thus appropriately termed as order parameter. A very important feature of order parameter is that, while describing the order of the molecules in the liquid crystalline materials, it also allows individual orientational deviation of the molecules from the director [26]. Typically the value of order parameter in liquid crystalline materials lie within a range of 0.3 to 0.9 depending on the temperature, with a value of unity for perfect order and a value of zero for the isotropic phase. The order parameters commonly considered in the study of liquid crystals are discussed here briefly which will help us in the discussion on classification of liquid crystals.

1.1.1.1 Orientational order:

The orientational order can be described as a measure of the tendency of the molecules to align along the director on a long range basis. In a nematic liquid crystal, for example, with a preferred direction $\hat{n}$ for the long molecular axis (called the director) an average orientational distribution function f(θ) exists, where θ is the angle between the long axis of the molecule and the director. This distribution function can be expanded in a series of Legendre polynomials as,

$$f(\theta) = S_0 P_2(\cos\theta) + S_2 P_2(\cos\theta) + S_4 P_4(\cos\theta) + S_6 P_6(\cos\theta) + ... + \qquad (1.1)$$

The Legendre polynomials are denoted by $P_n(\cos\theta)$ and S_n are the coefficients describing the orientational distribution function. Only even powers of the Legendre polynomials are retained since the director can be defined in either of two opposite directions, $\hat{n}$ or $-\hat{n}$. The dominant parameter is S_2 and when properly normalized, i.e.,

$$S_2 = \frac{1}{2}\left\langle 3\cos^2\theta - 1 \right\rangle, \tag{1.2}$$

then S_2 can be used as the orientational order parameter.

1.1.1.2 Bond Orientational order:

This is an order parameter which describes a line joining the centres of nearest neighbour molecules without requiring a regular spacing along that line. Thus, a relatively long range order with respect to the line of centres become possible by only short range positional order along that line. This order parameter plays a very important role in the phase transitions of the hexatic phases. To represent mathematically, the bond angle variation can be expressed as,

$$\psi_6 = I_6 e^{6i\phi} \tag{1.3}$$

where ϕ is the azimuthal angle and I_6 is the complex order parameter.

1.1.1.3 Translational order:

Positional order is used to describe the extent to which the position of an average molecule or group of molecules shows translational symmetry. For example, the layering tendency of the molecules can be described by an average

density of the centres of mass $\rho(z)$, which sinusoidally varies along the normal to the layers. The amplitude of the sinusoidal part, ψ, describes the amount of positional order and can be used as an order parameter:

$$\rho(z) = \rho_0\left[1 + \psi\cos\left(\frac{2\pi z}{d}\right)\right] \qquad (1.4)$$

where ρ_0 is the average density, and d is the distance between the layers.

On the basis of these order parameters and other properties, the liquid crystals are broadly classified into the following categories.

1.1.2 Calamitic Liquid Crystals:

These are the most common type of thermotropic liquid crystals and are composed of rod-like molecules with one molecular axis much longer than the other two. Depending on the structure and symmetry, calamitic liquid crystals are further divided into three main classes, viz., the nematic liquid crystals, the cholesteric liquid crystals and the smectic liquid crystals.

i) Nematic liquid crystals:

Liquid crystalline compound possessing only nematic phase is called nematic liquid crystal. If we consider liquid crystalline compounds in terms of the translational and orientational ordering of their individual molecules, then in nematic liquid crystals, there is only orientational ordering, but no translational ordering between the molecules. To be more specific, in the nematic phase the molecular centers of mass positions are disordered as in a liquid but have a statistically parallel orientation of the molecular long axes of each molecule along the director ($\hat{n}$).

Therefore, the molecular ordering in nematics is long range orientational order and there is no regular arrangement of the ends of the molecules. In the state of thermal equilibrium, the nematic phase has a symmetry ∞/mm and is therefore uniaxial. The direction of the director ($\hat{n}$) is arbitrary. The molecular arrangement of nematic liquid crystals is shown in Figure. 1.1a.

In some nematics, there exists a short-range smectic-like order in addition to the characteristic long-range orientational order. These nematics are termed as cybotactic nematics, skewed cybotactic nematics (N_{sc}) or normal cybotactic nematics (N_{nc}). In the first case, the smectic like order involves not only the layered arrangement of the molecules but also significant tilt of the molecules whereas in the second case, the molecules are parallel to the layer normal of the smectic like groups. The nematic phase exhibits schlieren, threaded, marbled, pseudo-isotropic and homogeneous textures when viewed through crossed polarizer.

ii) **Cholesteric or spontaneously twisted nematic liquid crystals:**

The cholesteric mesophase is similar to the nematic mesophase except that it is composed of optically active molecules. In this phase, the different layers orient at a slight angle relative to each other (rather than parallel as in nematic). So the directors in each layer are twisted with respect to those of the preceding layers to form a continuous helix about the layer normal. Cholesteric phase is also known as "spontaneously twisted nematic phase". The term cholesteric has been borrowed from the word cholesterol since this phase was first reported in the derivatives of cholesterol. The cholesteric liquid crystals are uniaxial (positive or negative) and

exhibit focal conic with Grandjean steps, homogeneous and isotropic textures. Apart from optical activity, this phase also exhibits circular dichroism. (Figure. 1.1b).

iii) **Smectic liquid crystals:**

Smectic liquid crystal phases are characterized by a one dimensional density wave along the average director giving rise to a layered structure. These liquid crystals have stratified structures but a variety of molecular arrangements are possible within each stratification [27-30]. There exists a number of smectic phases, but two of the most important cases occur when the director is parallel to the layer normal giving rise to orthogonal phases, and when the director is making an angle to the layer normal giving rise to the tilted phases. The smectic mesophase forms a one-dimensional periodic lattice in which the individual layers are two-dimensional liquids. The interlayer attractions are weak as compared with the lateral forces between molecules and, in consequence, the layers are able to slide over one another relatively easily. There are various modifications of the smectic phases, each with different combination of in-plane order and tilt angle. These have been named as the smectic A, B, C, D, E, F, G, H, I, J and K phase designated as, S_A, S_B, S_C, S_D, S_E, S_F, S_G, S_H, S_I, S_J, and S_K, with the letters denoting the chronological order of discovery of these phases. The sequence of their appearance is S_A, S_D, S_C, S_B, S_E, S_I, S_F, S_G, S_G' (S_J), S_H and S_H' (S_K) with decreasing temperature. S_B, S_G, S_J, S_E, S_H and S_K are found to be more crystalline than liquid crystalline phases. Therefore, at present, these phases are treated as soft crystalline phases and designated as the B phase, G phase, J phase, E phase, H phase and K phase. If a compound exhibits both nematic as well as smectic phases, the nematic phase always appears on the higher

temperature side. No single compound is found to exhibit all the smectic phases (modifications) so far. However, the maximum number of phases that a single compound can exhibit are found to be six so far, by terepthalylidene-bis-p-n-butyl aniline (TBDA) as well as N (p-n-pentoxy benzylidene) p-n-hexylaniline (5O.6). The structural identification of each smectic phase is briefly discussed below and their molecular arrangements are shown in the Figure. 1.1c.

SMECTIC A:

The molecular arrangement in this phase involves a parallel arrangement of the rod-like molecules with their ends in line to form layers in which the long axes of the molecules tend to be orthogonal to the layer planes. Rotational motion of the molecules is fairly free, but there is no long range packing of the centres of gravity of the molecules in the planes of the smectic layers. The layers are therefore liquid like in nature. The movement of the molecules from one layer to another, i.e., diffusion of molecules, occurs quite freely and the layers are free to slide on one another. The S_A phase is uniaxially positive. This phase usually exhibits pseudo-isotropic or homeotropic texture in which the smectic layers are parallel to the supporting surface and the optic axis is perpendicular to it. The characteristic textures observed are battonnets, focal conic fan and polygonal. If a liquid crystalline compound has S_A phase in addition to other smectic phases, the S_A phase is always found to be at the higher end of the temperature range.

SMECTIC B:

The smectic B phase generally exists along with S_A phase and occurs upon cooling the S_A phase. The molecules tend to be orthogonal to the layer planes and lamellar spacing is approximately equal to the molecular length. The layers in S_B phase are highly structured unlike in the case of S_A phase. The molecular centres lie on a hexagonal network and the molecules are free to rotate about their long axes. The dimensions of the hexagonal network are, however, small in relation to the size of the molecules, so that the molecular rotation can hardly be regarded as free, but is probably cooperative [31]. Three types of molecular stacking in smectic B phase are reported to be possible [32], namely AAA... (monolayer), ABA...(bilayer), which is also the most common one, and ABCA...(trilayer). The correlation between these layers was also reported in some compounds. Experimental studies [33] established a hexatic B phase which is different from the crystal S_B phase in a few compounds. The hexatic B exists at a higher temperature than the crystalline S_B phase and has short-range in-plane positional ordering and long range bond orientational ordering, both within and between the layers. Some compounds exhibit both types of smectic B phases [34]. If S_B follows the S_A phase upon cooling, S_B phase adopts all the textures exhibited by S_A phase with some modifications. This phenomenon is known as paramorphosis. However, the natural texture of S_B phase is mosaic, while the S_A -S_B transition is accompanied by the appearance of transient transition bars across the fans or focal conics while cooling from S_A phase. Hexatic B to crystal S_B phase transition also exhibits paramorphotic texture with difference in fans.

SMECTIC C:

This phase is the tilted analogue of the S_A phase i.e., the smectic layers have a liquid like, unsaturated arrangement of molecules where the molecular long axes or the directors ($\hat{n}$) are tilted with respect to the layer normal at an angle (θ) that varies from compound to compound. Three different tilt angles viz., one associated with the central atomic core region and the other two with the end alkyl chain regions of the smectic layers, are differentiated [35,36]. The tilt angle is temperature dependent [37] in some compounds and is temperature independent in some other compounds. The S_C phase either exhibits broken focal conic fan or schileren textures.

SMECTIC D:

Only a very few compounds [38,39] are known to exhibit this phase and the common variants observed are I- S_D- S_C or I- S_A -S_D- S_C. Diele et al [39] proposed a structural model for this phase with a cubic close packing of spherical units with each unit consisting of several molecules. No characteristic texture was observed because this phase is found to be optically isotropic. However, in the compound 4-hexyloxy-3-nitrobiphenyl-4-carboxylic acid, which exhibits S_D phase between S_A and S_C phases, a mosaic texture is observed initially which later transforms into an isotropic texture spontaneously.

SMECTIC E:

This phase is commonly observed [40] in the sequence N- S_A – S_B – S_E with decreasing temperature. The X-ray diffraction studies indicate (i) a high degree of

order in smectic layers with a distinctly non-hexagonal lattice, (ii) orthogonal arrangement of molecules with respect to the layers, and (iii) a three dimensional lattice. In some of the S_E modifications optically biaxial properties are observed [41]. Goodby [42] has reported it to be optically uniaxial. Some compounds exhibiting S_E phase are found to possess an orthorhombic cell in the S_E layers. This phase exhibits mosaic and the paramorphotic fan textures with concentric curves across the fans.

SMECTIC F:

This phase is observed in the homologues of pyridene derivatives [43], higher homologues of terepthalydene bis-p-n-alkylaniline (TB $\bar{A}$ A) series [43], Schiff base liquid crystal dimers [44] and a few N (p-n-alkoxy benzylidene) p-n-alkylaniline (nO.m) compounds [45]. The S_F phase has long range order of tilt direction (similar to S_C phase) and has a quasi-two-dimensional structure, with essentially no correlation of molecular positions between layers. The molecules are packed in hexagonal layers with their long axes tilted with respect to the layer planes. It has a c-centred monoclinic lattice with long range three-dimensional order of the lattice direction but does not have long range positional ordering. Shift distortions of the hexagonal net occur between layers, indicating poor correlation between the layers. However, since mono-domains can be obtained with a uniform tilt direction, the hexagonal symmetry is apparently preserved through the bulk of the sample, and it may be concluded that the layers are free to slide over, but not free to rotate relative to one another, i.e., the phase has extensive three dimensional bond orientational ordering. The S_F phase exhibits

stripped or chequered fan and schlieren textures under polarizing thermal microscope.

SMECTIC G:

The G phase is a common low temperature phase in N (p-n-alkoxy benzylidene) p-n-alkylaniline (nO.m) compounds. It has a pseudo-hexagonal structure with a local herringbone order. This phase, of course, has a three-dimensional structure but with a considerable disorder, i.e., the layer distribution is not sharp as in the case of crystals. Presumably this is associated with orientational disorder of the molecules about their long axes. As the layer thickness does not change discontinuously at the S_F -S_G transition, no change in tilt is expected and hence the tilt in S_G phase is of the same magnitude as in the S_F phase. The S_G phase exhibits paramorphotic focal conic fan or characteristic mosaic texture.

SMECTIC H:

Sakagami et al [46] had first differentiated S_G and S_H phases in the well known terepthalylidene bis-p-n-butylaniline (TBBA) and its higher homologues which are rich in S_G and S_H phases. In the S_H phase, the layers are highly structured and it is analogous to S_E phase with a tilt of the molecules. The arrangement of the molecules in the layers can be described as monoclinic when compared with the orthorhombic orthogonal arrangement of molecules in the S_E phase. The characteristic textures of S_H are mosaic which are different in the areas of the mosaic of S_G and the paramorphotic focal conic fan.

SMECTIC I:

Higher homologues of the TB$\bar{A}$A series (alkyl = nonyl, decyl, dodecyl) [47] exhibit the S_I phase. Esters like 4-(2'methylbutyl)phenyl 4'-n-octyloxybiphenyl-4'-carboxylate (8OSI) and amines, like N,N'-bis- (4'-n-heptyloxy benzylidene)-1, 4-phenylenediamine (7OBPD) also exhibit the S_I phase. The molecules are tilted in the layers and the tilt angle in this phase is equal to the tilt angle in the lower temperature S_G and S_F phases. It has more or less similar structure to that of the S_F phase. The only difference is that S_F phase has an in-plane short-range positional ordering whereas the S_I phase has a typical long range positional ordering. However, the S_F and S_I phases also differ in the direction of molecular tilt relative to the hexagonal packing of the molecular long axes. For the S_F phase the hexagon is tilted towards an edge, while for S_I phase, the tilt is towards an apex of the hexagon. The S_I phase exhibits broken fan, mosaic and schlieren textures.

SMECTIC J AND SMECTIC K:

Gane et al [48] first observed these phases in bis-(4'-heptyloxybenzylidene)-1,4'-phenylenediamine (HEPTOBPD) and confirmed that these are not new liquid crystalline phases, but two disordered crystal phases which are analogous to S_G and S_H phases except for the direction of tilt. Both the phases have monoclinic symmetry (with b>a) and pseudo-hexagonal packing of the molecules that are tilted towards the apex of the hexagon. The distortion from the hexagonal packing is greater in the lower temperature phases.

Leadbetter et al [49] confirmed the existence of S_J phase in 4-n-hexylphenyl 4-n pentyl phenyl 4-n-decyloxybenzothiolate.

Some of the smectic phases exhibit ferroelectricity when they are composed of chiral molecules. The potential applications of these ferroelectric liquid crystals are so immense that it is studied as a new branch of material science and technology. It is separately discussed in forthcoming sections later.

1.1.3 Discotic liquid crystals:

Discotic phases are formed on heating compounds that are composed of relatively flat, disc-shaped molecules. These have been recognized as a distinct class of liquid crystalline compounds where the short axis of the molecules maintains a preferred orientation. Evidence for the formation of the mesomorphic phases by disc-like molecules dates back to 1960 [50-52]; however, identification of the discotic phase was made by Chandrasekhar et al [11,13] in 1977 with benzene-hexa-n-alkanoate compounds. Investigations have revealed that not only does the extended columnar discotic system exists, discotic analogues of the nematics are also well recognized now a days. Polymorphism of the columnar discotic systems is also possible depending upon the nature of the lateral packing of the columns and the tilt angle of the column with respect to the normal to molecular planes. Some discotic liquid crystals, analogous to smectic liquid crystals, possess no positional order parallel to the director, making them behave like one-dimensional liquids. In the columnar phase the molecules are more likely to be found in columns rather than between the columns. This phase possesses the orientational order of the nematic phase and also positional order in directions

perpendicular to the director. The structures of a few discotic liquid crystals are shown in the Figure. 1.2.

1.1.4 Lyotropic liquid crystals:

Lyotropic liquid crystals are made up of two or more components. Generally, one of the components is an amphiphillic (containing a polar head group attached to one or more long hydrocarbon chains) and the other is water. A familiar example of such a system is soap (sodium dodecylsulphate) in water. As the water content is increased several mesophases are obtained. These phases differ from other liquid crystalline phases because these are multi-component systems and the concentration of the various components of the system is an important parameter in exhibiting the liquid crystalline properties by these systems [19,20,53].

A few modifications of lyotropic liquid crystals have been identified. In the lamellar, or the neat phase, water is sandwiched between the polar heads of adjacent layers, while the hydrocarbon tails, which are disordered or are in a liquid-like configuration, are in a non-polar environment. In the cubic, or the viscous isotropic phase, the layers are bent to form spherical units with a body-centred cubic arrangement. In the hexagonal or middle phase, the layers are rolled up into cylindrical units of indefinite length arranged parallel to one another in a hexagonal array. A nematic type ordering has also been observed in some soap systems. In hydrophobic dominated compositions, such as aerosol OT-water system, inverted middle and inverted viscous isotropic phases can occur in which the tails point outward towards the hydrophobic medium while water is trapped inside. Cholesteric liquid crystals are formed by the solutions of synthetic polypeptides, e.g.,

poly-γ-benzyl-L-glutamate, in organic liquids when the concentration exceeds a certain critical value. Lyotropic liquid crystals occur abundantly in nature, being ubiquitous in living systems. (Figure. 1.3.)

1.1.5 Defect phases:

One of the most important recent developments in the science of liquid crystals is the appreciation of liquid crystal phases which are possible only through the incorporation of periodic and non-periodic defects [54,55]. Defects in a liquid crystalline phase are points, lines or surfaces at which the orientational or positional ordering is not defined. These defects, thought to be energetically unfavourable, are a part of the structure of the new phases. These phases can be thought of as super structures in which individual regions exhibit liquid crystallinity and the regions are separated by defects. These defects may have the order of an isotropic liquid in analogy with a 'melted lattice.' Two of the important defect phases are the smectic twist grain boundary (TGB) phase and the blue phases formed by some highly chiral molecules. In the TGB phase, the tendency of the molecules to form a twisted phase is frustrated by an additional tendency to form layers. The result is a smectic A structure periodically interrupted by the grain boundaries where the smectic A structure twists by a small angle. In blue phases, regions with liquid crystalline order slightly different from the chiral nematic phase are separated by a lattice of line defects. A few of the defect phases are shown in Figure. 1.4.

1.2 FERROELECTRIC LIQUID CRYSTALS

The ferroelectric effect was first observed in 1921 by Valasek [56] during experiments on crystals of Rochelle salt (potassium sodium tartarate). A ferroelectric material is characterized by an electric dipole moment even in the absence of an external electric field. In these materials the centre of positive charge do not coincide with the centre of negative charge, resulting in the development of spontaneous polarization [57]. This spontaneous polarization, which is the most characteristic property of a ferroelectric material, usually vanishes above a certain temperature called the Curie temperature. There is an intimate relationship between the ferroelectric properties and the atomic arrangement of the ferroelectric materials. Two viewpoints contribute to the understanding of occurrence of ferroelectricity. One is the idea of polarization catastrophe where the local field caused by polarization increase faster than the elastic restoring force on an ion in the crystal, thereby leading to an asymmetrical shift in ionic positions. The other idea is that the static dielectric constant increases when the transverse optical phonon frequency decreases. Both of these ideas have been used to describe the origin of ferroelectricity in different types of materials [58].

In 1975, the American physicist Meyer using symmetry arguments suggested that the tilted smectic phases made up of chiral molecules should also exhibit ferroelectricity. [59,60] Ferroelectricity in the tilted smectic phases requires the molecules to be chiral. The concept of chirality and how it influences the tilted smectic phase, is discussed in the following section. We have confined our discussion to the chiral smectic S_C^* phase since materials exhibiting this phase are used for device applications. However, the same arguments apply equally to other

tilted chiral smectic phases like S_F*, S_I* and also the crystal smectic phases H*, J*, K* and G*.

The ferroelectric liquid crystals, the first group of compounds with fluid properties can be thought of as the most recent members of the already rich family of ferroelectric materials,. They are very similar to the ferroelectric solids in some respects, like, they exhibit spontaneous polarization, have a Curie point and their macroscopic polarization vanishes as the system approaches this temperature. The electro-optic properties of the ferroelectric liquid crystals are widely different from those of the other kinds of liquid crystals. Ferroelectric liquid crystals switch at a very fast rate (~ 1μs) with a large change in the refractive index (Δn~0.1). With such a fast response, ferroelectric liquid crystals have opened new avenues in the field of display technology. Today commercial applications of the ferroelectric liquid crystals include flat panel displays, miniature xerographic devices and high-resolution printheads, etc., to name a few. The principal focus of research in the field of ferroelectric liquid crystals has been the surface stabilized ferroelectric liquid crystals (SSFLC).

1.2.1 Chirality and the Smectic C* Phase:

The smectic C liquid crystalline phase is a layered modification composed of molecules whose long molecular axes are inclined at a temperature dependent tilt angle, θ, to the layer normal. Within each layer there is no positional order of the molecules with the correlation length extending only over a few molecular centres, but the tilt direction remains relatively uniform over large domains. The smectic C phase may be thought of as having been derived from the orthogonal smectic A

phase by simple ordering of the random tilt in the A phase, a relationship which is reflected in a low enthalpy change in the transition from the smectic A to the smectic C phase. The chiral smectic C* phase is composed of optically active molecules and the optical activity arises due to the molecular asymmetry of the enantiomers. In such a case, a macroscopic helical arrangement of the molecules is formed as a result of a precession of the molecular tilt about an axis perpendicular to the layer planes as shown in Figure. 1.5a. The tilt direction is rotated through an azimuthal angle (ϕ) on moving from one layer to the next. As the rotation is in a constant direction, a helix is formed which is either left or right handed. The helical twist sense is determined by the nature and position of the chiral centre with respect to the central core of the mesogenic molecule. A 360° rotation of the helix for the S_{C^*} phase usually extends over hundreds of layers and the azimuthal angle is generally found to be of the order of 0.1—0.01°.

1.2.2 Ferroelectricity in Chiral, Tilted Smectic liquid crystal phases.

In the smectic C* phase, the spontaneous polarization (P_s) arises when the system is cooled from the preceding smectic A, cholesteric or isotropic phase, initially rising very rapidly but thereafter rising very slowly. Typically, for a second order phase transition, the spontaneous polarization is coupled to the change in tilt angle which occurs on cooling the mesophase. The tilt angle varies in the following way:

$$\theta_T = A(T_C - T)^{\alpha} \qquad (1.5)$$

where θ_T is the tilt angle at temperature T, A is a constant, T_C is the transition temperature for the smectic A to smectic C transition, and α is an exponent which is expected to be 0.5 as per the mean field theory but in practice it is found to be less than 0.5. The spontaneous polarization, which varies in a similar way, is expressed as:

$$P_S = P_o(T_C - T)^{\beta} \qquad (1.6)$$

where P_s is the spontaneous polarization at temperature T and β is an exponent which is nearly equal to 0.5. The spontaneous polarization is usually measured in units of nanocoulombs per square centimeter (nC cm^{-2}). With the decrease of temperature, the rotational freedom of the molecules, and the conformation of the molecules change to some extent as the tilt angle increases.

For an achiral smectic C phase, the environment or local symmetry elements consist of a centre of inversion, a mirror plane normal to the layers and a C_2 axis parallel to the layers and normal to the tilt direction (Figure. 1.5b). This combination of symmetry elements gives C_{2h} symmetry.

When some of the molecules in the mesophase are chiral, the centre of symmetry and the mirror planes are lost and only the C_2 axis remains. As the molecules are polar, an imbalance arises with respect to molecular dipoles along the C_2 axis. This imbalance occurs even though the molecules are undergoing rapid reorientational motion about their long molecular axes. This time-dependent alignment of the dipoles along the C_2 axis causes the spontaneous polarization (P_s) to develop along this direction and parallel to the layer planes [61]. Each individual layer, therefore, essentially has a spontaneous polarization associated with it, and

since the layers are stacked one on top of the other in a helical arrangement, the layer polarizations are consequently averaged out to zero and the phase is therefore described as helielectric. However, if the helix is unwound, the layer polarizations point in particular direction and the phase then becomes ferroelectric. The unwinding of the helix can be achieved by applying electric field and is extensively used in surface stabilized ferroelectric liquid crystal (SSFLC) displays.

1.2.3 Surface stabilized ferroelectric liquid crystal cells (SSFLC):

Clark and Lagerwell in 1980 [62] proposed a method to suppress the helix in a ferroelectric liquid crystal and developed the SSFLC arrangement as shown-in the Figure. 1.5c. The helix is constrained by using a cell of thickness that is less than the helical pitch. The surface anchoring forces between the liquid crystal and the boundary plates unwind the intrinsic helix. Symmetry arguments show that this boundary also causes the molecular orientation for each layer to be the same and the materials exhibit ferroelectric behaviour. The director is favoured to lie in the plane of the bounding plates. Because of this condition and the fact that the director is constrained to be at a certain angle from the layer normal to the layer (i.e., to lie on the intersection of a cone and the bounding plate), there are two stable states. The polarization vector, therefore, must be normal to the bounding plates and its two states are in opposite directions. Later it had been established that there are two commonly found layer geometries in SSFLC cells, called the bookshelf and the chevron.

Electro-optical effects are achieved by applying an electric field that induces changes in the director orientation. Since the polarization vector is coupled to the

director, it can be switched between the two stable states by the electric field. This process is known as Clark-Lagerwall effect [63]. The development of the SSFLC's was a major step, not only from the point of view of academic interest, but it has successfully been used in commercial direct-view displays and print bars since 1989.

The bistability by the SSFLC devices makes them ideal where low energy consumption is a major concern, for still images once created in these cells do not require any additional power. Yet, their switching time is fast enough to provide the high frame rates required for video. The fast switching also allows full colour on each pixel which means higher quality on a display of a given size.

1.2.4 Other liquid crystal phases exhibiting spontaneous polarization.

Apart from the ferroelectric liquid crystals, there exists another class of liquid crystals that exhibit spontaneous polarization, viz., the antiferroelectric liquid crystals. Anti- ferroelectric liquid crystals (AFLCs) were first reported by Chandani et al, [64] in a compound named DOBAMC and was designated as the S_{CA}* phase. In this phase the molecules in the neighbouring layers tilt in almost the same direction but in the opposite sense [65,66,67]; the spontaneous polarizations in the neighbouring layers point in the opposite sense of the direction perpendicular to the tilting plane, thereby canceling each other (Figure. 1.6a). Therefore no spontaneous polarization is observed. However, the chirality of the S_{CA}* phase induces a slight precession from layer to layer in the tilting and hence the in-plane spontaneous polarization which leads to the formation of a helicoidal structure with the axis parallel to the smectic layer normal.

Another phase, the ferrielectric phase, consists of layers that are stacked in such a way that there is a net overall spontaneous polarization. In this phase, the number of layers of opposite polarization is not equal (Figure. 1.6b).

1.3 Experimental studies on liquid crystals.

Studies on liquid crystals have been conducted using a number of experimental techniques such as X-ray diffractometry [68,69], dilatometric analysis [70,71], nuclear magnetic resonance (NMR) [72,73], electron spin resonance (ESR) / electron paramagnetic resonance (EPR) [74,75], Fourier Transform Infrared Spectroscopy (FTIR) [76,77] and Raman Spectroscopy [78,79]. These techniques have divulged an enormous volume of experimental data, which has been interpreted to understand the phase transitions in liquid crystalline systems and the associated changes in the various physical and chemical properties, including the electro-optic properties. In this regard, both Laser Raman and FTIR spectroscopies have proved very important techniques as they are able to provide information both at the microscopic (molecular) as well as the macroscopic levels. In Laser Raman spectroscopy, variation of some physical quantities are found to affect the polarizability tensor that results in changes in measurable parameters of certain vibrational modes of the Raman spectrum of the system. FTIR spectroscopy, on the other hand, has been developed during recent past as a very fast technique based on interferometry and can be used to obtain information in a time-resolved setup. Both of these techniques are found to be very effective in the study of phase transitions in liquid crystals, the latter being very much useful in the study of microsecond range switching of ferroelectric liquid crystals under an externally applied electric field.

Therefore, in this thesis, both of these techniques have been employed in the study of phase transitions and molecular dynamics of some thermotropic as well as ferroelectric liquid crystals.

1.3.1 Raman spectroscopic studies on non-ferroelectric liquid crystals.

Raman spectroscopy is one of the most important techniques used in the study of vibrational dynamics of the liquid crystals. Apart from being bond specific, the variation of physical quantities of the liquid crystalline phases affect the polarizability tensor which are reflected as changes in measurable parameters of the Raman spectra. In the past couple of decades Raman spectroscopy has been extensively used in the study of liquid crystals to extract spectral information [80-94], more specifically on the molecular structure [80-88] and intra/inter-molecular interactions [95-97] in the liquid crystalline phases. During recent past, most of the studies using Raman techniques have concentrated on the ferroelectric [98,99] and polymer liquid crystals [100]. However, many basic aspects of the orientational and conformational changes during the process of phase transitions in non-ferroelectric liquid crystals are yet to be explored.

The N(p-n-alkyloxy benzylidene) p-n alkylanilines homologous series of compounds exhibit smectic mesomorphism [101]. This series is popularly known as the nO.m series, where n refers to the number of carbon atoms in the alkoxy chain part of the molecule, whereas m refers to the number of carbons in the alkyl chain part of the molecule, as is illustrated below.

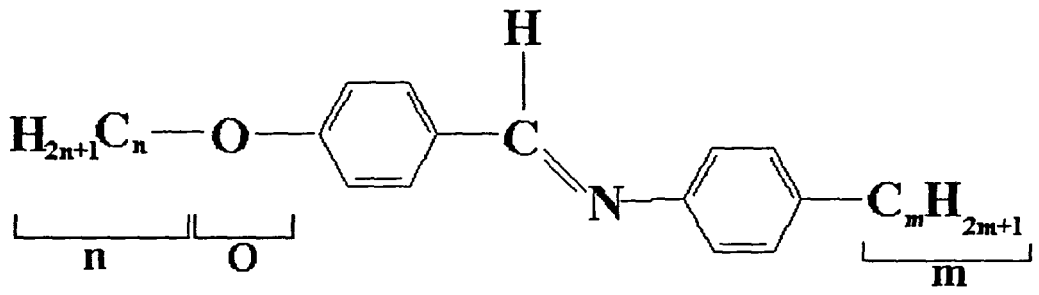

This group consists of compounds containing phenyl groups connected by Schiff base linkages. These compounds are primarily thermotropic liquid crystals exhibiting a wide variety of mesophases.

The first room temperature nematic compound N(p-n-methyloxy benzylidene)-p-n-butylaniline, popularly known as MBBA [102] was reported in 1969 and has paved the way for a new era in liquid crystal research and applications. The simplicity of the synthesis and purification of the Schiff base compounds compared with other compounds, in spite of their susceptible nature to atmosphere, present a wide scope of basic research in these compounds.

The importance of nO.m compounds stems from the following reasons: in addition to nematic phase a wide variety of smectic phases are exhibited by these compounds within a relatively low range of temperatures (room temperature to 85 °C). Some of the compounds of the nO.m series exhibit first order N-S_A transition and some compounds exhibit second order transition with the existence of a tricritical point (where first–order transition crosses over to second order transition) of N-S_A transition among nO.m compounds in 5O.m series, exhibiting large number of phases in compounds (six phases in a single compound 5O.6) are a few important aspects of nO.m series of compounds from the point of view of basic research.

Of these nO.m compounds N(p-n-pentyloxy benzylidene) p-n alkylaniline (5O.m) series of compounds are a fascinating group as the intermediate compounds of this group viz., 5O.5 and 5O.6 exhibit a rich variety of smectic mesomorphism in addition to the presence of nematic phase. The lower homologues of the series such as 5O.2 exhibit nematic and smectic G phases while the higher homologues show the nematic, smectic A and the smectic B phases. This particular series of compounds (5O.m) deserves more attention because the smectic C phases found in these compounds exhibit large tilt angle variation within a small temperature range. For example, the smectic C phase in 5O.5 exhibits a tilt angle variation of $0^{\circ} - 23^{\circ}$ within a small temperature range of 4 °C. Further curiosity is aroused because of the presence of an exotic smectic F phase both in 5O.5 and 5O.6 (the only other nO.m compound that exhibits the S_F phase is 9O.4), which is an extremely rare phase. The compounds 5O.5 and 5O.6 are N-S_A-S_C-S_F-S_G and N-S_A-S_C-S_B-S_F-S_G phase variants respectively. A very interesting and intriguing aspect of the phase sequence of 5O.5 and 5O.6 is just that an increase of one CH_2 group in the end alkyl chain of the molecule 5O.5, an orthogonal (smectic B) phase is induced between two tilted phases (smectic C and smectic F) in 5O.6.

Although the phase transitions and the structural changes in the nO.m compounds have been studied extensively using various techniques experimental, a detailed spectroscopic analysis to probe the microscopic details of the different phases exhibited by nO.m compounds has not been reported so far, to the best of the author's knowledge. Therefore, the compounds 5O.5 and 5O.6 which present a challenging area for understanding the origin of the various intriguing aspects

mentioned above are chosen for a detailed and comparative study using Laser Raman spectroscopy as a part of the work described in this thesis.

1.3.2 FTIR spectroscopic studies on ferroelectric liquid crystals.

Ferroelectric liquid crystals have acquired immense importance in research, both academically as well as commercially, because of their potential applications. But non-availability of suitable time-resolved techniques had proved to be a major stumbling block in the study of the dynamics of electric field induced reorientation of the ferroelectric liquid crystal molecules. The development of time-resolved FTIR spectroscopy [103-105] has led to some major advancement in the studies of the ferroelectric liquid crystals. During recent past, time-resolved FTIR spectrometers have been developed which are capable of providing submicrosecond time-resolution for the time-resolved studies [106-111]. Time-resolved FTIR spectroscopy has now become a widely used tool in determining the switching dynamics of the different molecular segments in the ferroelectric liquid crystals [112-120]. These studies on the switching dynamics and the segmental mobility of the ferroelectric liquid crystals have clarified many ambiguities in the literature. Most earlier workers believed that the whole molecule behaves like a single rigid unit with simultaneous reorientation of all molecular segments [112-115], whereas recent studies have shown that the different molecular segments, i.e., the core, the chiral portion and the alkyl chain region, respond to the electric field as individual units and reorient at different intervals of time [116-120]. Some recent studies have, also, pointed out the hindered rotation of the different molecular segments in the ferroelectric/ antiferroelectric liquid crystals [121-123] as well as explored the

orientational dynamics and the mobility of the different segments in polymeric liquid crystals. [124,125]. Even then, many basic aspects of dynamical switching of the ferroelectric liquid crystals remain to be properly understood.

The sample that we have used in our experiments, 4-(1-methylheptyloxy carbonyl) phenyl 4-(4'-octyloxy benzoylxy) benzoate, named as Chisso 2061, is a chiral antiferroelectric liquid crystal. It belongs to the family of non Schiff's base antiferroelectric liquid crystals composed of unsubstituted phenyl groups connected by ester linkages. When this antiferroelectric liquid crystal is confined in a suitable SSFLC cell, and an electric field is applied, we obtain electric field induced ferroelectric liquid crystal phase. These molecules can then be switched just like the normal ferroelectric liquid crystal molecules.

In recent years, FTIR spectroscopy has gained immense popularity in the study of ferroelectric and antiferroelectric liquid crystals as it is able to extract information related to dynamics of selected groups. The switching dynamics of ferroelectric liquid crystals at molecular segmental level is a very complicated process and many basic aspects of dynamical behaviour have yet to be understood properly. We have employed time-resolved FTIR technique to monitor the response of the different molecular segments under pulsed electric field in the electric field induced S_C^* phase of a chiral, antiferroelectric liquid crystal.

REFERENCES

1. de Gennes, P. G., and Prost, J., "*The Physics of Liquid Crystals*", Oxford University Press, 2nd ed., 1993.

2. Reinitzer, F., *Monatsch. Wiener. Chem. Ges.*, **9**, 421,1888.

3. Lehmann, O., *Z. Physics. Chem.*, **4**, 462, 1889.

4. Blinov, L. M., "*Electro-optical and magneto-optical properties of Liquid Crystals*", John Wiley and Sons Ltd, 1st ed., 1983.

5. Priestley, E. B., Wojtowicz, and P. J., Sheng, P., "*Introduction to Liquid Crystals*", Plenum Press, 1974.

6. Friedel, G., *Ann. Physique*, **18**, 273, 1922.

7. Bouligand, Y., (a) *J. Phys. (Paris)*, **30**, 90, 1969, (b). *J. Phys. (Paris)*, **33**, 525, 1972, (c) *J. Phys. (Paris)*, **34**, 603, 1973, (d) *J. Microscop. (Paris)*, **17**, 145, 1973.

8. Leadbetter, A. J., "*Thermptropic Liquid Crystals*", (ed. Gray, G. W.) Wiley, Chichester, 1987.

9. Pershan, P. S., "*Structure of Liquid Crystal Phases*," World Scientific, Singapore, 1988.

10. Birgeneau, R. J., and Lilster, J. D., *J de Physique Lettres*, **39**, 399,1978.

11. Chandrasekhar, S., Sadasiva, B. K., and Suresh K. A., *Pramana*, **9**, 471, 1977.

12. Levelut, A. M., *J. Chim. Phys.*,**88**, 149, 1983.

13. Chandrasekhar, S., *Phil Trans Roy Soc London*, **A309**, 93, 1983.

14. Ohta, K., Muroki, M., Takagi, A., Hatad, K. I., Ema, H., Yamamoto, I., and Matsuraki, K., *Mol. Cryst. Liq. Cryst.*, **140**, 131, 1981.

15. Ribeiro, A. C., Martins, A. F., and Giroud-Godquin, M. A., *Mol. Cryst. Liq. Lett.*, **5**, 133, 1988.

16. Luzzati, V., and Tardieu, A., *Ann. Rev. Phys. Chem.*, **25**, 79, 1974.

17. Friberg, S, *J. Am. Oil. Chem. Soc.*, **48**, 578, 1971.

18. Lawson, K. D., and Flautt, T. J., *J. Am. Chem. Soc.*, **89**, 5489,1967.

19. Khetrapal, C. L., Kunwar, A. C., Tracey, A. S., and Diehl, P., "*NMR- Basic, Principles and progress*," **9**, (eds. Diehl, P., Fluck, E., and Kosfield, R.) Springer-Verlag, Berlin, 1975.

20. Safran, S., " *Statistical Thermodynamics of Surfaces, Interfaces and Membranes*", Addision Wesley, 1994.

21. Brazovskii, S. A., and Dmitriev, S. G., *Zh. Eksp. Teor. Fiz.*, **69**, 979, 1975.

22. Hornreich, R. M., Luban, M., and Shtrikman, S., *Phys. Rev. Lett.*, **35**, 1678, 1975.

23. Wright, D. C., and Mermin, N. D., *Rev. Mod. Phys.*, **61**, 385, 1975.

24. de Gennes, P. G., *Solid State Commun.*, **10**, 753, 1972.

25. Halperin, B. I., Lubensky, T. C., and Ma, S. K., *Phys. Rev. Lett.*, **32**, 292, 1974.

26. Collings, P .J., and Patel, J. S., "*Handbook of Liquid Crystals Research*", Oxford University Press, 1997.

27. Sackmann, H. and Demus, D., *Mol. Cryst. Liq. Cryst.* **21**, 239, 1973.

28. Coates, D., and Gray, G. W., *Microscop.*, **24**, 117, 1973.

29. Gray, G. W., and Goodby, J. W., "*Smectic Liquid Crystals : Textures and Structures*", Leonard Hill, London, 1984.

30. Demus, D., and Richter, L., "*Textures of Liquid Crystals*", Verlag Chemie, New York, 1978.

31. Gray, G. W., *Mol. Cryst. Liq. Cryst.*, **66**, 270, 1981.

32. Goodby, J. W., Gray, G. W., Leadbetter A. J., and Mazid, M. A., "*Liquid Crystal of one and two dimensional order*" (eds. Helfrich, W., Heppke,) G., Springer-Verlag, New York, pp-3 1980.

33. Goodby, J. W., and Pindak, R., *Mol. Cryst. Liq. Cryst.*, **75**, 233, 1981.

34. Poeti, G., Fanelli, E., and Guillon, D., *Mol. Cryst. Liq. Cryst.*, **82**, 107, 1982.

35. Bartolino, R. Doucet, J. and Durand, G., *Ann. Phys.*, **3**, 389, 1978.

36. Taylor, T. R., Fergason, J. C., and Arora, S. L., *Phys. Rev. Lett.*, **24**, 359, 1970.

37. Luckhurst, G. R., Timmimi, B.A., Pisipati, V.G.K.M., and Rao, N.V.S., *Mol. Cryst. Liq. Cryst. Letter*, **1**, 45, 1985.

38. Demus, D., Kunicke, G., Nelson and Sackmann, H., *Z. Naturfrosch*, **23A**, 84, 1968.

39. Diele, S., Brand, P., and Sackmann, H., *Mol. Cryst. Liq. Cryst.*, **17**, 163, 1972.

40. Goodby J. W., and Gray, G. W., *Mol. Cryst. Liq. Cryst.*, **56**, 43, 1979.

41. Biering, A., Demus, D., and Gray, G. W., and Sackman, H., *Z. Naturforsch*, **23A**, 84, 1986.

42. Goodby, G. W., *Liq., Cryst., Ordered fluid*, **4**,175, 1984.

43. Sackman, H., "*Advances in Liquid Crystals*", (ed. Bata, L.) p-27, 1981.

44. Attard, G. S., Date, R. W., Imrie., C. T., Luckhurst, G. R., Roskilly, S. J., Seddon, J. M., and Tayler, L., *Liq. Cryst*, **16**, 525, 1994.

45. Alapati, P.R., Potukuchi, D.M., Rao, P.B., Rao. N.V.S., Pisipati, V.G.K.M., and Paranjpe, A.S., *Liq. Cryst.*, **5**, 545, 1989.

46. Sakagami, S., Takase, A., and Nikamizo, M., *Mol. Cryst. Liq. Cryst.*, **36**, 261, 1976.

47. Weigelben, A., Ritcher, L., Deresch, J., and Demus, D., *Mol. Cryst. Liq., Cryst.*, **59**, 329, 1980.

48. Gane, P. A. C., Leadbetter, A. J., Wrighton, P. G., Goodby, J. W., Gray, G. W., and Tajbkhsh, A. R., *Mol. Cryst. Liq. Cryst.*, **100**, 67, 1983.

49. Leadbetter, A. J., Tucker, P. A., Gray, G. W., and Tajbakhsh, *Mol. Cryst. Liq. Cryst. Lett.*, **1**, 19, 1985.

50. Brook, J. D., and Tayler, G. H., in "*Chemistry and Physics of Carbon*", Vol-3, (ed. Philip, L.Walker Jr.), pp-243-283, New York.

51. Tanford, C., "*The Hydrophobic Effect*", Wiley, New York, 1973.

52. Tanford, C., *J. Phys. Chem.*, **78**, 2469, 1974.

53. Renn, S. R., and Lubensky, T. C., *Phys. Rev. A.*, **38**, 2132, 1988.

54. Brazovskii, S. A., and Filev, V. M., *Zh. Eksp. Teor. Fiz.*, **75**, 1140, 1978.

55. Sethna, J. P., *Phys. Rev. B.*, **31**, 6278, 1985.

56. Valasek, J., *Phys. Rev.*, **17**, 425, 1921.

57. Halblutzel, J., *Helv. Phys. Acta.*, **12**, 489, 1939.

58. Kittel, C., *"Introduction to Solid State Physics"*, Wiley Eastern Limited, 5th ed., 399, 1987.

59. Meyer, R. B., Liebert, L., Strzelecki, L., and Keller, P. *J., Physique. Lett.*, **36**, 69, 1975.

60. Meyer, R. B., *Mol. Cryst. Liq. Cryst.*, **40**, 74, 1976.

61. Brand, H. R., Cladis, P. E., and Fin, P. L., *Phys. Rev. A.*, **31**, 361, 1985.

62. Clark, N. A., and Lagerwall, S. T., *"Liquid Crystals of One and Two-Dimensional Order"*, (eds. Helfrich, W, Heppke, G.) p-222, Berlin, Springer, 1980.

63. Clark, N. A., and Lagerwall, S. T., *Appl. Phys. Lett.*, **36**, 899.1980.

64. Chandani, A. D. L., Ouchi, Y., Takezoe, H., Fukuda, A., Terashima, K., Furukawa, K., and Kishi, A., *Japan. J. Appl. Phys. Lett.*, **29**, 987, 1990.

65. Gorecka, E., Chandani, A. D. L., Ouchi, Y., Takezoe, H., and Fukuda, A., *Japan. J. Appl. Phys.*, **29**,131,1990.

66. Inui, S., Kawano, S., Saito, M., Takanishi, Y., Hiraoka, K., ., Ouchi, Y., Takezoe, H., and Fukuda, A., *Japan. J. Appl. Phys. Lett.*, **29**, 987,1990.

67. Goodby, J. W., Blinc, R., Clark. N.A., Lagerwell, S. T., Osipov, M. A., Pikin, S. A., Sakurai, T., Yoshino, K., and Zeks, B., *"Ferroelectric Liquid Crystals: Principles, Properties and Applications* ", Gordon and Breach, Philadelphia, 1991.

68. Kaganer, M. V., Ostrovskii, B. I., and de Jeu, W. H., *Phys. Rev. A*, **44**, 8158, 1991.

69. Hou, J., Tashiro, K., Kobayashi, M., and Inoue, T., *J. Phys. Chem.*, **96**, 484, 1992.

70. Rao, N. V. S., Pisipati, V. G. K. M., Alapati, P. R., and Potukuchi, D. M., *Mol. Cryst. Liq. Cryst.*, **162B**, 119, 1988.

71. Kiefer, R., and Baur, G., *Liq. Cryst.*, **7**, 815, 1990.

72. Martins, A. F., Esnault, P., and Volino, F., *Phys. Rev. Lett.*, **57**, 1745, 1986.

73. Fan, S. M., Luckhurst, G. R., and Picken, S. J., *J. Chem. Phys.*, **101**, 3255, 1994.

74. Rananavare, S. B., Pisipati, V. G. K. M., and Freed, J. H., *Liq. Cryst.*, **3**, 752, 1988.

75. Luckhurst, G. R., and Poupko, R., *Chem. Phys. Lett.*, **29**, 191, 1974.

76. Verma, A. L., Zhao, B., Ziang, S. M., Shen, J. C., and Ozaki, Y., *Phys. Rev. E.*, **56**, 3053, 1997.

77. Verma, A. L., Zhao, B., Terauchi, H., and Ozaki, Y., *Phys. Rev. E.*, **59**, 1868, 1999.

78. Galbiati, E., and Zerbi, G., *J. Chem. Phys.*, **84**, 3509, 1986.

79. Kirov, N., Dozov, I., and Fontana, M. P., *J. Chem. Phys.*, **83**, 5267, 1985.

80. Schnur, J. M., *Phys. Rev. Lett.*, **29**, 1141, 1972.

81. Amer, N. M., and Shen, Y. R., *Phys. Rev. Lett.*, **27**, 718, 1970.

82. Borer, W. J., Mitra, S. S., and Brown, C. W., *Phys. Rev. Lett.*, **27**, 379, 1971.

83. Chang, R., *Mol. Cryst. Liq. Cryst.*, **12**, 105, 1971.

84. Schnur, J. M., Sheriden, J., and Fontana, M., in *"Liquid crystals"* (ed. Chandrasekhar, S.), 1975.

85. Bulkin, B. J., and. Prochaska, F. T., *J. Chem. Phys.*, **54**, 635, 1971.

86. Schnur, J. M., and Fontana, M., *J. Phys. (Paris).*, **35**, L53, 1974.

87. Fontana, M., and Bini, S., *Phys. Rev. A* **14**, 1555, 1976.

88. Yoshida, H., Nakajima, Y., Kobinata, S., and Maeda, S., *J. Phys. Soc. Jpn.*, **50**, 3525,1981.

89. Dalmolen, L. G. P., Egberts, E., and de Jeu, W. H., *J. Phys. (Paris).*,**45**, 129, 1984.

90. Wrobel, D., Biophys. Chem., 26, 91, 1987.

91. Vanwinkle, D. H., Dierkker, S. B., and Clark, N. A., *J. Chem. Phys.*, **91**, 5212, 1989.

92. Watanabe, K., and Klein, M. L., *J. Phys. Chem.*, **95**, 4158, 1991.

93. Yokovenko, S. Y., Minko, A. A., Arnscheidt, B., and Pelzl, J., *Liq. Cryst.*, **19**, 449, 1995.

94. Shao, Y., and Zerda, T. W., *J. Phys. Chem. B.*, **102**, 3387, 1998.

95. Dash, S. K., Singh, R. K., Alapati, P. R., and Verma, A. L., *Mol. Cryst. Liq.Cryst.*, **319**, 147, 1997.

96. Dash, S. K, Singh, R. K., Alapati, P. R., and Verma, A. L., *J. Phys. Condensed Matter*, **9**, 7809, 1997.

97. Dash, S. K., Singh, R. K., Alapati, P. R., and Verma, A. L., *Liq. Cryst.*, **25**, 459, 1998.

98. He, L., Shen, Z. X., Yin, Z., Zhang, M. S., Li, W. S., and Tang, S. H., *Ferroelectrics.*, **230**, 345, 1999.

99. Clarke, M. J., Meyer, S. C., and Coles, H. J., *Ferroelectrics.*, **245**, 707, 2000.

100. Mihara, T., and Koide, N., *Mol. Cryst. Liq. Cryst.*, **367**, 605, 2001.

101. G.W. Smith, and Z.G. Gardlung, *J. Chem. Phys.*, **59**, 3214, 1973.

102. Kelker, A. A., and Scheurle, B., *Angen. Chem. Enternal.*, **8**, 884, 1969.

103. Toriumi, H., Sugisawa, H., and Watanabe, H., *Jap. J. Appl. Phys.*, **27**, L935, 1988.

104. Gregoriu, V. G., Chao, J. L., Toriumi, H., and Palmer, R. A., Chem Phys. Lett., **179**,491, 1991.

105. Urano, T. I., and Hamaguchi, H., Chem Phys. Lett., **195**, 287, 1992.

106. Czarnecki, M. A., Katayama, N., Ozaki, Y., Satoh, M., Yoshio, K., Watanabe, T., and Yanagi, T., Appl Spectrosc, 47, 1382, 1993.

107. Katayama, N., Czarnecki, M. A., Ozaki, Y., Murashiro, M., Kikuchi, M., Saito, S., and Demus, D., Ferroelectrics, **147**, 441, 1993.

108. Masutani, K.,Sugisawa, H., Yokota, A., Furukawa, Y., Tasumi, M., *Appl. Spectrosc.*, **46**, 560, 1992.

109. Masutani, K., Yokota, A., Furukawa, Y., Tasumi, M., *Proc. 5th Int. Conf. On Time-Resolved Vibrational Spectroscopy*, P32, Wasedaukin, 1991.

110. Czarnecki, M. A., Katayama, N., Satoh, M., Watanabe, T., and Ozaki,Y., J.Phys. Chem.,**99**, 14101, 1995.

111. Masutani, K., Numahata, K., Nishimura, K., Ochiai, S., Nagasaki, Y., Katayama, N., Ozaki, Y., *Appl. Spectrocs.*, **53**, 588, 1999.

112. Katayama, N., Czarnecki, M. A., Satoh, M., Watanabe, T., and Ozaki, Y., *Appl. Spectrosc.* **51**, 487, 1997.

113. Shilov, S. V., Skupin, H., Kremer, F., Gebhard, E., and Zentle, R., *Liq. Cryst.*, **22**, 203, 1997.

114. Shilov, S. V., Okretic, S., Siesler, H. W., and Czarnecki, M. A., *Appl. Spectrosc. Rev.*, **31**, 82, 1996.

115. Shilov, S. V., Skupin, H., Kremer, F., Wittig, T., and Zentle, R., *Phys. Rev. Lett.* **79**, 1686, 1997.

116. Hide, F., Clark, N. A., Nito, K., Yasuda, A., and Walba, D. M., *Phys. Rev. Lett.* **75**, 2344, 1995.

117. Nagasaki, Y., Masutani, K., Yoshihara, T., and Ozaki, Y., *J. Phys. Chem.*, **104**, 7881, 2000.

118. Nagasaki, Y., Yoshihara, T., and Ozaki, Y., *J. Phys. Chem.* **104**, 2846, 2000.

119. Nagasaki, Y., and Ozaki, Y., *Phys. Chem. Chem. Phys.* **2**, 3037, 2000.

120. Tian, Y., Xu, X., Zhao, Y., Tang, X., Su, F., Zhao, X., and Zhou, E., *Liq. Cryst.* **19**, 295, 1995.

121. Kocot, A., Wzralik, R., Orgasingka, B., Perova T., Vij, J. K, and Nguyen, H. T., *Phys. Rev. E* **59**, 551 1999.

122. Verma, A. L., Zhao, B., Bhattacharjee, A., and Ozaki, Y., *Phys. Rev. E* **63**, 051704, 2001.

123. Vij, J. K., Kocot, A., Kruk, G., Wrzalik, R., and. Zentel, R., *Mol. Cryst. Liq. Cryst*, Sci. Technol., Sect.A, **237**, 337, 1993.

124. Shilov, S. V., Okretic, S., Siesler, H. W., and Czarnecki, M. A., *Appl. Spectrosc. Rev.*, **31**, 82, 1996.

125. Czarnecki, M. A., Okretic, S., and Siesler, H. W., *J. Phys. Chem. Rev.*, **101**, 374, 1997.

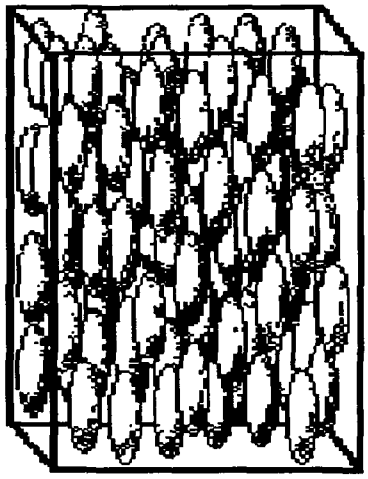

Nematic

Fig. 1.1a Nematic liquid crystals

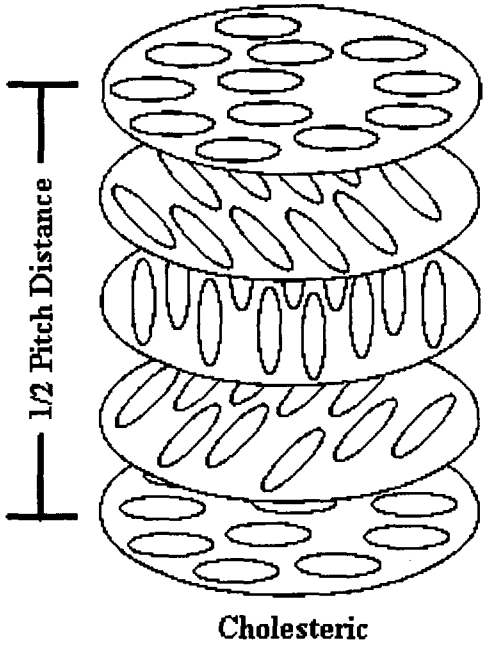

Cholesteric

Fig 1.1b Cholesteric liquid crystals

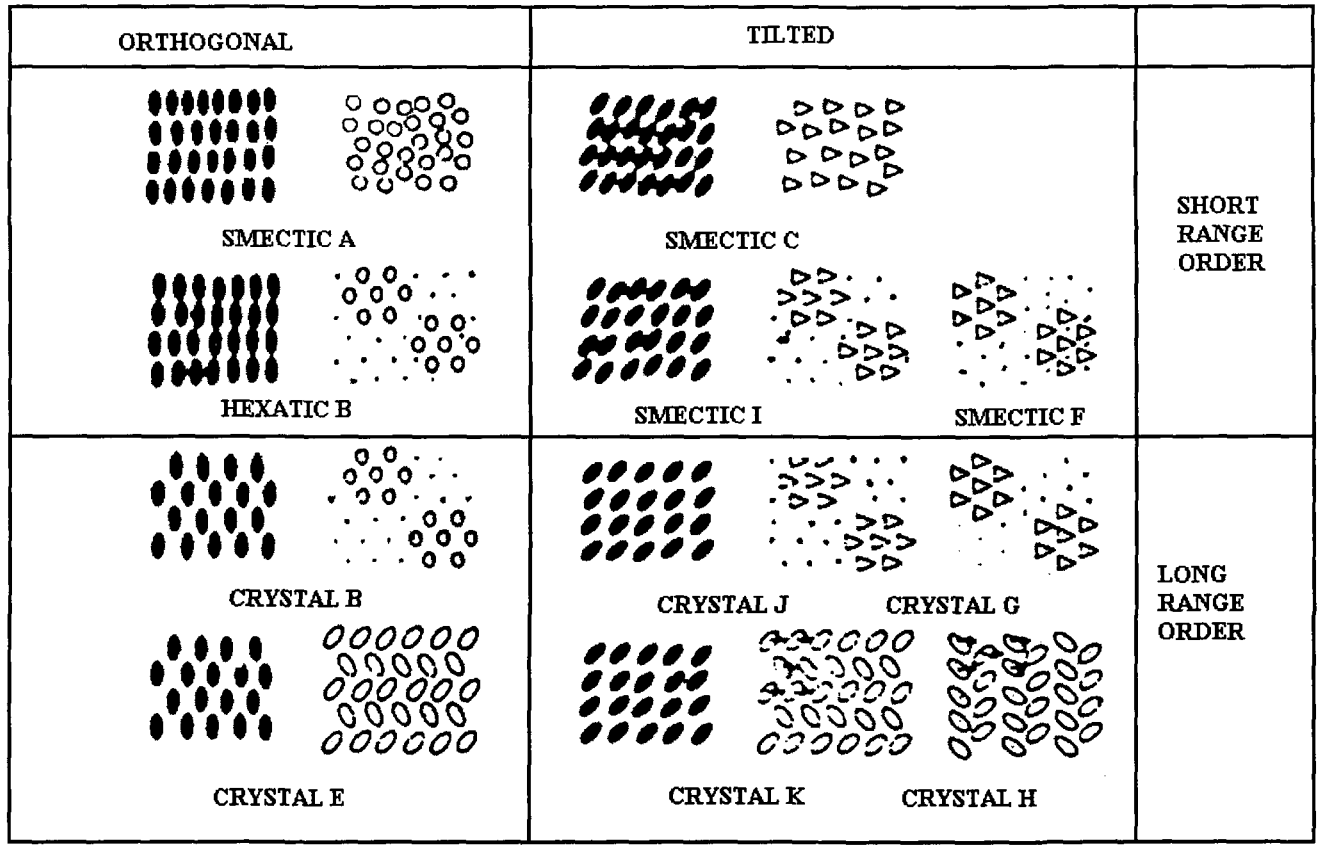

The structures of lamellar smectic mesophases. The side of the lath-like molecules are shown by black ellipses.

Fig 1.1c Various types of Smectic liquid crystals

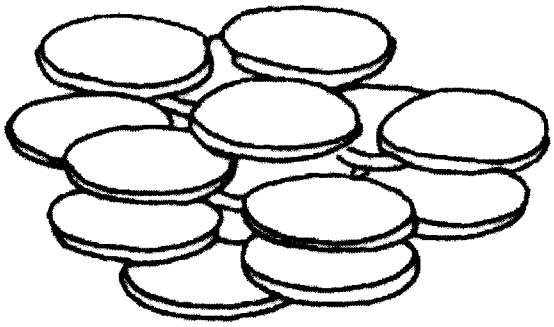

(a) Discotic Phase. (Nematic type)

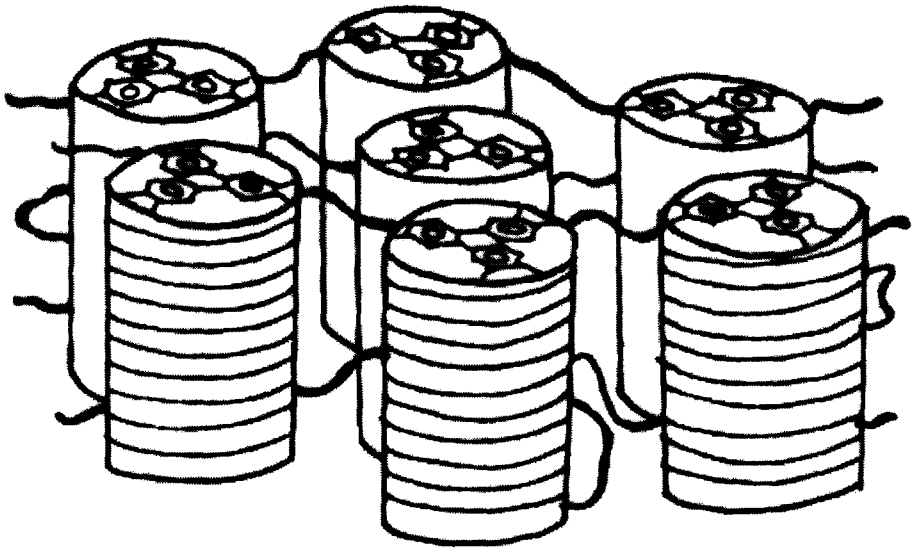

(b) Discotic phase (columnar type).

Fig. 1.2 Two different types of discotic liquid crystals

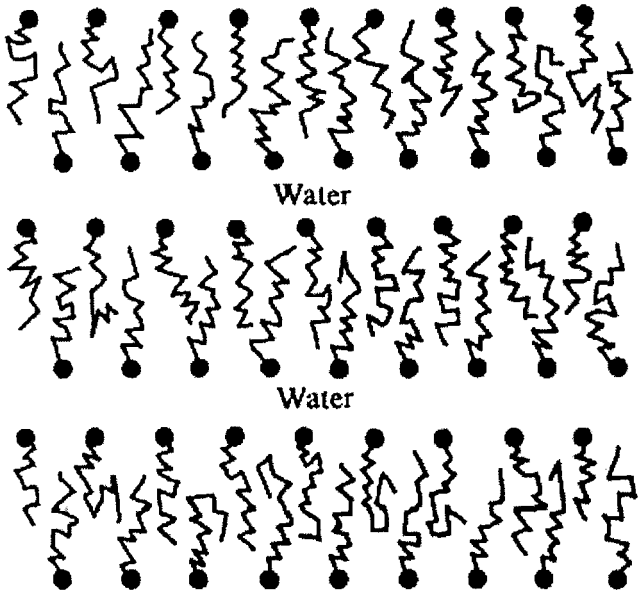

(a) The lamellar or neat phase of soaps.

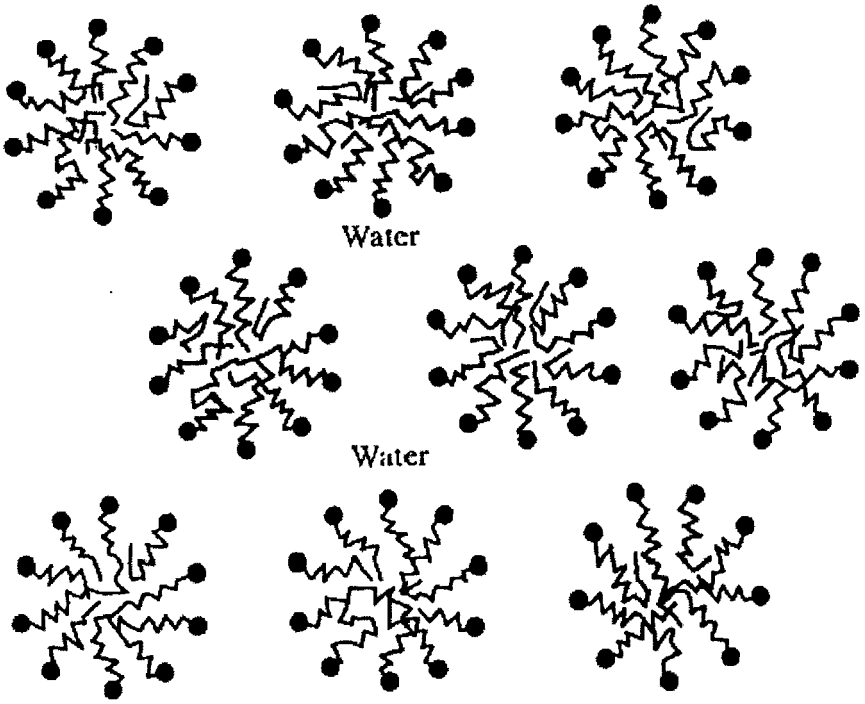

(b) The hexagonal or middle phase of soaps.

Fig 1.3 Different types of Lyotropic liquid crystals.

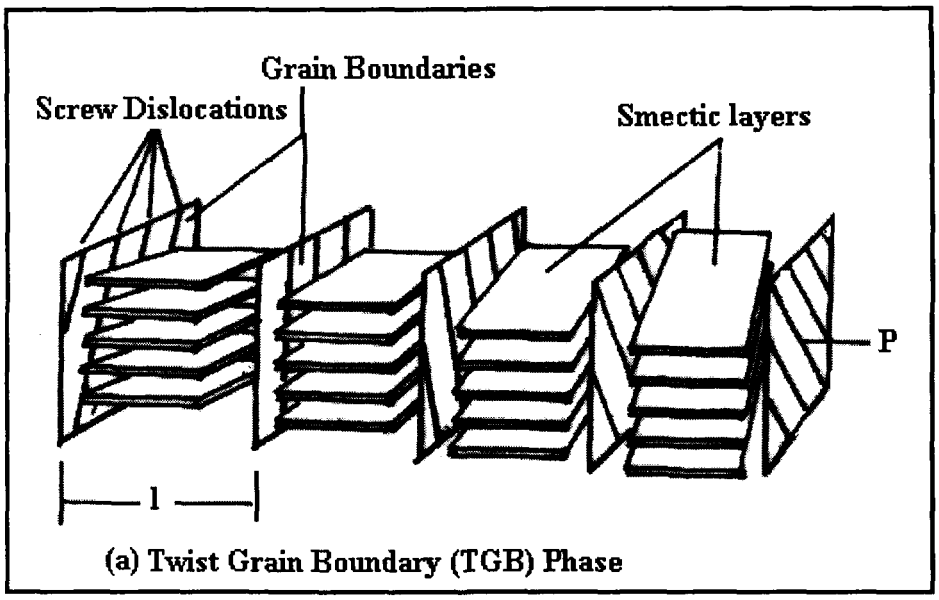

(a) Twist Grain Boundary (TGB) Phase

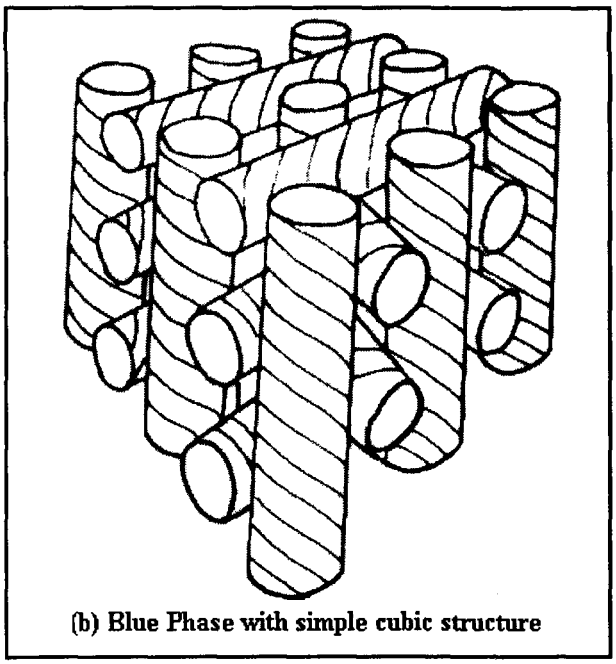

(b) Blue Phase with simple cubic structure

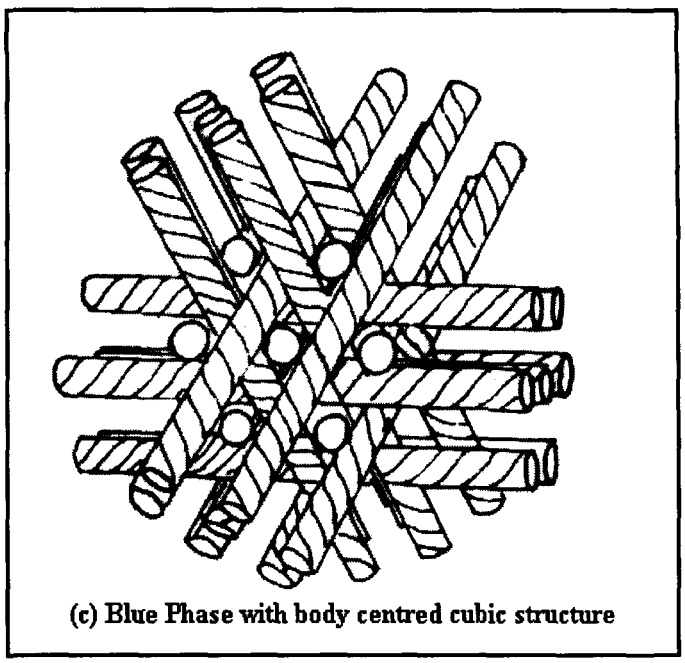

(c) Blue Phase with body centred cubic structure

Fig 1.4 Different types of defect phases

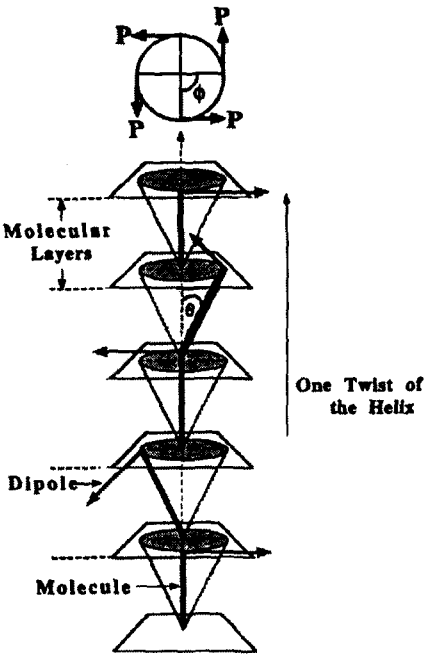

Helielectric Structure of the Smectic C* Phase

(a) The structure of the chiral smectic C* phase.

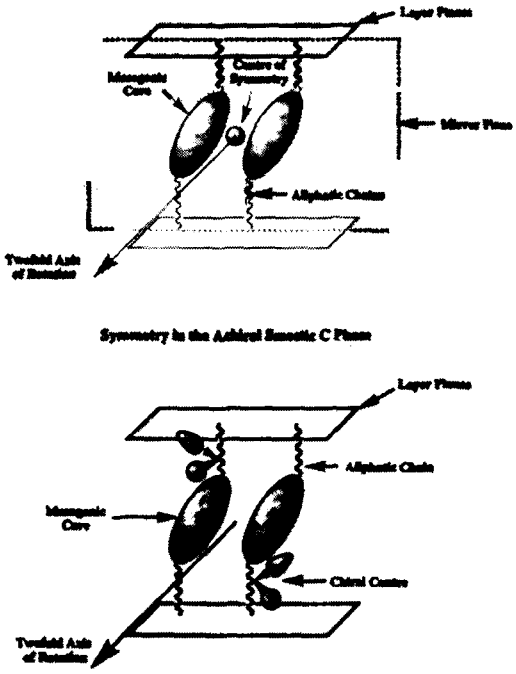

(b) The symmetry in SmC and SmC* phases.

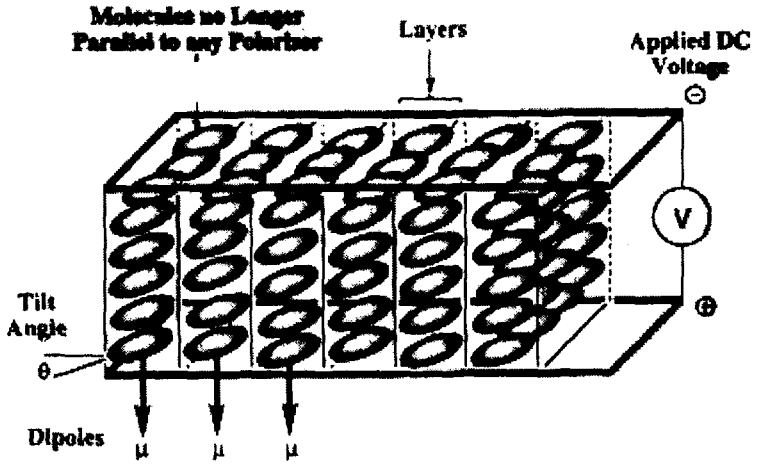

Bistable switching states

(c) Optical transmission in surface stabilized ferroelectric liquid crystal (SSFLC) display.

Fig. 1.5 Ferroelectric phase and SSFLC display.

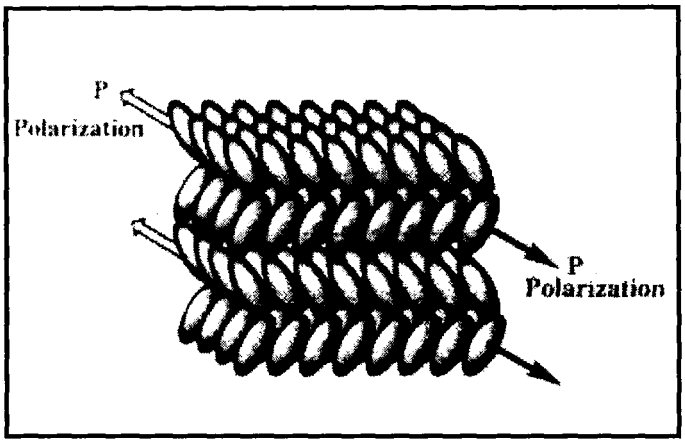

Fig. 1.6a. Structure of the antiferroelectric smectic C* phase.

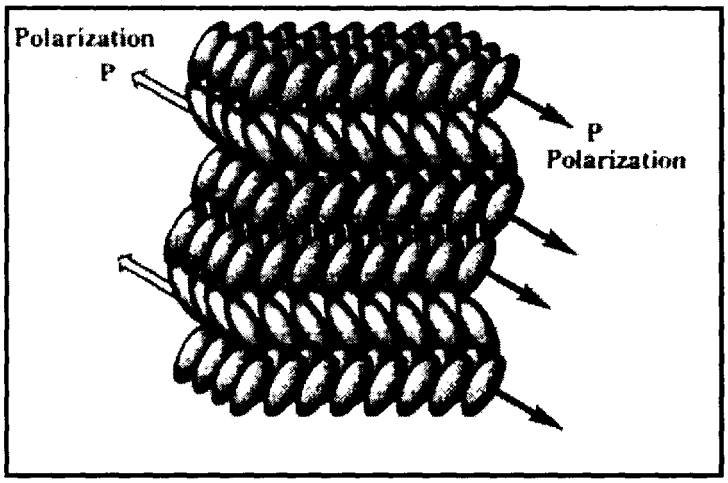

Fig. 1.6b. Structure of the ferrielectric smectic C* phase.

Chapter 2

THEORETICAL BACKGROUND OF RAMAN AND FTIR SPECTROSCOPY AND INSTRUMENTATION FOR THE EXPERIMENTAL TECHNIQUES.

This chapter is divided into two major sections. In the first section theories of Raman and FTIR spectroscopies are given, which are the two important techniques used in this thesis. The other section describes the details of sample preparation, instruments used and related matters.

2.1. THEORETICAL ASPECTS OF EXPERIMENTAL TECHNIQUES.

2.1.1 Raman Effect

Light incident upon a molecule can interact with the molecule either by the absorption of light or by scattering phenomena. When a substance is irradiated by an intense beam of monochromatic light of frequency ν_o, most of the incident radiation passes through the sample undeflected. But, a small part will be scattered by the molecules in all directions, except in the direction of the incident beam. It is found that a major proportion of the scattered light has the same frequency (ν_o) which is called Rayleigh scattering or elastic scattering, and its intensity is proportional to the fourth power of frequency of the incident radiation. Apart from the Rayleigh line, the scattered light contains radiation of frequencies different from frequency of incident radiation. These lines due to inelastic scattering, are characteristic of the molecule on which light is incident and is known as Raman scattering. A Raman band is not characterized by its absolute wavenumber $\nu_o + \nu_r$, but by the magnitude

of wavenumber shifts $|\Delta\nu|$ from ν_0 where $|\Delta\bar{\nu}| = |\bar{\nu}_o - \bar{\nu}| = \bar{\nu}_r$. Raman scattering is always accompanied by Rayleigh scattering. The pattern of frequencies on the lower frequency side, known as Stokes lines are mirrored by an identical pattern of lesser intensity on the higher frequency side of the exciting line, and is known as the anti-Stokes lines (Figure. 2.1). As the anti-Stokes Raman scattering originates from higher vibrational levels of ground electronic state, the intensity of such Raman lines is much weaker compared to those from Stokes Raman scattering and is governed by Boltzmann distribution. A Raman band is characterized not only by its wavenumber shift but also by its polarization characteristics, shape and bandwidth. These parameters provide useful structural information [1-3].

It is found that generally Raman frequencies correspond to the vibrational and rotational transitions of the scattering molecule. Raman effect can be understood by considering the light scattering process as collisions of photons of incident light with the scattering molecules, as it is an extremely feeble two-photon process.

2.1.2 Theory of Raman scattering

The simple classical treatment, which assumes fluctuations of polarizability due to the oscillating induced dipole moment during vibrational or rotational motions of the molecules, is insufficient to explain the precise nature of interaction of radiation with matter. The semi-classical treatment by Kramer and Hiesenberg [4], which correlates the scattering tensor to the wavefunctions and the energy levels of scattering molecules is quite sufficient to understand scattering phenomenon. In this model, the incident radiation treated, classically, is regarded as a source of

perturbation of the energy levels of the scattering system. The quantum mechanical techniques are applied to investigate the transitions between quantized energy levels of the perturbed system.

A non-rotating molecule considered at the origin of a space fixed coordinate system interacts with an oscillating electric field that is represented as,

$$\bar{E}_\sigma = \bar{E}_\sigma^\circ e^{i(\bar{k}\cdot\bar{r}-\varpi t)} \tag{2.1}$$

where, $\bar{k}$ and ϖ are respectively the direction of propagation and angular frequency of the field. The oscillating electric dipole moment induced in the molecule due to interaction with radiation is expressed as,

$$(\bar{\mu}_\rho)_{mn} = (\bar{\alpha}_{\rho\sigma})_{mn}\,\bar{E}_\sigma \tag{2.2}$$

where,

$$(\mu)mn = \langle \psi_m | \bar{e}_\rho | \psi_n \rangle \tag{2.3}$$

is the amplitude of the transition moment, and ψ_m and ψ_n are the time independent wavefunctions of the initial and the final states, respectively. The polarizability tensor for the transitions from the state m to n is given by $(\bar{\alpha}_{\rho\sigma})_{mn}$, where ρ and σ are the molecular cartesian coordinates of the scattering tensor. The scattered light intensity I_{mn} in terms of photons per molecule per second scattered into a 4π solid angle after averaging over all orientations of the molecule can be expressed as,

$$I_{mn} = \frac{128\pi^5}{9c^4}(\nu_o \pm \nu_{mn})^4 I_o \sum_{\rho,\sigma} \left|(\alpha_{\rho\sigma})_{mn}\right|^2 \tag{2.4}$$

where $|m\rangle$ and $|n\rangle$ are the initial and the final vibrionic states, ν_o and I_o the frequency and the intensity of the plane polarized incident radiation, and $(\nu_o \pm \nu_{mn})$ the frequency of the scattered radiation. ν_{mn} is the frequency of vibration involved

in Raman scattering, c is the velocity of light and $\alpha_{\rho\sigma}(\rho,\sigma = x,y,z)$ is the ρ^{th} component of the polarizability tensor.

As is seen from expression (2.3), the intensity of the scattered radiation depends more critically on the square of the polarizability tensor $(\alpha_{\rho\sigma})_{mn}$. Therefore the main basis for developing a theory of Raman effect is to provide a theoretical framework for calculating the polarizability tensor components $(\alpha_{\rho\sigma})_{mn}$ in terms of the molecular parameters.

To determine the polarizability, the distortions of the wavefunctions of the molecule due to periodic perturbation by the electromagnetic wave are calculated. By applying time dependent perturbation theory, the transition dipole moment is evaluated using new wavefunctions. The time dependent Schrodinger equation is:

$$i\hbar\frac{\partial}{\partial t}|\psi\rangle = (H_o + H')|\psi\rangle \tag{2.5}$$

where H_o is the unperturbed Hamiltonian and,

$$i\hbar\frac{\partial}{\partial t}|\psi_o\rangle = H_o|\psi_k^o\rangle \tag{2.6}$$

The time dependency is incorporated through,

$$|\psi\rangle = \sum_k a_k(t)|\psi_k^o(t)\rangle \tag{2.7}$$

where,

$$|\psi_k^o(t)\rangle = |\psi_k^o\rangle e^{\left[\frac{-iH_o t}{\hbar}\right]} \tag{2.8}$$

This is the solution in the absence of perturbation. The perturbation by the electric field of the incident electromagnetic radiation can be represented by,

$$H' = -\frac{1}{2}\left[\mu_\rho E_\rho^o \left\{e^{i\omega t} + e^{-i\omega t}\right\}\right] \qquad (2.9)$$

where, $\mu_\rho = \sum e_j \rho_j$, e_j and ρ_j representing the charge and the position coordinates of the j^{th} particle of the system.

The $(\rho\sigma)^{th}$ component of the molecular polarizability for transition from $|m\rangle$ to $|n\rangle$ state is given Kramer Heisenberg Dirac equation, [5]

$$(\alpha_{\rho\sigma})_{mn} = \frac{1}{h}\sum_e \left[\frac{\langle n|\mu_\sigma|e\rangle\langle e|\mu_\rho|m\rangle}{\nu_{em} - \nu_o + i\Gamma_e} + \frac{\langle n|\mu_\rho|e\rangle\langle e|\mu_\sigma|m\rangle}{\nu_{en} + \nu_o + i\Gamma_e}\right] \qquad (2.10)$$

where μ_ρ and μ_σ are the dipole moment operators and the summation is over all the excited eigen states $|e\rangle$ of the molecule. $i\Gamma_e$ is the damping term related to the width of the excited state $|e\rangle$.

When $\langle e|\mu|m\rangle$ is finite for a real state $|e\rangle$, the transition from $|m\rangle$ to $|e\rangle$ is accompanied by light absorption with centre frequency ν_{em} and full-width at half maxima of $2\Gamma_e$, and the absorption intensity would be proportional to $|\langle e|\mu|m\rangle|^2$. If the photon energy $(h\nu_o)$ of Raman excitation were close to the energy of the electronic transition, the first term of $(\alpha_{\rho\sigma})_{mn}$ and thus I_{mn} would be remarkably large. This is called resonance Raman scattering.

2.1.3 The Polarizability tensor and depolarization Ratio.

As mentioned earlier, when electromagnetic radiation interacts with the charge distribution of a molecule, the polarization of the charge cloud induced by

the electric field of the incident radiation results in an induced dipole moment. The dipole moment so induced is proportional to the electric field and the polarizability α for the small electric field strength is given by:

$$\bar{\mu} = \alpha \bar{E} \tag{2.11}$$

For an isotropically polarizable molecule, the induced dipole moment vector $\bar{\mu}$ is in the same direction as that of the electric field vector $\bar{E}$. However, for an anisotropic molecule, the induced dipole moment in any direction is given by

$$\mu_{ij} = \sum \alpha_{ij} \bar{E}_j \tag{2.12}$$

where i, j = x, y, z. The polarizability tensor α_{ij} can be expressed as,

$$\alpha_{ij} = \begin{bmatrix} \alpha_{xx} & \alpha_{xy} & \alpha_{xz} \\ \alpha_{yx} & \alpha_{yy} & \alpha_{yz} \\ \alpha_{zx} & \alpha_{zy} & \alpha_{zz} \end{bmatrix} \tag{2.13}$$

Because of the symmetry there are only six polarizability tensor components. The elements α_{ij} generally depend on the frequency of the incident radiation, wavefunctions and electronic properties of the molecular system. However, certain components of polarizability elements remain invariant with respect to change of coordinate system and are given by,

$$(\bar{\alpha})^2 = \frac{1}{9}\left[\alpha_{xx} + \alpha_{yy} + \alpha_{zz}\right]^2 \tag{2.14}$$

$$\gamma_s^2 = \frac{1}{2}\left[(\alpha_{xx} - \alpha_{yy})^2 + (\alpha_{yy} - \alpha_{zz})^2 + (\alpha_{zz} - \alpha_{xx})^2\right] + \frac{3}{2}\left[(\alpha_{xy} + \alpha_{yx})^2 + (\alpha_{yz} + \alpha_{zy})^2 + (\alpha_{zx} + \alpha_{xz})^2\right] \tag{2.15}$$

$$\gamma_{as}^2 = \frac{3}{4}\left[(\alpha_{xy} - \alpha_{yx})^2 + (\alpha_{yz} - \alpha_{zy})^2 + (\alpha_{zx} - \alpha_{xz})^2\right] \tag{2.16}$$

where $\bar{\alpha}$, γ_s and γ_{as} represent the isotopic, symmetric isotropic and the antisymmetric anisotropic tensor invariants.

The depolarization ratio for randomly oriented molecules in the fluid state in 90° scattering geometry is defined as follows:

$$\rho_l(\theta = 90^o) = \frac{I_\perp}{I_{\text{II}}} \tag{2.17}$$

The subscript on ρ_l indicates that it is defined for linearly polarized radiation. In terms of polarizability components,

$$\rho_l = \frac{3\gamma_s^2 + 5\gamma_{as}^2}{45(\bar{\alpha})^2 + 4\gamma_s^2} \tag{2.18}$$

For normal Raman effect, the tensor is symmetric and $\alpha_{ij} = \alpha_{ji}$. Hence $\gamma_{as}^2 = 0$ and ρ_l has its well known form for non-resonant Raman scattering given by,

$$\rho_l = \frac{3\gamma_s^2}{45(\bar{\alpha})^2 + 4\gamma_s^2} \tag{2.19}$$

and equation 2.15 reduces to,

$$\gamma_s^2 = \frac{1}{2}\left[(\alpha_{xx} - \alpha_{yy})^2 + (\alpha_{yy} - \alpha_{zz})^2 + (\alpha_{zz} - \alpha_{xx})^2\right]$$

$$+3\left[(\alpha_{xy})^2 + (\alpha_{yz})^2 + (\alpha_{zx})^2\right] \tag{2.20}$$

For Raman scattering from non-totally symmetric modes, $(\bar{\alpha})^2 = 0$ and $\rho_l = \frac{3}{4} + \frac{5\gamma_{as}^2}{4\gamma_s^2}$. If $\gamma_{as}^2 = 0$, we have normal polarization with $\rho_l = \frac{3}{4}$.

Under resonance Raman scattering the tensor need not remain symmetric, i.e., $\alpha_{ij} \neq \alpha_{ji}$.

If $\gamma_{as}^2 \neq 0$, then $\gamma_s^2 \neq 0$ and we have anomalous polarization provided $\gamma_s^2 \neq 0$; if $\gamma_s^2 = 0$, then $\rho_l = \infty$ (inverse polarization).

For totally symmetric modes, where, $(\bar{\alpha})^2 \neq 0$ and $\gamma_{as}^2 = 0$;

$$\rho_l = \frac{3}{\left\{\frac{45(\bar{\alpha})^2}{\gamma_s^2}\right\} + 4} \tag{2.21}$$

and so $0 \leq \rho_l < \frac{3}{4}$ according as $\infty \geq \frac{45(\bar{\alpha})^2}{\gamma_s^2} > 0$.

Group theoretical considerations can provide information about the invariants which are non-zero for particular vibrational modes in molecules of a given symmetry, and thus the symmetry properties of the general polarizability tensor. Dispersion of ρ_l with exciting frequency provides valuable information about the symmetry of the molecule.

2.1.4 Parameters of Raman profiles:

In order to obtain useful information from the Raman spectra, a number of parameters of Raman profiles need to be analyzed. Some of the basic features obtained in Raman spectroscopy are peak position, integrated intensity and linewidth. These are extremely helpful in applicational aspects of Raman spectroscopy in different fields such as molecular dynamics, structural phase transitions and molecular order parameter calculations. In view of this, the spectroscopic origin of these parameters are discussed below briefly.

2.1.4.1 Peak Positions:

If the Raman spectra originate from molecular vibrations, then the Raman bands characterize a particular mode of vibration at definite frequency due to a group of atoms. However, depending upon the symmetry properties of molecular vibration, Raman modes may be active, inactive or weakly active. The peak positions usually indicate energy of vibration of the molecules. Shift in peak position, therefore indicate, increase or decrease of energy of bond that is undergoing vibration. Peak positions of certain characteristic modes are sensitive towards different physical parameters such as temperature, pressure, solvents and other perturbations which affect the intermolecular interactions and bonding arrangements.

2.1.4.2 Integrated Intensity:

The absolute or integrated intensity of Raman bands provides information about molecular structure. It shows the modulation of the molecular polarizability by a vibration. Placzek's theory [6], which treats molecules as quantum objects and electromagnetic fields classically, satisfactorily describes the Raman effect with the condition that the exciting frequency differs considerably from the frequencies of electronic as well as of vibrational transitions. If a sample is irradiated by a laser radiation whose electric vector is oriented perpendicularly to the plane of irradiation and observation, then the observed radiant power is proportional to the absolute differential Raman scattering cross-section (or integral Raman scattering coefficient)

$\left(\frac{d\sigma}{d\Omega}\right)$, where σ is the cross-section and Ω is the solid angle. In case of 'Stokes line' of a Raman-active vibration of frequency ν, scattering coefficient is given by [7],

$$\left(\frac{d\sigma}{d\Omega}\right)_{\perp}^{-} = \frac{\pi^2 b^2 (\nu_o - \nu)^4}{45\varepsilon_o^2 \nu \left[1 - e^{\frac{hc\nu}{kT}}\right]} g_j \left(45\alpha'^2 + 7\gamma'^2\right) L \qquad (2.22)$$

Here ν_0 and ν represent the frequency of the exciting radiation and the excited vibration, respectively and g_j is the degree of degeneracy of the vibration. The expression g_j $(45\alpha'^2+7\gamma'^2)$ is known as the *scattering activity*, $b^2 = h/8\pi^2 c\nu$ is the square of the 'zero point amplitude' of the vibration. Therefore, equation (2.22) can be rewritten in simplified form as:

$$\left(\frac{d\sigma}{d\Omega}\right)_{\perp}^{-} = \frac{\pi^2 b^2 (\nu_o - \nu)^4}{8c\varepsilon_o^2 \nu \left[1 - e^{\frac{hc\nu}{kT}}\right]} g_j \left(\alpha'^2 + \frac{7}{45}\gamma'^2\right) L \qquad (2.23)$$

In equation (2.23), L represents internal *field factor* that could be given by

$$L = \frac{1}{3^4}\left[\left(\frac{n_R}{n_o}\right)\left(n_R^2 + 2\right)^2 \left(n_o^2 + 2\right)^2\right] \qquad (2.24)$$

where n_o and n_R are the refractive indices at the wavelength of the exciting and Raman radiation respectively. The increase of the incident and scattered electric field due to the dielectric nature of the scattering medium are generally taken into account by the internal field factor [8]. Therefore, barring L, the differential Raman scattering cross-section of a vibration of degeneracy g_j, frequency ν, excited by radiation with frequency ν_0, could be represented by:

$$\left(\frac{d\sigma}{d\Omega}\right)_{\perp} = \frac{\pi^2 b^2 (\nu_o - \nu)^4}{8c\varepsilon_o^2 \nu\left[1 - e^{\frac{hc\nu}{kT}}\right]} g_J \left(\alpha'^2 + \frac{7}{45}\gamma'^2\right) \qquad (2.25)$$

Now, redefining ν_0 as the reference frequency ν_{ref}, and dividing the above equation by $(\nu_{ref}-\nu)^4$ one gets

$$\left(\frac{d\sigma}{d\Omega}\right)_{\perp} (\nu_{ref} - \nu)^{-4} = \frac{h}{8c\varepsilon_o^2 \nu\left[1 - e^{\frac{hc\nu}{kT}}\right]} g_J \left(\alpha'^2 + \frac{7}{45}\gamma'^2\right) \qquad (2.26)$$

The left hand side of equation (2.26) is known as *'absolute normalized Raman scattering cross-section'* and is equal to the intensity of the observed band. From equation (2.26) it is also inferred that intensity of the scattered radiation is proportional to ν^4 factor of the exciting frequency.

2.1.4.3 Width of spectral line (Linewidth)

It is a well-known fact that all the spectral lines have an *intrinsic linewidth*, which is independent of any detection system used for their observation. This intrinsic linewidth has got its origin from the fact that an atom or a molecule, in an excited state, has got a finite life time and accordingly it has some energy (or frequency) spread. This (linewidth) is commonly known as *natural linewidth*. The natural linewidth, however can not be observed without very special techniques because it is completely concealed by some other broadening effects like doppler broadening, collision induced broadening, instrumental broadening, stark broadening and time of flight broadening. The spectral lines of discrete absorption or emission spectra are, therefore, never strictly monochromatic, but have got a

frequency spread and hence a spectral distribution I(ν) of intensity around the central frequency $\nu_o = (E_i - E_k)/h$, where E_i and E_k are the energies of the two states involved in the transition. The function I(ν) in the vicinity of ν_0 is called the line profile. The frequency interval $\Delta\nu = |\nu_2 - \nu_1|$ between the two frequencies ν_1 and ν_2, such that $I(\nu_1) = I(\nu_2) = I(\nu_0)/2$, is called the full width at half maximum (FWHM) of the line or often called linewidth (Γ) of the spectral line. Raman linewidth is a cumulative effect of the linewidths originating from the temperature independent vibrational dephasing and temperature dependent orientational/rotational motion. For a particular Raman linewidth, orientational/rotational motion contributes towards its wings whereas vibrational dephasing contributes towards its middle portion. In order to get an overall idea on different processes that contribute to linewidths, a brief discussion is given here on isotropic Raman line shapes and widths which provides a direct and useful probe of vibrational dephasing along with the origin of other contributions to linewidth.

The different microscopic processes affect the vibrational relaxation and energy transfer processes in systems in many ways and result in a finite correlation time for the vibrational mode. The correlation time is the time during which a well-defined phase relationship among an ensemble of identically prepared excited molecules is irreversibly scrambled and destroyed. The primary cause of vibrational relaxation and dephasing is the interaction of forces from the environment with the cubic and quartic anharmonicities of the vibrational modes which changes its instantaneous vibrational frequency and result in loss of its phase memory [9,10]. The population and energy relaxations involve inelastic processes in which a

vibration undergoes an inelastic scattering and exchanges energy with other intra-molecular and inter-molecular vibrational degrees of freedom resulting in energy dissipation as well as a loss of phase memory and correspond to the so called T_1-processes (spin-lattice relaxation). The phase relaxation involves elastic scattering of the vibration which results in the loss of phase memory without changing its quantum state. These are called T_2'-processes (pure dephasing) which contribute to the overall dephasing process T_2 (spin-spin). Although T_1 relaxation contributes to T_2, there are processes other than T_1 relaxation, which may provide a dominant mechanism for dephasing.

Vibrational dephasing is accessible to experiments primarily through two types of measurements. Spectral line shape measurements and coherent pico-second time-resolved studies. The width of a homogeneously broadened line is related to the energy (T_1) and pure dephasing (T_2') lifetimes of the excitation by the relation $2\pi\Gamma_{hom} = \frac{1}{T_1} + \frac{2}{T_2'}$. One may measure T_1 relaxation by ordinary emission experiment and an absorption experiment would give T_2 and thus we may obtain T_2', at least in principle. However, study of isotropic Raman line shapes and widths provides a direct and useful probe of vibrational dephasing. In condensed phase at room temperature, vibrational relaxation processes are very rapid and line width data is very difficult to interpret because a large number of physical processes contribute to the observed lineshapes. The main line broadening factors include the orientational and rotational motions, vibrational population and energy relaxation, phase relaxation, isotopic splitting, hot bands, and statistical distribution of vibrational

frequencies due to inhomogeneities and disorder in solids [9,10]. Under certain assumptions and suitable choice of Raman scattering geometry, it is possible to separate out the orientational contribution from other contributions from the intrinsic vibrational part.

2.1.4.4 Brief discussion on Line Broadening and Line Shapes.

The orientational motion of molecular groups in the lattice contributes to the spectral bandwidth and line shape in the following way. If the orientational motion is treated approximately as a jump motion between the available orientation sites, angular jumps may occur randomly taking the ion from one configuration to an equivalent one where it resumes all its normal vibrations over again. The temperature dependence of linewidth of a Raman band due to this process can be expressed by an Arrhenius type equation:

$$\Gamma_{(T)} = \Gamma_o e^{\left(\frac{-E^*}{kT}\right)} \qquad (2.27)$$

where Γ_0 is a constant parameter related to the entropy of the system, E* is the activation energy needed for reorientational motion and T is the temperature. This process contributes to the anisotropic part (off diagonal) of Raman scattering, which also includes contributions from vibrational relaxation and non-rigidity of the molecular groups. Therefore, for extracting meaningful information about orientational dynamics from measured off-diagonal Raman line shapes, intrinsic vibrational contribution must be separated out. The intrinsic part of vibrational relaxation arises due to anharmonic interactions and coupling of the vibrational mode of the molecular unit with other intermolecular vibrations as well as with the

intra-molecular translational and lattice modes of the system [11]. The phase correlation of an ensemble of oscillators will decay in time due to interactions of a vibration with its surroundings, which result in modulation of transition frequency. The linewidth, thus determined by the distribution of the oscillator frequencies $(\delta\varpi)$ and time scale (τ_c) at which the modulation of the transition frequency occurs, is theoretically obtained by the expression:

$$\Gamma_{T_2'}^{(4)} = \frac{1}{T_{qj}^{*} \exp\left(\frac{\hbar\omega_{qj}}{kT}\right)} \tag{2.28}$$

with a frequency shift of,

$$\Delta\omega_{Qi}^{4} = \frac{\delta\omega_{qj} \exp\left(-\beta\hbar\omega_{qj}\right)}{1+\left(\delta\omega_{qj}T_{qj}^{*}\right)^{2}} \tag{2.29}$$

where $\delta\omega_{qj}$ (measure of the strength of coupling) is a change in frequency of a mode q_j due to excitation of the internal mode Q_i. T_{qj}^{*} is the T_1 spin lattice relaxation.

For practical purposes though, instead of this theoretical approach, the lie width is calculated by using mathematical programs. It is well known that the frequency dependence of the transition probability in the vicinity of absorption determines the line shape. Two most commonly observed line shapes are the Lorentzian and the Gaussian. The Lorentzian line shape is very similar to that of the Gaussian but falls off more gradually at the wings (Figure. 2.2). The general form of the Lorentzian shape is represented by,

$$y = \frac{a}{[(v-v_o)^2 + b^2)]} \tag{2.30}$$

where 'a' and 'b' are characteristic constants, which depend on lifetimes. The maximum occurs at $\nu = \nu_o$ and it is equal to $\frac{a}{b^2}$. The width at half maximum is b.

The general form of the Gaussian shape is represented as,

$$y = ce^{\left[-d(\nu-\nu_o)^2\right]} \tag{2.31}$$

where 'c' and 'd' are constants.

For a modern double monochromator, the slit function, for small slit widths, can, to a good approximation be represented by a Gaussian function. Also, for small slit widths the true Raman lineshape can be approximated by a Lorentzian. The measured profile will be a convolution of a Gaussian slit function with a Lorentzian lineshape. This convoluted function is known as the 'Voigt function'. For extracting information on the various Raman parameters, the Voigt profiles are deconvoluted using a computer software called GRAMS. This software initially makes rough fittings of the spectra based on input data and then makes a tentative polynomial fitting. An iteration process is then initiated which continues till the exact solution is converged leading to the nearly complete fitting of the spectra. The parameters like linewidth, peak position and area are automatically displayed. Peak area was used to calculate integrated intensity. The line width obtained from this calculation was used to obtain the true linewidth (Γ_L) using a method of least square fitting by the relation,

$$\Gamma_L = \left(\Delta\nu_{1/2}\right)_{Raman}\left[1-\left\{\frac{S}{\left(\Delta\nu_{1/2}\right)_{Raman}}\right\}^2\right] \tag{2.32}$$

where $\left(\Delta\nu_{\frac{1}{2}}\right)_{Raman}$ is the linewidth obtained from the iterative calculations and S is the slit function.

2.2 Fourier Transform Infrared Spectroscopy.

Fourier transform is a technique that has acquired immense importance in chemical analysis, as it is able to provide near real time data. In this technique the absorption spectrum is obtained by interference technique and the structural information from the observed diffraction patterns is obtained through a mathematical manipulation known as Fourier transformation. This is possible since all the diffraction based methods also depend on interference effects. Interferometry provides a very good alternative to the conventional IR spectroscopy, as the entrance beam is not limited by the slit. Another inherent advantage is that the energy at all wavelengths emitted by the source is measured simultaneously [11-14].

The basic theory underlying the operation of a Fourier transform infrared spectrometer is as follows. Any arbitrary state can be expanded in terms of a suitable set of states, e.g.,

$$f(x) = \sum_{k=0}^{\infty} (a_k \sin kx + b_k \cos kx) \qquad (2.33)$$

or can be written in the integral form as,

$$f(t) = (2\pi)^{-\frac{1}{2}} \int_{-\infty}^{+\infty} g(\nu) e^{i\nu t} d\nu \qquad (2.34)$$

where, t (time) and ν (frequency) are Fourier Transform pairs.

Such an expansion can be carried out with any set as long as it is complete and may use any function like sine, cosine, spherical harmonics, Hermite polynomials, etc. The principle of interferometry lies in the simple concept of interference of radiation. Two radiation beams with the same wavelength (λ) and amplitude (a) lead to the phenomena of optical interference if they are coherent. The interference is constructive if the two radiation beams interfere in phase and destructive if out of phase by an half-integral multiple of the wavelength. At intermediate phase differences, the amplitude is given by the equation,

$$\frac{1}{2}\left(1 \pm \cos\frac{2\pi\theta}{\lambda}\right) \tag{2.35}$$

where θ is the phase difference.

A rather complex interference pattern is obtained when two radiation beams of different wavelengths interfere and the amplitude is then given by the equation,

$$\frac{1}{2}\left[\sum_{n=1,2}\left(1.0 + \cos\frac{2\pi\theta}{\lambda_n}\right)\right] \tag{2.36}$$

The interference pattern becomes less regular when more wavelengths are allowed to interfere.

The heart of any FTIR spectrometer is an amplitude division interferometer (Figure. 2.3a). The original Michelson design, still employed in a majority of laboratory FTIR's, consists of a beam splitter, a compensating plate and a pair of mirrors. The difference in path length of the two arms is varied by mechanically scanning the position of one of the mirrors. This gives rise to a time dependent variation in the transmitted optical intensity, commonly known as the interferogram (Figure. 2.3b). When the interferometer is illuminated by a monochromatic source

such as a single frequency laser, the interferogram will be a sine wave of intensity versus mirror position. On the other hand, if the source is characterized by a broad infrared spectrum, the interferogram will correspond to the superposition of an infinite number of sine waves having different periods but a common zero-phase point (or the central maxima) which occurs when the lengths of the two interferometer arms are equal.

Present day FTIR spectrometers use a dedicated digital computer to perform a rapid Fourier transform of the interferogram, thereby directly yielding the composite spectrum of the source, the instrument, and any sample interposed in the optical path.

Some very important advantages of the FTIR spectrometers are the multiplex advantage, the throughput advantage, greater frequency accuracy and suppression of stray light. Of these, multiplex advantage is most important and it is derived from the fact that FTIR measures spectra generated by all wavelengths simultaneously instead of sequentially stepping from wavelength to wavelength. In principle this implies that the time required to obtain a spectrum having a given signal-to-noise ratio can be reduced in proportion to the number of data points in the spectrum.

2.3 Experimental Techniques and Instrumental Details.

In this section, details are given about the samples, their preparation and characterization, experimental techniques and the various instruments used to obtain the Raman and the time-resolved FTIR data described in this thesis.

2.3.1. RAMAN STUDIES

2.3.1.1. Synthesis and characterization of the 5O.5 and 5O.6 compounds:

The N(p-n-alkyloxy benzylidene) p-n alkylaniline, (nO.m) compounds 5O.5 and 5O.6 were synthesized by following a standard procedure [15,16]. The chemicals used were purchased from Aldrich Chemical Co. USA. The method of preparation involves the condensation of p-n-alkylaniline (alkyl=5,6) with p-n-pentlyoxy benzaldehyde,

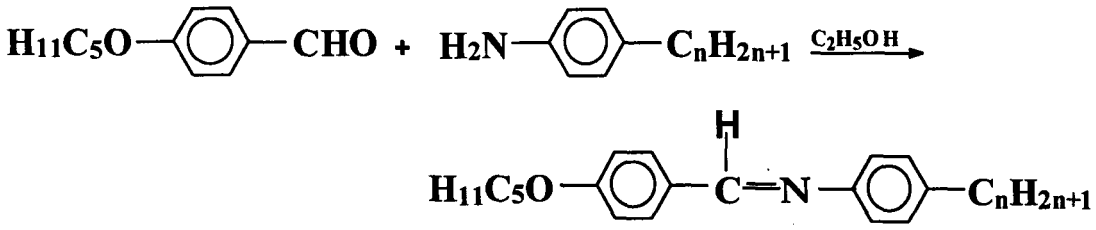

n=5

and **m**= 5 and 6 for 5O.5 and 5O.6 respectively.

The samples were recrystallized repeatedly several times in absolute ethanol until observed transition temperatures were constant. The purity of the compounds was established by observing the sharpness of the DSC peak at their melting point. Special precautions were taken to prevent atmospheric hydrolysis, as the compounds of this homologous series are prone to decomposition due to prolonged heating at high temperature. The transition temperatures were determined by Differential Scanning Calorimetry (DSC, Model Perkin Elmer series-7) and the liquid crystal were identified from their characteristic textures using polarizing microscope (Model – METZ –782 POL) attached with a indigenously fabricated heating attachment. The phase sequence, transition temperatures and transition enthalpy

values were found to be in excellent agreement with the data available in literature. The molecular structure and the phase transition sequence of the two N(p-n-pentyloxy benzylidene) p-n alkylanilines, 5O.5 and 5O.6 are given below.

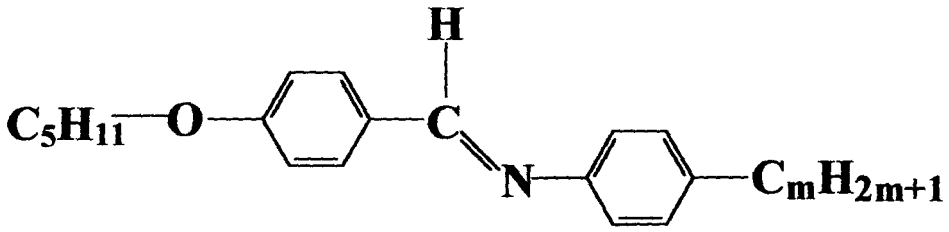

m= 5 and 6

(a) 5O.5

(b) 5O.6

2.3.1.2 Sample preparation for the Raman study of 5O.5 and 5O.6.

For recording the Raman spectra in the bulk form, the samples were encapsulated in quartz capillary tubes of 0.8 mm diameter in an inert atmosphere and were sealed. These sealed sample tubes were used in recording both high and low temperature spectra. For measuring the spectra in the solution form, molar solutions of the samples were prepared in CS_2. The solution was then transferred to sealed quartz cuvettes for recording the Raman spectra. In order to record the Raman spectra of the samples in thin films, free-standing thin films were prepared. For drawing the free-standing films the following procedure was adopted. A conical hole of 1-2 mm vertex diameter was made in a glass or hylam slab. Sample placed on the slab near the conical hole was heated to smectic A phase and was spread across the

hole using a glass cover slip. Free-standing film so drawn were found to be more stable in hylam slab than in the glass slab. The film thickness was roughly estimated from the interference pattern of the laser beam and was about 100 μm. The Raman spectra were recorded using the SPEX Ramalog 1403 Double monochromator.

2.3.2 TEMPERATURE CONTROL AND MONITORING DEVICES.

2.3.2.1 High temperature cell for Raman studies of bulk samples.

In order to record the Raman spectra in bulk samples of 5O.5 and 5O.6, a small glass cell was fabricated where the temperature could be easily monitored and varied while recording the Raman spectra. As shown in the Figure. 2.4a, the cell may be divided into two portions: an inner chamber and an outer chamber. The lower part of the inner chamber was compact (solid glass) on which a groove of 2 cm depth and 1mm diameter was made to place the encapsulated sample for spectral study. The upper part of the inner chamber is hollow in order to place the temperature sensor close to the sample. Heating element is compactly wound around the inner chamber uniformly on both sides of the sample groove (leaving enough space for laser radiation to excite the sample) which gives a symmetric thermal distribution around the sample. The outer hollow chamber is especially designed for creating a vacuum around the inner chamber for maintaining temperature stability. An outlet has been provided on one side of the outer chamber for vacuum purposes with a lid protection. Two in-built metallic leads and outlets are also made on the outer chamber for heating elements. A temperature controller (Century Model no. CT-806) was used to monitor and control the temperature by keeping its sensor in

close contact with the sample. Before using the cell, the heat chamber is subjected to several stages of calibration using encapsulated samples of organic compounds of known melting points in different temperature ranges. The apparent and the actual melting point of these samples were measured and plotted graphically which is shown in the Figure. 2.4b. From this figure, it is observed that the temperature gradient increases with increase in melting point of the samples. The linearity of the curve shows that this gradient is uniform. Moreover, the fluctuations in the measured temperatures were well within the experimental error of ±0.2 °C. The actual transition temperatures were extrapolated from the graph and the sample was kept at a particular temperature for at least 45 minutes before recording the spectra. The temperature rise of the sample due to laser heating was minimized by employing low laser power.

2.3.2.2. High temperature cell for Raman studies in thin films.

In order to record the Raman spectra of the samples in homeotropically aligned freestanding thin films a heating cell was fabricated. As shown in Figure. 2.5, the cell is fabricated on a base of aluminum of dimensions 62 x 28 x 6 mm. Grooves were cut at both the ends of this base for placing two heating coils which could heat the base uniformly from both sides. At the geometrical center of the plate a cylindrical hole of 6 mm diameter was drilled through which laser radiation could enter. On the upper surface of the plate, in the region around this hole a square of size 22 mm and depth 2 mm was cut. In this square one could place sheets of ITO coated glass or Hylam, with conical holes of 1 mm diameter at their center on which the films of a liquid crystal could be drawn with the help of a glass spreader. A small

hole at the side of the base was drilled through which a temperature sensor could be inserted to continuously monitor the temperature during the course of the experiment. The whole assembly was placed in a cell of Hylam to achieve good thermal stability. Temperature of this cell could be varied from room temperature to around 200 °C with an accuracy of ±0.3 °C. The temperature was monitored by a Micron Model-MPT-02 digital temperature controller.

2.3.2.3. Low temperature cell for Raman studies of bulk samples.

Low temperature studies on the samples were conducted using an Air Products' helium Cryocooler (Model Displex CSA 202E). This unit is capable of cooling the sample up to 10 K. Temperature control was attained by using a controller Model APD-E with a precision of ±0.5 K. Temperature measurement was done with the help of a pre-calibrated Gold-Chromel thermocouple.

The closed cycle helium cryocooler consists mainly of a compressor unit module 202 and the expander module DE202. This has an air cooled compressor unit which supplies helium gas at a pressure of 260 Psi to the expander module. The compressed gas at high pressure is then allowed to expand in the expander assembly (Figure. 2.6). In the process of expansion, the heat station temperature decreases because of Joule- Thomson effect, and the helium gas at 110 Psi pressure returns to the compressor unit. Through the repetition of this cycle, cryogenic temperature upto 10 K can be achieved at the heat station, with refrigeration capacity of 1.8 watts at 20 K. The temperature at any other intermediate value between 20 K and the room temperature was obtained by using the temperature controller.

The liquid crystal under investigation was sealed in a quartz capillary tube and mounted with the help of a conducting glue on to the sample holder made up of copper which is mechanically mounted to the second stage heat station. Vacuum shroud Model DMX 1E is connected at the vacuum shroud mount and the system is thoroughly evacuated (10^{-5} torr) by a Hind HiVac Model VS114D pumping system. In addition, to obtain good thermal stability "radiation shield" is connected to the final stage heat station. DMX-1X interface extension is used to obtain Raman spectra. An indigenously made stand along with necessary arrangements for adjustment along three dimensions was used to support the expander module.

2.3.2.4. High temperature cell for studies of liquid crystalline samples. (Mettler Toledo FP900 Thermo-system)

The Mettler-Toledo FP900 thermosystem comprises of the FP90 central processor and the FP82 hot stage for the determination of a wide range of thermal data.

The FP90 central processor is a control and evaluation unit in which the FP82 hot stage can be attached without the need for temperature re-calibration. The measurement parameters are entered in a dialog box with a 6-line liquid crystal display on the keypad of the FP90 control unit. The system provides for the programming and storing of the different heating/cooling cycles with very precise rates of variation of temperature. After measurement, the analyses of results appear on the alphanumeric display and can be documented using an optional dot matrix printer. It is also possible to display, store and program data into a computer by using special interfaces provided with the system.

The FP82 hot stage is used to observe the thermal behaviour of a sample under a microscope, under laser radiation and also during Raman and FTIR spectroscopy. Using cross polarizers, it can be effectively used in experiments involving polarizing microscopy and other kinds of spectroscopies for studying the intensity pattern during the phase transitions of the liquid crystals. This device uses a flat electrical furnace with a Pt100 sensor and its essential features are shown in the Figure. 2.7. It has a temperature range of –60 °C to 375 °C under external cooling whereas the temperature range without external cooling ranges from the room temperature to 375 °C. The accuracy of this instrument varies from ±0.4 to ±0.6 °C depending on the range of temperature in which the experiment is being carried out. The heating or cooling rate of this instrument can be adjusted between ±0.0 (isothermal condition) to ±20 °C/min. With the remote handset provided with the FP82 hot stage, the heating or cooling rate of the system can be easily varied and also isothermal settings can be achieved during the course of an ongoing experiment. A photomonitor can also be connected to the system to perform thermo-optical analysis of the liquid crystal samples.

2.3.3. Measurement of Raman Spectra

Raman spectra of the compounds 5O.5 and 5O.6 were recorded in 90° scattering geometry in the bulk samples and in the solutions whereas, in thin films the back scattering geometry at 180° was used. A SPEX Ramalog 1403 double monochromator equipped with an RCA 31034 photo-multiplier tube (with photon counting arrangement) and also a charge-coupled detector (CCD) was used to record the Raman spectra. The spectrometer control and data processing were accomplished

with the help of a microprocessor based DM3000R series computer with the SPEX DM3000 software package. Excitation lines were obtained from a Spectra-Physics Model 165-09 Argon ion laser. High temperature studies of the liquid crystals were done using an indigenous high temperature glass cell whereas low temperature studies were undertaken with a close-cycle Helium cryocooler (Displex Model CSA 202E). High temperature studies in homeotropically aligned free standing thin films were carried out using an indigenously fabricated heating cell as well as Mettler hot stage. Details of the Argon Ion laser and spectrometer are given in the later sections of this chapter.

2.3.3.1. Spectra-Physics Model 165-09 Argon Ion Laser

This model consists of the laser head with a CW output and Model 265 exciter. The laser head consists of a rugged beryllium oxide (BeO) plasma tube closed at both ends by fused silica Brewster windows, a solenoid for providing necessary magnetic field and an optical resonator. The plasma tube is mounted in an optical cavity resonator formed by a spherical reflector at the output and a prism assisted by a flat mirror (to select the wavelength) at the high reflector end. The whole assembly of the resonator is held firmly against the quartz rods with springs to minimize microphonic frequency shifts. The plasma tube is supported on a kinematically adjustable mount and is adjusted in such a way that the plasma tube is exactly centered. An external thumb wheel is provided for wavelength selection and for changing the intra-cavity aperture. The plane of polarization of the output beam can be changed to the desired plane by using the polarizer for recording the polarized Raman spectra.

The Spectra-Physics Model 265 exciter is fully equipped with the necessary electronic circuits to create, sustain and regulate the ion discharge in the plasma tube and to control the output power from the laser by simultaneously regulating the solenoid current. An arrangement is provided for a desired constant output optical power when operated in the "light control" mode. The 265 Exciter is fed with a stabilized three-phase 380V (phase to phase) power supply. This unit requires cooling of the transistor pass bank in the exciter, the solenoid and the BeO plasma tube which is achieved by circulating distilled, deionized water at 15 °C at 40 PSI from a closed cycle water chiller plant from Neslab, Model HX-500.

2.3.3.2 Spex model Ramalog 1403 double monochromator.

Raman spectra of the samples were measured with the help of the Spex model Ramalog 1403 double monochromator equipped with a RCA 31034 photo-multiplier tube and CCD. Figure. 2.8a schematically illustrates the essential parts of the instrument. The Spex 1403 double monochromator is a f/7.8 instrument with a spectral coverage from 11000 to 31000cm^{-1} with an accuracy of ±1 cm^{-1} in the 10000 cm^{-1} range. The spectral repeatability of ±0.2 cm^{-1} and a resolution of 0.15 cm^{-1} at 5791 Å (Hg line FWHM) can be achieved by this instrument. The holographic type instrument used in the instrument has 1800 grooves/mm blazed 5000Å. The gratings are mounted on a modified Czerny-Turner mount (Figure. 2.8b) using the fundamental grating equation:

$$d(\sin\alpha + \sin\beta) = n\lambda \qquad (2.37)$$

where n in the spectral order, λ the wavelength, d the grating spacing, and α and β, the angle of incidence and diffraction respectively. If $\alpha = \theta + \phi$ and $\beta = \theta - \phi$, where θ is the angle of rotation of the grating measured from zero as shown in the Figure. 2.8b and is a constant depending on the design of the instrument, then equation (2.37) can be recast as

$$2d \sin\theta \cos\phi = n\lambda \qquad (2.38)$$

The Raman peaks are measured in terms of the frequency shifts in cm^{-1} on a linear x-axis by utilizing a cosecant drive for grating rotation with $\phi = 10^{\circ}$ and thus $\text{cosec}\phi = 0.984$ (values supplied by manufacturer). To record the Raman spectra, the laser beam is passed through the Spex Model 1459 UVISIR illuminator after being diffracted from the Spex Model 1460 "Lasermate," which is a small unit consisting of a grating with 1200lines/mm blazed at 5000 Å and a mirror assembly to isolate and filter the spurious plasma lines. The beam is then focussed on to the sample, after deflection (through 90°) by a mirror to a spot of diameter 10μm by a fused silica condensing lens. Scattered radiation from the sample is then passed through the polarization analyzer (optional) which works on the principle of birefringence and total reflection or of dichroism. The polarization state of the observed Raman bands can be obtained by using this analyzer. The scattered radiation is then collected by an elliptical mirror (f/1.4) and focussed on to the entrance slit (S_3) of the spectrometer after reflection from the mirror (M_7) and passing through the polarization scrambler (Figure. 2.8a). The polarization scrambler converts the plane polarized scattered radiation to a randomly polarized radiation before it reaches the spectrometer and thus cancels any variation in spectrometer response that result

from polarization dependent efficiencies. The polychromatic scattered radiation that is focussed on to the entrance slit gets dispersed by the 1800 lines/mm holographic gratings (G_2 and G_3). Finally, a nearly monochromatic light signal of a particular frequency selected by spectrometer control reaches the exit slit (S_7) or to the mirror (S_8) of the double monochromator. From here the beam can be either focussed on to a photomultiplier tube or a charge-coupled detector or, optionally to a third monochromator.

2.3.3.3 Spectrometer control and data processing.

The spectrometer control (frequency scanning) and data processing were accomplished using a DM-3000R series computer employing the DM3000 software package for Raman Spectroscopy. The DM3000 series of spectroscopy computers are based on an integrated comprehensive approach for controlling the spectroscopy setup and managing the obtained data with its unique combination of software and hardware. This software enables the user to manipulate the spectral data by allowing operations like background subtraction, addition, division, integration, differentiation, and frequency and intensity range expansion/reduction etc. The exceptional menu driven software package includes features that completely automate the data acquisition process. The DM3000 computers have up to 24 digital inputs /outputs to control any of the monochromator drives such as grating turrets, swing-away mirrors and other similar devices which provide a lot of flexibility and versatility to these systems. With DM3000 it is possible to acquire radiometrically corrected data in a wide variety of spectrometric units. For incremental scanning, the DM3000 allows to specify integration intervals as fast as 1 millisecond or as slow as

100 second per data point, and up to 4000 data points can be recorded in a single scan. The DM3000 has a dot-matrix graphic printer that can reproduce all the displays with comprehensive file identification.

The raw data is obtained from the output of the preamplifier. The anode of the photomultiplier tube is the input of the preamplifier, which has a gain of 400. The high voltage (1750 volts) required for operating the photomultiplier tube is also provided by the DM3000 with a stability of 0.002 % after an hour's warm up.

The photomultiplier tube Model RCA 31034 used with the experimental setup is a 2" diameter, head-on, 11-stage QUANTACON photomultiplier having a Gallium-Arsenide chip as its photocathode, an ultraviolet transmitting glass window and an in-line Copper-Beryllium dyanode structure. This tube is cooled to –30 °C by a thermoelectric cooling device and has almost absolute linear absolute response in the 3000 Å to 8500 Å wavelength range. It operates with a current gain of 10^6 with a maximum dark pulse simulation of 12CPS (counts per second).

2.4 TIME-RESOLVED FTIR STUDIES

2.4.1 Antiferroelectric liquid crystal Chisso 2061.

Chiral antiferroelectric liquid crystal, 4-(1-methylheptyloxy carbonyl) phenyl 4-(4'-octyloxy benzoylxy) benzoate, named as Chisso 2061, was obtained from the Chisso Petrochemical Corporation, Tokyo. The standard procedure for the synthesis of this compound is reported in literature [17]. This was a highly purified sample and therefore, it was used as such in our experiments without any further purification. As an extra precaution, a small portion of the sample was observed

under a polarizing microscope, both while heating and cooling to verify the consistency of the various phase transition temperatures with the reported values. The molecular structure and the sequence of phase transitions of 4-(1-methylheptyloxy carbonyl) phenyl 4-(4'-octyloxy benzoylxy) benzoate, (Chisso 2061), is shown below.

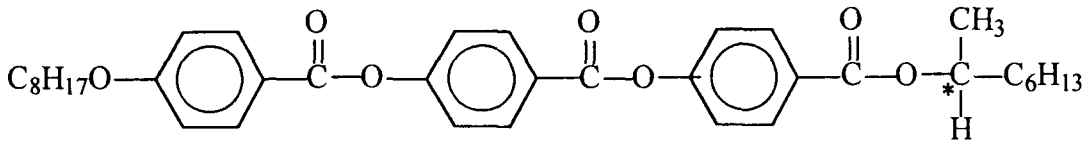

$$Cr \underset{}{\overset{52.0}{\rightleftharpoons}} S^{*}_{IA} \underset{}{\overset{68.4}{\rightleftharpoons}} S^{*}_{CA} \underset{}{\overset{88.2}{\rightleftharpoons}} S_{A} \underset{}{\overset{142.3\ ^{0}C}{\rightleftharpoons}} I$$

As can be seen, the $S_{CA}*$ phase has a wide range of temperature (≈20 °C) which enabled us to concentrate on the study of dynamical switching and segmental mobility in this phase.

2.4.2. Sample preparation for the time-resolved FTIR study Chisso 2061.

The FTIR spectra of Chisso 2061 was recorded in surface stabilized ferroelectric liquid crystal (SSFLC) cells. These commercially obtained SSFLC cells consists of two BaF_2 plates with conducting layers of indium-tin oxide. The plates were rubbed with polyvinyl alcohol in one direction so that uniform microscopic grooves were formed. The thickness between the two plates, as determined from the interference fringe pattern, was adjusted to about 3-4 μm using a polyethylene spacer. The cell was filled with sample by capillary action by heating the sample to the isotropic phase and then slowly cooling it down to a temperature in the $S_{C}*$

phase. Monodomains of the sample inside the cell were obtained by employing cyclic and slow temperature treatment under an electric field of ±15 V.

2.4.3 FTIR Spectrometer and Time-Resolved studies.

Fourier transform infrared spectroscopy of the sample was performed using a JOEL JIR-6500 Fourier transform infrared spectrometer equipped with a micro-attachment (JEOL IR-MAU 110) and a mercury-cadmium-telluride (MCT) detector was used for obtaining the data. A wire grid polarizer was provided with the system that could be rotated about the direction of the IR radiation. The polarization direction was fixed at 45° to the rubbing direction of the ITO plated windows of the SSFLC cells. The theoretical details regarding the principle of FTIR spectroscopy has been explained in a previous section of this chapter. In order to make time-resolved measurements the same instrument equipped with a boxcar integrator (SRS Model-250) was used. Rectangular wave electric field of ±15 V at 5 kHz repetition rate was applied between the electrodes of the cell from a function generator (Kenwood FG-273).

A noble multi-channel asynchronous time-resolving system with 16 time-resolving channels developed by Ozaki et al [18] was used for making time-resolved FTIR measurements improving on previous methods [19,20]. To understand the system we refer to the Figure. 2.9. The time-resolving module, shown in the bottom of Figure. 2.9, has 16 time-resolving units, each of which consists of a gate circuit, a low pass filter, and an A/D converter. Time-resolving is carried out by setting each gate at a different time delay. The purpose of the low pass filters, placed between each gate circuit and its A/D converter, is to eliminate

high-frequency components from the discrete time-resolved signals created by the gate circuit and to convert them to analog signals. The analog signals are then processed by the A/D converter at the sampling rate of the FTIR spectrophotometer itself, as shown by the trigger signal for sampling in figure, which has no relation to the gate timing for time-resolution.

The sample is excited by repetitive stimuli at constant intervals, which do not depend upon the sampling timing of the FTIR spectrophotometer and yet are restricted on the basis of the sampling theorem; that is, the repeat rate of the sample excitation must be no less than twice the highest frequency in the spectral range [14]. The sample excitations result in transient transmission differences, so that the analog interferogram is modulated at a very high frequency due to the repetitive excitation of the sample. However, if we could observe the sample only at the timing of a constant time after each excitation, it would appear that the sample is held static at one point in the decay of its transition state. The gate circuit effectively carries out this stroboscopic process with the help of the delay circuit. Consequently, the gated discrete interferogram becomes a time-resolved spectra of the sample at a constant point in its dynamic transient decay itself in the frequency domain. The A/D converter samples the analog time-resolved interferogram after the higher harmonics have been eliminated by the low pass filter to convert the discrete interferogram to the analog one. This present system has a time-resolution of 50 ns. It depends only on the specification of the delay circuit. While, in principle, there is no shortest limit in time-resolution, the system is limited by the rise time of the detector used [14].

REFERENCES

1. Szymanski, H, A, (ed.), "*Raman Spectroscopy*", Vol 1 (1967) and Vol 2 (1970), Plenum Press, New York.

2. Tobin, M. C., "*Laser Raman Spectroscopy*", Wiley-Inter-Science, New York, 1971.

3. Long, D. A., *Raman Spectroscopy,* McGraw Hill International Book Company, New York, 1977.

4. Kramers, M. A., and Heisenberg, W. *Z., Physik*, **31**, 681, 1925.

5. Dirac, P. A. M., *Proc. Roy. Soc (London).*, **114**, 710, 1927.

6. Placzek, G., in *Handbuch der Radiologie*, **Vol-6,** Part-2, pp-209, 1934.

7. Schrotter, H. W., and Klockner, H. W., "*Raman Spectroscopy of Glasses and Liquids;* Topics in Current Physics", (ed., Waber, A.) Springer Verlag, **Ch.4**, 1979.

8. Nester, R. J., and Lippon Coutt, E. R., *J. Raman Spectroscopy,* **1**, 309, 1973.

9. Jones, K. E., and Zewail, A. H., in *Advances in Laser Chemistry*, Ed., A.H. Zewail, Vol. 3, Springer, 1978.

10. Harris, C. B., Shelby, R. M. and Cornelius, *Phys. Rev. Lett.*, **38**, 1415, 1977.

11. Bell, R. J., "*Introductory Fourier Transform Spectroscopy*", Wiley, New York, 1972.

12. Alpert, N. L., Keiser, W. E., and Szymanski, H. A., *"IR - Theory and Practice of Infrared Spectroscopy"*, Plenum, New York, 1970.

13. Sathyanarayana, D. N., "*Vibrational Spectroscopy- Theory and Applications*", New Age, New Delhi, 1996.

14. Griffiths, P. R., de Haseth, J. A., " *Fourier Transform Infrared Spectroscopy*", Wiley Interscience, New York, 1986.

15. Alapati, P. R., Potukuchi, D. M., Rao, N. V. S., Pisipati, V.G. K. M., Paranjpe A.S., and Rao, U. R. K., *Liq. Cryst.*, **3**, 1461, 1988 and references therein.

16. Alapati, P. R., Potukuchi, D. M., Rao, P. B., Rao, N. V. S., Pisipati, V.G. K. M., and Paranjpe, A.S., *Liq. Cryst.*, **5**, 545, 1989.

17. Inukai, T., Furukawa. K., Terashima, M., Saito, S., Isogai, M., Kitamura, T., Mukoh, A., *Proc. 12th Jpn. Liq. Cryst. Conf.*, 112, 1986.

18. Masutani, K., Numahata, K., Nishimura, K., Ochiai, S., Nagasaki, Y., Katayama, N., Ozaki, Y., *Appl. Spectrocs.*, **53**, 588, 1999.

19. Masutani, K., Yokota, A., Furukawa, Y., Tasumi, M., *Proc. 5th Int. Conf. On Time-Resolved Vibrational Spectroscopy*, P32, Wasedaukin, 1991.

20. Masutani, K.,Sugisawa, H., Yokota, A., Furukawa, Y., Tasumi, M., *Appl. Spectrosc.*, **46**, 560, 1992.

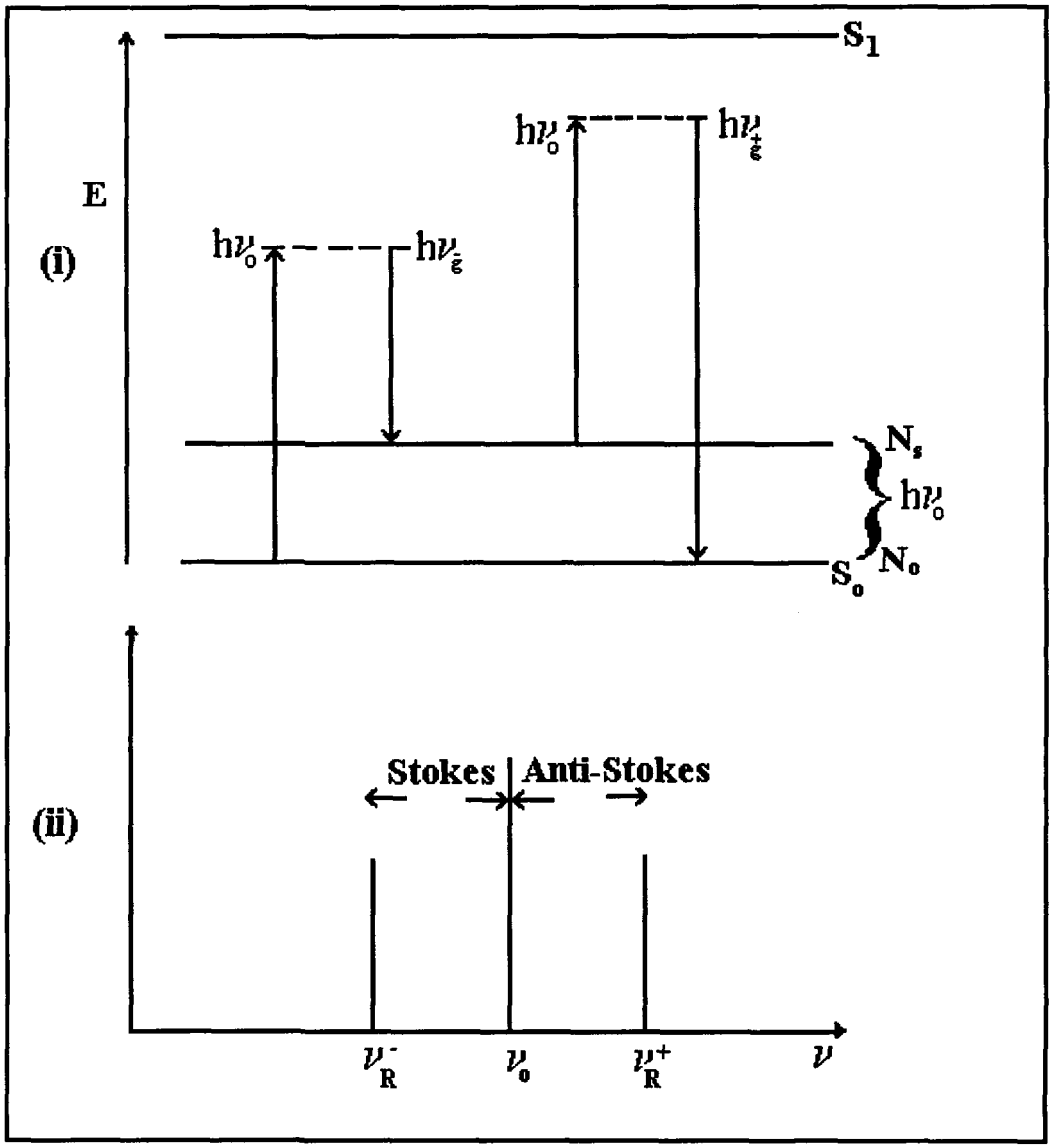

Fig 2.1. Diagrammatic representation of (i) Raman scattering process and (ii) Stokes and Anti-Stokes lines.

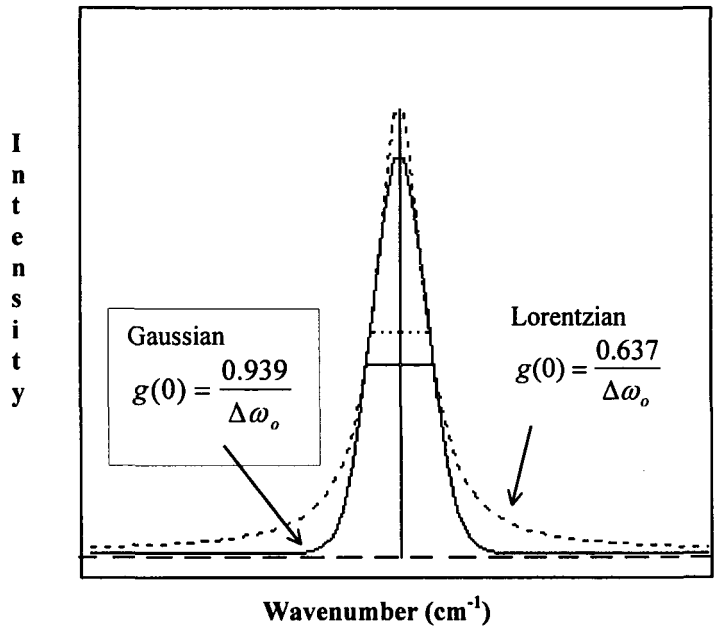

Fig 2.2. A comparison of the lineshapes, _____ Gaussian and _ _ _ _ _ _ Lorentzian.

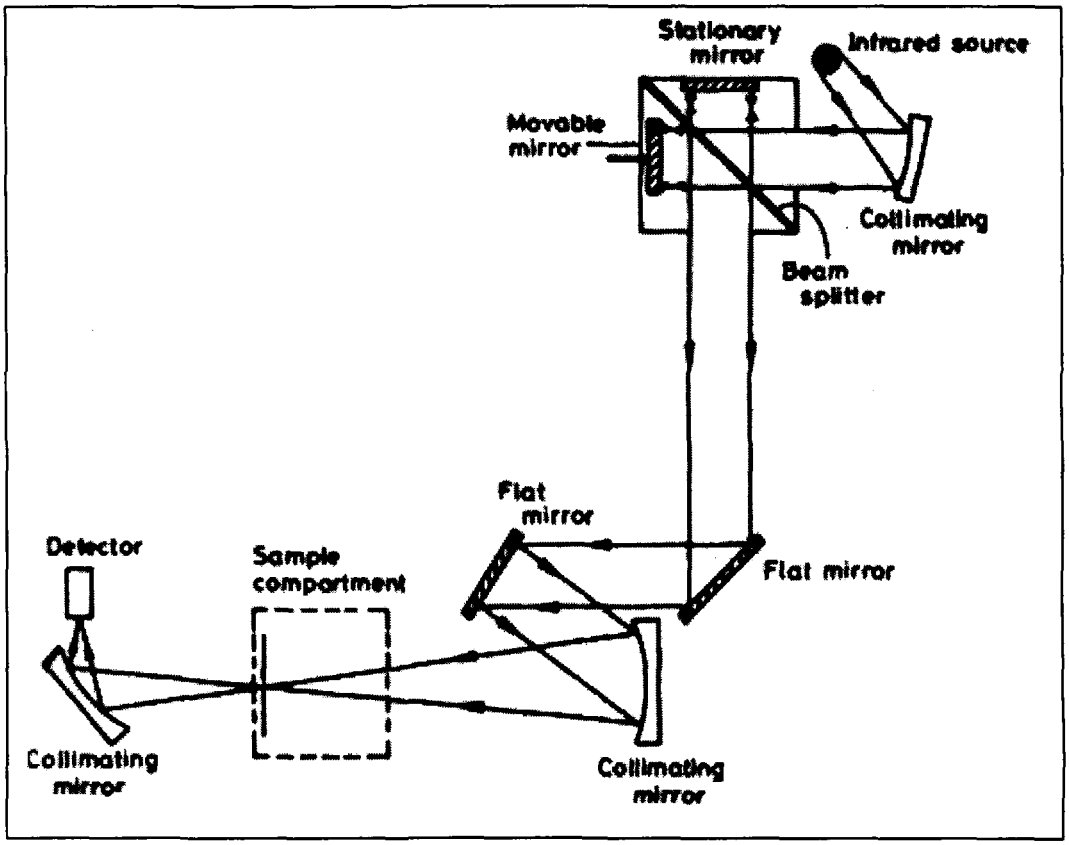

Fig. 2.3a. Simplified diagram of a Fourier transform infrared spectrophotometer.

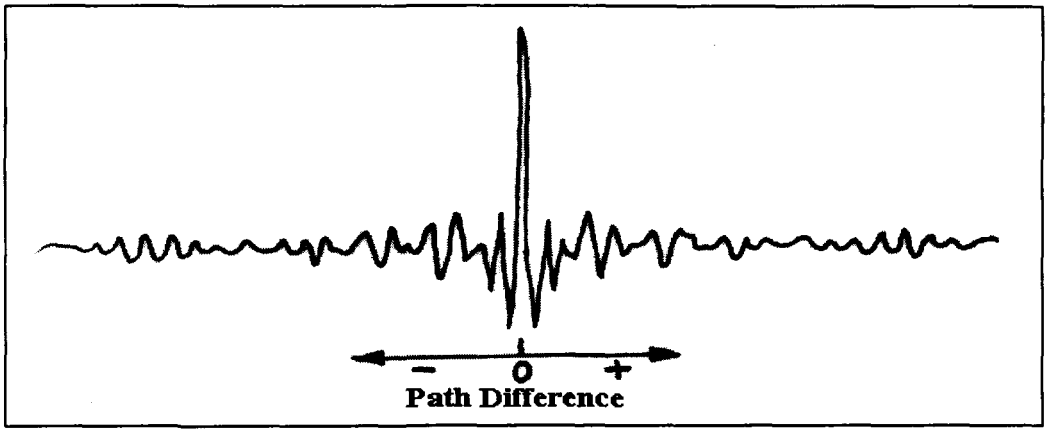

Fig. 2.3b. Interferogram from a Michelsons interferometer.

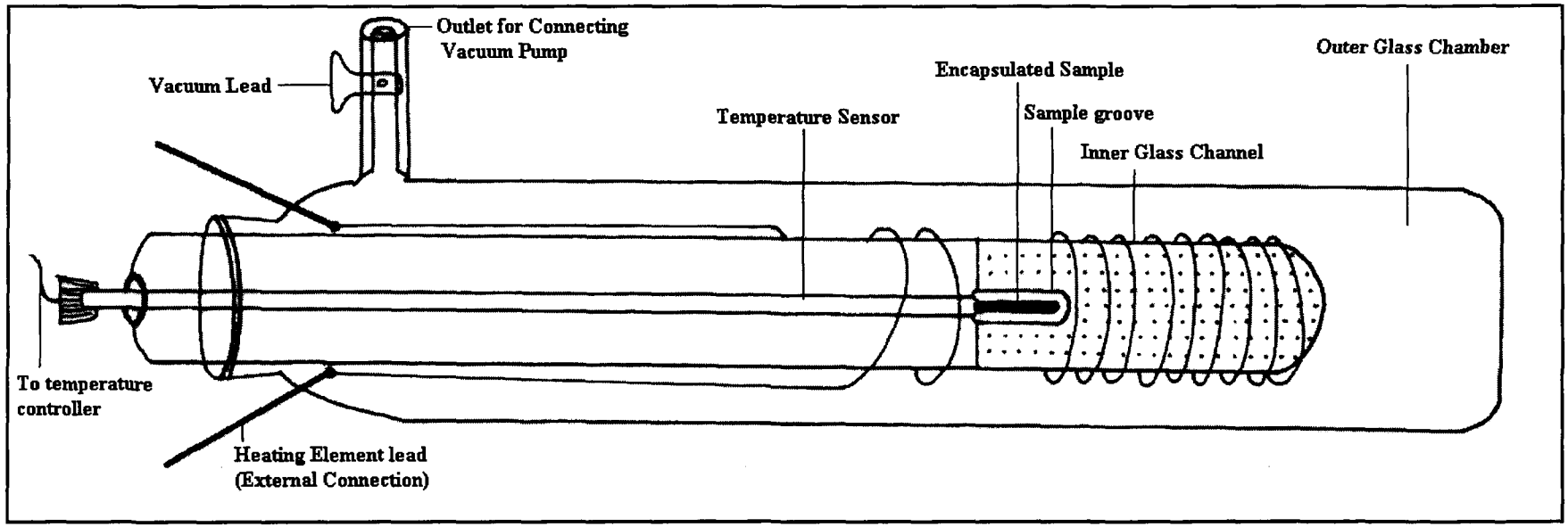

Fig 2.4a. High temperature cell for Raman studies in bulk form.

M.P. Temp. VS Observed Temp.

Calibration of the High Temperature Cell

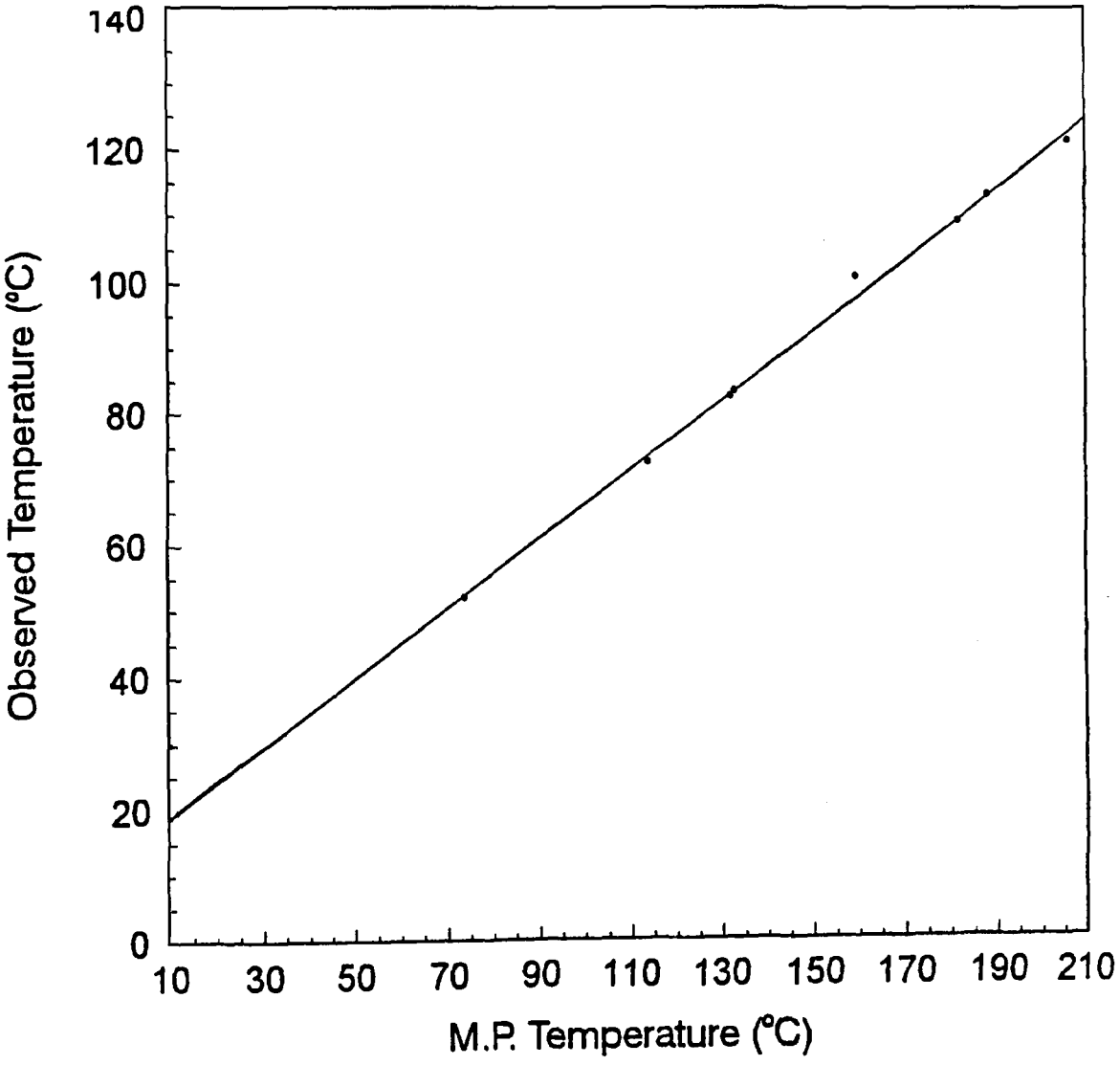

Fig 2.4b Calibration curve for the high temperature cell.

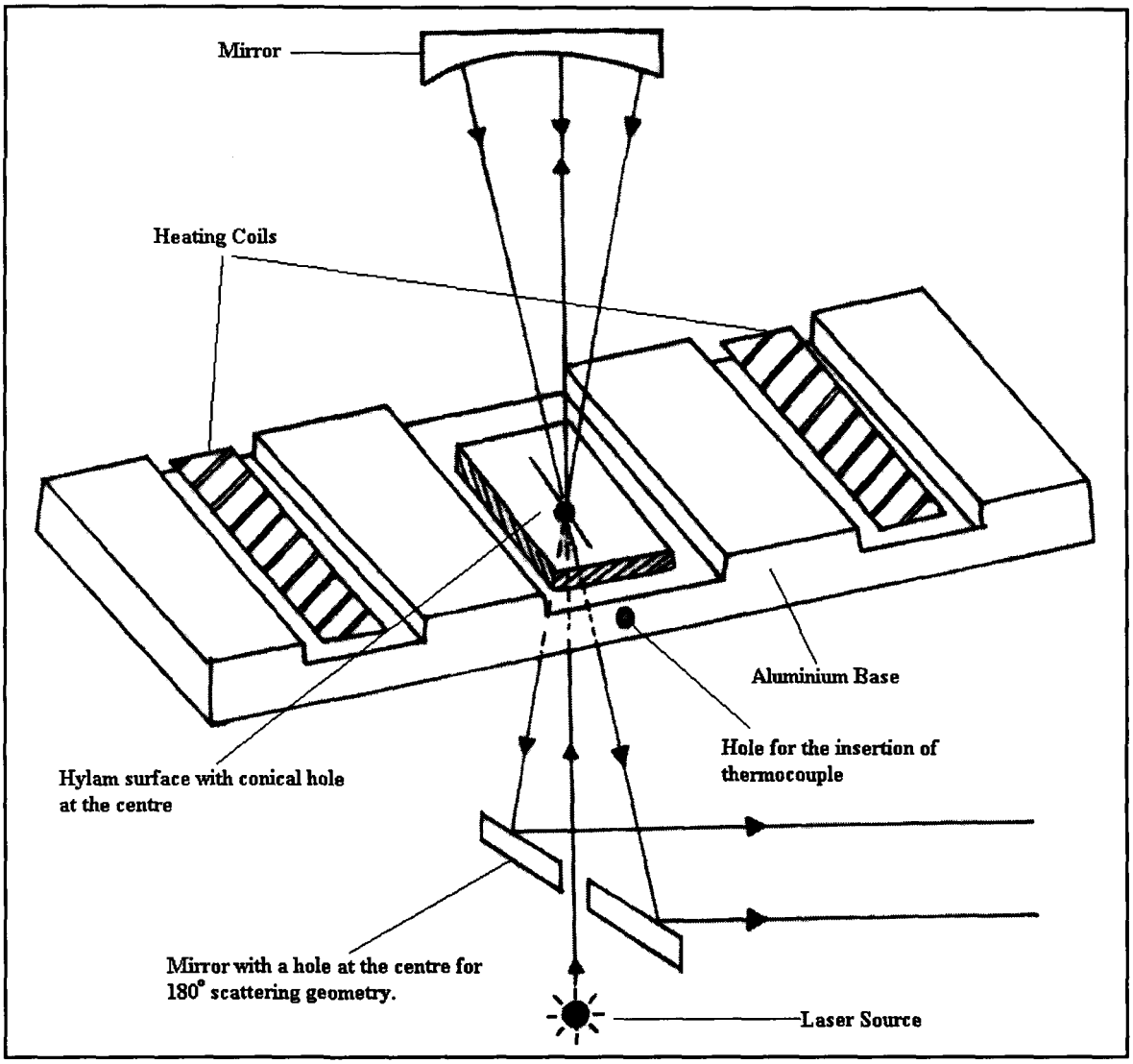

Fig. 2.5. High temperature cell for Raman studies in free-standing thin films.

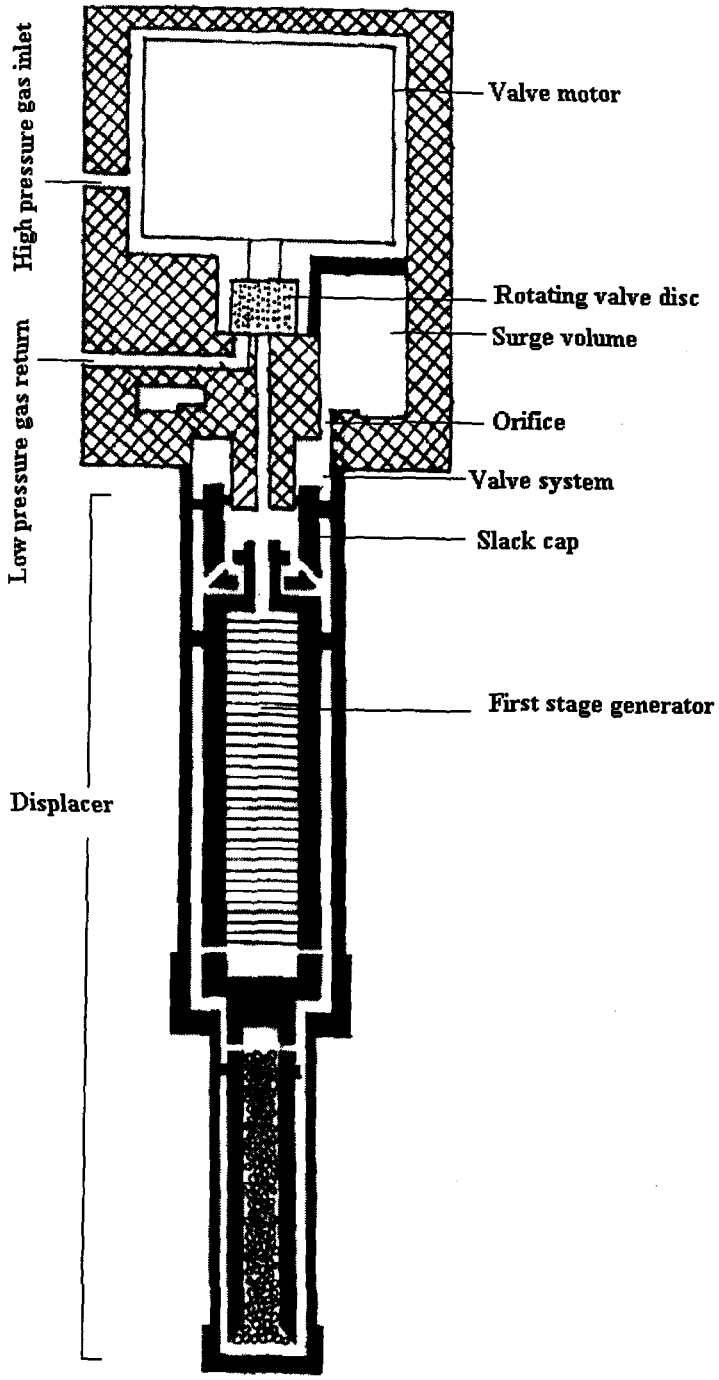

Fig 2.6. Section diagram of the expander module DE202 of the helium cryo-cooler Model Displex CSA 202E

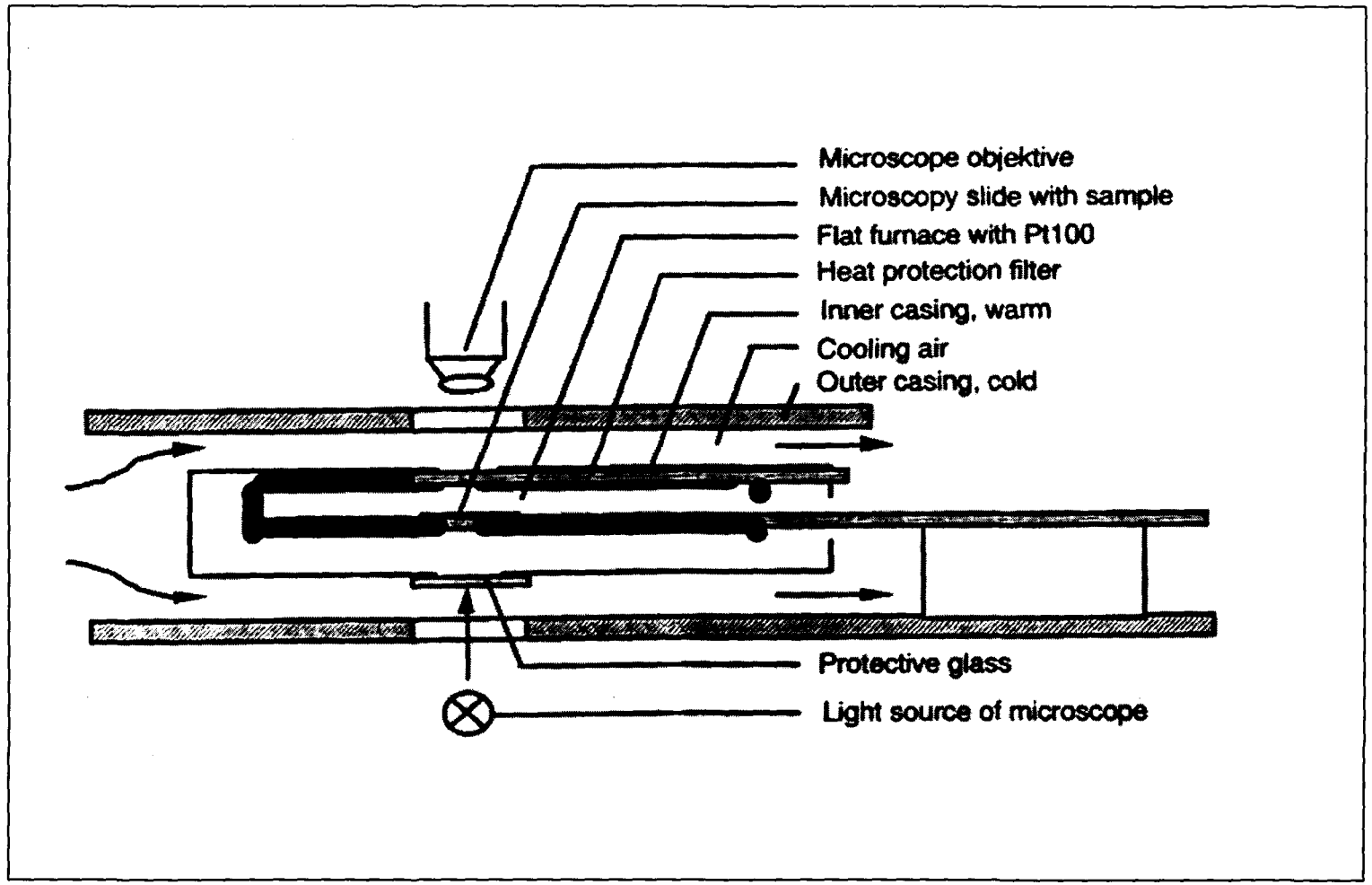

Fig 2.7 Mettler Toledo High temperature hot stage.

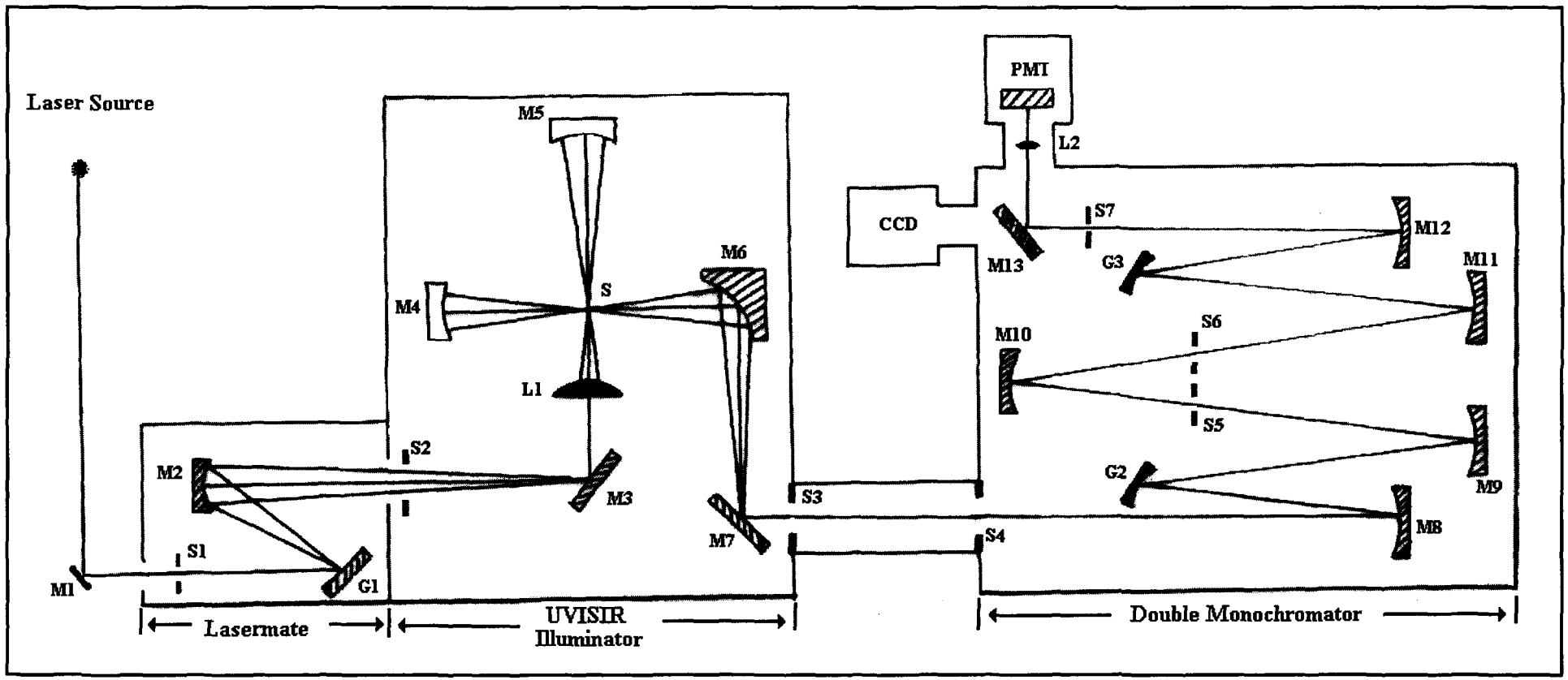

Fig. 2.8a. Optical diagram of a Spex Ramalog 1403 Spectrophotometer including the Lasermate and UVISIR illuminator. M1, M3, M7 and M13 are plane mirrors; M2, M4, M5 and M8-M12 are concave mirrors; M6 is an elliptical mirror; S1to S7 are slits; L1 is a fused silica condenser lens and L2 is a field lens; S is the sample: G1 to G3 are gratings, PMT is the photomutiplier tube and CCD is the charge couple detector.

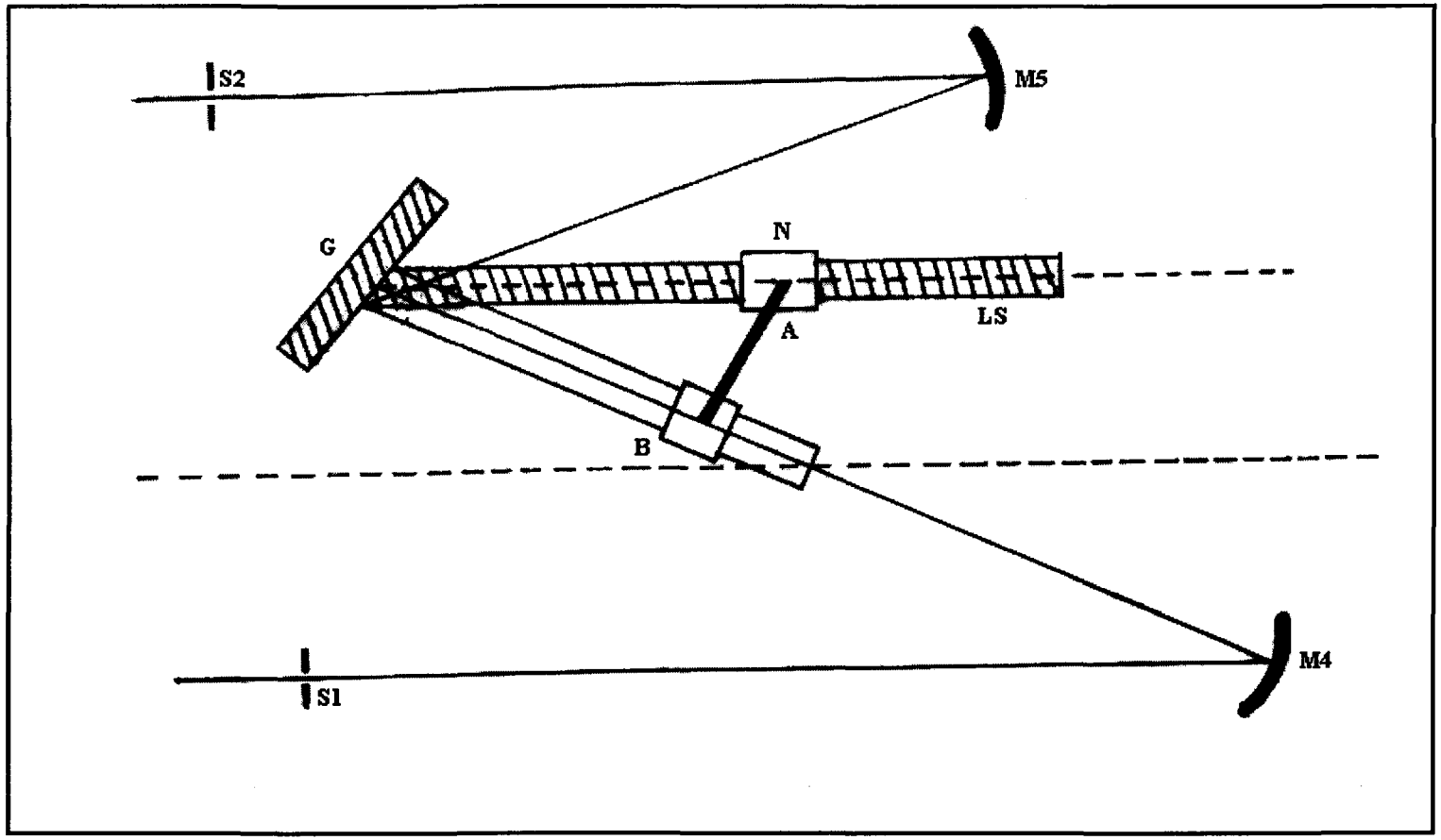

Fig. 2.8b. Mechanical cosecant drive mechanism for the Czerny-Turner mount of gratings for the SPEX Ramalog 1403 double monochromator. S1, S2 are slits, M4and M5 are mirrors, G is the grating, N is a nut, LS is the Leadscrew, B is the slide and A is the arm. The input nut N moves along leadscrew Ls while the slide B moves along a bar at right angles to the grating G. the grating rotates as the arm A moves along the bar.

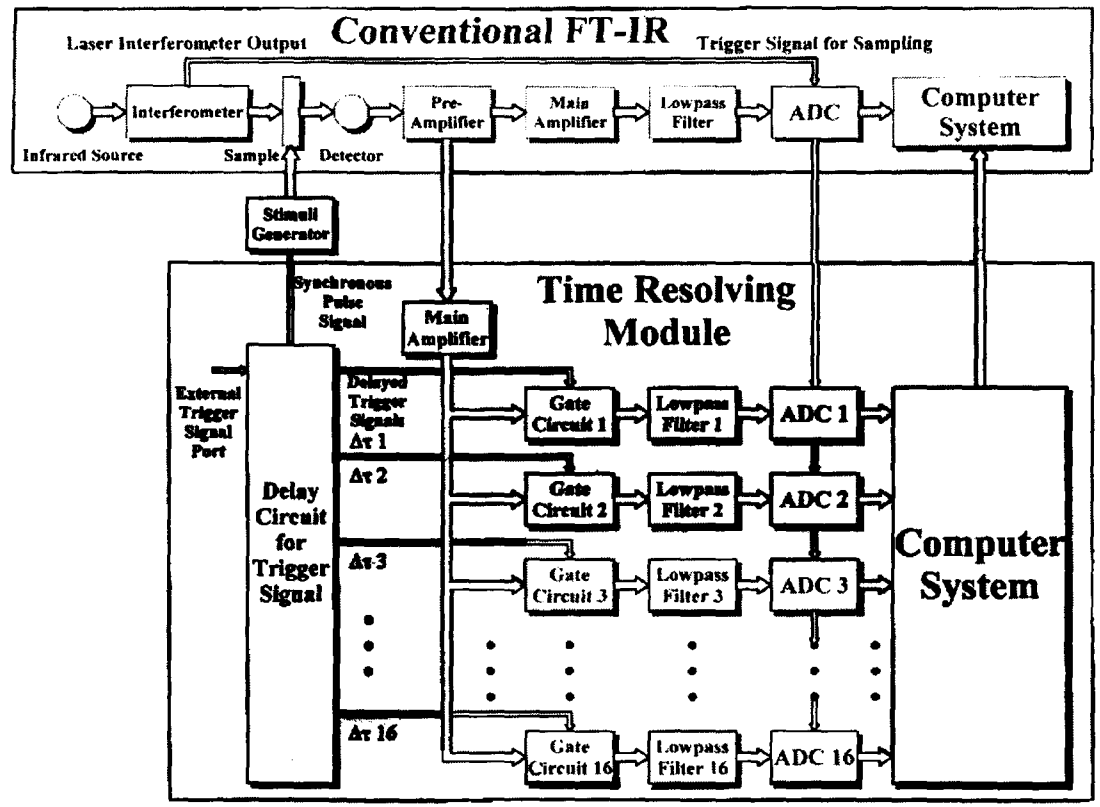

Fig 2.9 The time resolved arrangement using a conventional FTIR spectrometer.

Chapter 3

DYNAMICS OF PHASE TRANSITION IN A LIQUID CRYSTALLINE COMPOUND 5O.5 PROBED LASER RAMAN SPECTROSCOPY

Raman spectra of the schiff base liquid crystalline compound N-(4-n-Pentyloxybenzylidene)-4'-n-pentylaniline, (5O.5) has been recorded as a function of temperature from 22 to 80 °C in the 1140-1220 cm^{-1} and 1550-1640 cm^{-1} regions for studies reported in this chapter. From careful deconvolution of the spectral features using Lorentzian profiles, precise values of peak positions, integrated intensities and linewidths of some selected Raman bands were obtained. The variation of the Raman spectral parameters with temperature have been discussed in terms of changes in the molecular alignment and its effect on intra /inter-molecular interactions at the Crystal-*G*, *G*-S_F, S_F-S_C and S_A-N phase transitions. From a detailed analysis it is inferred that the increased orientational/vibrational freedom of the alkyl chains as well as the delocalization of the electron clouds are responsible for the spectral anomalies at the K-G transition. Loss of positional ordering and twist around the -ϕ-N= bond takes place at the S_F-S_C transition. In the S_A -N transition we have observed some evidence for the formation of cybotactic clusters.

3.1. INTRODUCTION.

Vibrational spectroscopy has been a subject of great interest for both experimental and theoretical research for a long time. Especially, in recent years, Raman spectroscopy has emerged as a very powerful tool in the investigation of vibrational dynamics of liquid crystalline compounds. The importance of this technique is further realized in view of the fact that the phase transitions in liquid crystals are reflected as variation in measurable parameters of certain Raman bands associated with vibrational modes of the system. The analysis of linewidths and peak positions yield information about the structure and dynamics of the system undergoing phase transitions. Integrated intensity, on the other hand, provides crucial information about the fluctuation of some physical quantities undergoing changes during phase transition. Extensive studies on the dynamics of phase transitions of liquid crystals using Raman spectroscopic technique have been reported in the past [1-14]. Most of these studies have focussed attention on analyzing either the region involving the lattice modes (50 – 200cm^{-1}) [1-6] or the 200—900 cm^{-1} region which consists of the conformationally sensitive alkyl chain modes [7-9]. The lattice mode region is found to show some abrupt changes in intensity of certain modes with change in temperature which have been associated with the changes in the intermolecular interactions as well as positional ordering. Intensity changes in the alkyl chain mode region are ascribed to the fact that at higher temperatures the increased lateral gap between the different molecular layers facilitates orientational and translational motions of the long alkyl tail along with their molecular axis. However, it is necessary to monitor the behaviour of the Raman

bands associated with the core and alkyl chain parts separately as a function of temperature to understand the role of these units on the dynamics of phase changes.

In this chapter we have carried out extensive studies of the liquid crystalline compound 5O.5 using Laser Raman spectroscopy. We have investigated the behaviour of the various core-related bands as a function of temperature in different phases. The results obtained provide evidence for the existence of a lateral dipole moment at the core. We have also observed evidence of the transition between well defined three-dimensional phases and also on the loss of positional ordering and twisting of the molecular segments about the -ϕ-N= bond.

3.2. Experimental Details.

The preparation of sample, its characterization [15-17] and sampling arrangement are the same as discussed in the previous chapter. The Raman spectra of the sample 5O.5 were recorded at various temperatures on a Spex Ramalog 1403 double monochromator, equipped with a RCA-31034 photomultiplier tube and a CCD detector, in the 1140-1220 cm^{-1} and 1550-1640 cm^{-1} regions. The spectra were recorded over a wide range of temperatures starting from 22 °C (crystalline phase) to 76 °C (isotropic liquid) at intervals of 0.3 °C near phase transitions and 2 °C elsewhere. The excitation source used was the 488.0 nm line from an Ar^+ laser. In order to avoid laser heating of the sample, very low laser power (20-30 mW) was employed. A scanning increment of 0.1 cm^{-1} with an integration time of 0.5 sec were found suitable to record the spectra with a reasonably good signal to noise ratio with the slit combination of 200-400-400-200 μm. Our data had a very high reproducibility with the uncertainty in the peak positions being within ± 0.20 cm^{-1}

while the band areas and linewidth (FWHM) being accurate within ± 2 %. Few spectra at low temperature (30K) were also recorded to ascertain the number and resolve the overlapping bands in broad spectral regions. As the spectral parameters, viz., peak position, linewidth and integrated intensity, were required to be precisely measured, the laser plasma lines were recorded at the same slit setting as used for recording Raman spectra to eliminate the slit width effect. The slit function, S=2.62 cm^{-1} was calculated as the full width at half maxima (FWHM) of the plasma line recorded at 1576.60 cm^{-1} from the Ar^+ laser. In an ideal case, the plasma line should be very close to the position of the Raman band of interest. To approach the bands under study as close as possible, two more plasma lines at 1138.85 cm^{-1} and 1172.50 cm^{-1} from the Ar^+ laser were recorded. The FWHM of these two lines were also found equal to 2.62 cm^{-1}. This value of the slit function was used in fitting the curves and determining their true linewidths. The spectral curve fitting, deconvolution and determination of the various spectral parameters were done using the GRAMS software.

3.3. Results and Discussion

3.3.1. Molecular Structure.

The structure and sequence of phase transitions in N-(4-n- Pentyloxy benzylidene)-4'-n-pentylaniline are shown in Figure. 3.1. The molecule is composed of two portions, the two benzene rings with the [—C(H)=N-] linkage forming the core; and the $C_5H_{11}O$ and C_5H_{11} alkyl chains forming the zigzag tails, which are attached to the two ends of the core. The Raman spectrum showed a

triplet in the 1160—1171 cm^{-1} region (Figure.3.2). Similarly, doublets were observed in the 1570—1575 cm^{-1} and the 1594—1598 cm^{-1} regions (Figure. 3.2). The figure clearly shows that the bands are overlapped, especially at the wings. In order to obtain precise data on the linewidth and peak position, it is desirable to deconvolute the bands. It has been achieved by fitting the spectral features in the 1140—1220 cm^{-1} and 1550—1640 cm^{-1} regions with Lorentzian profiles. Figure. 3.3 shows the deconvoluted spectra after separating and fitting the spectral features of the respective region using GRAMS software.

The observation of the triplets and doublets in the spectrum can be attributed to the presence of the oxygen atom adjacent to the core part of the molecule. A question is likely to arise here that whether the origin of the triplet and the doublets is due to the delocalization of the charges or due to the presence of different rotational isomers. The possibility of the occurrence of the rotational isomers can be eliminated because of two main reasons. The splittings in the triplet as well as the doublets became much clear in the Raman spectrum at low temperatures (≈30K). If rotational isomers were present we would have expected at least a reduction in the splitting, if not the complete replacement of the doublets by singlets. Another important evidence in support of the above assumption is that at low temperatures and also up to a temperature of 51 °C the band at 1167 cm^{-1} is found to be more intense than the band at 1162 cm^{-1} whereas at still higher temperatures the relative intensity of these bands exhibit a reverse trend. Such an effect would not be observed in the case of rotational isomers as the intensity of Raman bands is a function of population of the two forms. The band at 1171 cm^{-1} is assigned to the C-O stretching mode of the molecule. The bands observed at 1162 and 1167 cm^{-1} are

the in-plane C-H bending modes of the two aromatic rings. Similarly the bands at 1572, 1575, 1594 and 1598 cm^{-1} are due to the quadrant stretching modes of the aromatic rings [10-12,20]. The oxygen atom adjacent to one of the aromatic rings strongly affects the band positions. The electronegativity of oxygen (3.5) is higher compared to that of carbon (2.5). Due to this reason a large change in the electron cloud distribution takes place resulting in the development of slight negative charge at the oxygen atom with respect to the aromatic ring. On the other hand, there is a nitrogen atom attached to the second aromatic ring. This will also disturb the electron cloud distribution of the aromatic ring but not to the same extent as the oxygen atom since the difference of electronegativity in this case is slightly lower (electronegativity for N= 3 and for C= 2.5). To explore this aspect in detail, we consider the electronic configuration of oxygen,

$$(1s_\sigma{}^b)^2\,(1s_\sigma{}^a)^2\,(2s_\sigma{}^b)^2\,(2s_\sigma{}^a)^2\,(2p_\sigma{}^b)^2\,(2p_\pi{}^b)^4\,(2p\pi^a)^2$$

where 'b' and 'a' stand for bonding and anti-bonding orbitals respectively. The delocalization of the π-electrons takes place due to the mesomeric effect [20]. In such a case a lateral dipole develops along the central linkage [21]. Such a dipole would show a tendency for reduction in the extent of positional correlation of the molecules which is actually observed in our experiments as will be seen later in this chapter. We can thus conclude that the charge redistribution of the two aromatic rings are different and independent of each other to a large extent. This suggests that the bands at 1162, 1572 and 1594 cm^{-1} are associated with the benzene ring adjoining the nitrogen atom and those at 1167, 1575 and 1598 cm^{-1} are associated with the benzene ring adjacent to the oxygen atom. This is established by the fact that we have observed doublets for each of the aromatic ring modes instead of

singlets. Further support to this view is provided by previous experiments on similar schiff base compounds without the oxygen atom (e.g., TBBA, TBDA, TBH_PA, etc.,) [10-14] where only singlets were observed for these particular modes of the aromatic rings. In Table 3.1, a tentative assignment of all the peak positions has been made on the basis of the expected group frequencies and reported assignments for similar schiff base compounds [10-14,20].

3.3.2. The Crystal (K) - G phase transition.

For a detailed analysis, the bands were deconvoluted by fitting the spectral features in the 1140-1220 cm^{-1} and the 1550-1640 cm^{-1} regions (Figure. 3.3) into Lorentzian profiles at every temperature. The values of peak positions, linewidths and integrated intensities thus obtained are shown in Table 3.2a, b and c and the values are plotted in Figures. 3.4, 3.5 and 3.6 respectively. The percentage contribution of individual bands to their respective overlapping spectral regions was calculated and taken as a measure of the integrated intensity. Measurement of integrated intensity with respect to some internal standard is avoided because doping may change the liquid crystalline characteristics of the sample. In this study we have concentrated on the structural disorder of the core and therefore we consider only nine prominent Raman bands observed at 1162, 1167, 1171, 1194, 1572, 1575, 1594, 1598 and 1627 cm^{-1}, which are all associated with the core.

A careful examination of the Figures. 3.4, 3.5, and 3.6 reveal an anomalous behaviour of the spectral features for all the Raman bands at a temperature of 28 °C, which is the crystal -*G* transition temperature of the compound 5O.5. This transition is an example of a transition between two well-defined three-dimensional structures

[22,23]. The only difference between the two phases is that G is a highly viscous liquid crystalline phase where the molecules are arranged in a monoclinic lattice whereas K is a crystalline phase. As in most of the liquid crystal molecules, the alkyl chain part of the molecule is expected to attain a higher degree of orientational and vibrational freedom at the melting process involving a phase transition from crystalline to a crystal like smectic phase. In contrast, the core part of the molecule including the aromatic rings is expected to be rigid with very small orientational freedom. Moreover, the *G* phase has a pseudo-hexagonal packing with a local herring-bone structure. In such a packing, very little translational freedom between the molecules is possible. But a lateral gap exists among each of the pseudo-hexagonal clusters, which facilitate a relatively free lateral motion (vibrational) of the alkyl chains, thereby exerting some strain on the core part of the molecule. Due to this reason abnormalities are expected to arise in those vibrational modes which are connected to the core.

A careful study of Figure.3.4 shows that the peak positions of the Raman bands at 1167 and 1594 cm^{-1} at the K-*G* transition show a shift towards higher wavenumber side. But the band due to the -ϕ–N= stretching mode at 1194 cm^{-1} shows an opposite behaviour and the peak position is shifted to a lower wavenumber. This is because of the increased orientational freedom of the terminal alkyl chains in the G phase which exerts strain on the core and softens the -ϕ-N= bond. The Raman bands due to the C=N and the C-O modes at 1627 and 1171 cm^{-1} respectively, do not show appreciable shift in the peak positions because the total energy of the bonds remains unchanged. For the aromatic ring modes the observed

upward shift in the peak position indicates that the aromatic rings in the solid state are constrained due to higher interactions in close packing form.

An abrupt increase in the integrated intensity at the K-*G* transition for all the representative bands is observed in Figure 3.6, which can be attributed to the increase in the electron cloud density related to these modes. As the two lone pair of electrons lie in bonding orbitals, it is possible that the 5O.5 molecule suffers a twist along one of the single bonds at the K-G transition. Since softening of the -ϕ–N= is taking place as discussed in the previous paragraph and that all the bands associated with benzene rings are shifting to higher wavenumber side as well as showing an increase in intensity, it may be concluded that the two benzene ring sections of the molecule are twisting about the -ϕ–N= bond thereby affecting the electron cloud distribution and the -ϕ–O– bond also. In that case a drift of the electron cloud is expected to take place. Also, in the molecular orbital approach [24] the magnitude of resonance and hence the strength of a covalent bond is approximately proportional to the amount of overlap of the atomic orbitals of the electrons constituting the bond. In such a case the core related modes in 5O.5 molecule are expected to show an increase in the intensity and also shift to a higher position. This is exactly what has been observed in the spectra obtained, where there is an upward shift of the peak positions along with increase in the integrated intensity of the related modes in the *G* phase. Due to this disturbance of the charge density, a broadening of the linewidth also takes place which is evident in Figure.3.5.

3.3.3. The G - Smectic F (S_F) phase transition.

As is apparent from the Figures. 3.4, 3.5 and 3.6, there is a gradual increase in the peak positions, integrated intensities and the linewidths with increasing temperature from 30 to 47 ^{0}C. No abnormal change in the peak positions, linewidths and the integrated intensities of any of the bands is observed at the G-S_F transition temperature. A close look on the structures of the G and S_F phases reveal that basically both of these phases have a c-centred monoclinic lattice [22,23]. The major difference of these two structures is that in the S_F phase there is a strong in-plane short range positional correlation, whereas no such interlayer positional correlation is found to exist in the G phase. The gradual increase in the peak positions and the linewidths of all the Raman bands indicates higher freedom of the individual molecules in the S_F phase. But integrated intensity does not show any significant change in this region. This confirms that the only change that takes place at this transition is the loss of intermolecular ordering with almost no change in the intramolecular parameters, both with respect to position and orientation. Further, the observed behaviour at G—S_F transition is consistent with the reported second order nature of this transition by monitoring the bulk physical parameters such as entropy change and variation of density with temperature at this transition [25].

3.3.4. The Smectic F (S_F) – Smectic C (S_C) phase transition.

The S_F—S_C transition is marked by an abrupt increase in the peak positions whereas there is a sharp decrease in the linewidths and integrated intensities of the bands confirming the first order nature of this transition. This behaviour is due to

large structural differences between the S_F and the S_C phases. The S_F—S_C transition is a phase transition between the highly ordered S_F phase to the liquid-like molecular arrangement in layers in S_C phase. Both S_F and S_C are tilted phases. The S_F phase is characterized by a monoclinic lattice structure with hexagonal close packed molecules and short range positional ordering (bond orientational order) [22,23]. Accordingly, the direction of the tilt is towards the edge of the hexagon. The S_C phase with its liquid-like two-dimensional structure possesses a short range correlation between the molecular positions (centre of masses) over certain distances (known as clusters). Because of the fluid like character, neither the distance between the centre of clusters is related to the local spacing nor are the inter-molecular interactions correlated.

As the intermolecular interactions are weak in the S_C phase, intra-molecular dynamics is the reason behind the changes in the Raman parameters of the different modes. Therefore in the S_C phase there is a higher degree of both the positional and orientational freedom of the molecules. Due to the freedom enjoyed by the molecules in this state the bonds become stronger as well as twisting around the single bonds also become possible. Figure. 3.4 exhibits a small but noticeable change in peak positions at this transition. On the other hand, the changes observed in the integrated intensity and linewidth are much prominent (Figures. 3.5 and 3.6), especially for the -ϕ-N= and the -C=N- modes. It is well known that the Raman linewidth is a cumulative effect of the linewidths originating from the temperature dependent reorientational motion as well as the temperature independent vibrational dephasing [11]. Therefore, there must be some rotational motion taking place around the -ϕ-N= bond. The abrupt change of integrated intensity of the bands due to the -

ϕ-N= mode indicates an appreciable σ-electron cloud distortion due to rotation about this bond. In such a case we also expect a redistribution of the π-electron cloud over the -C=N- bond, which is reflected as a change in integrated intensity. Also, a rotation about the -ϕ-N= bond would lead to a modification of the core of the molecule. Because of higher freedom and comparatively weak intermolecular interactions in the S_C phase the alkyl chains in this phase will try to stabilize themselves in the lowest energy configuration by reorienting the peripheral benzene rings around a flexible single bond (-ϕ-N=) without affecting its backbone significantly.

A gradual change in the peak positions, integrated intensities and the linewidths for all the bands were observed at the S_A—N transition indicating the second order nature of this transition. However, increase of integrated intensity for all the bands at the transition indicates that the restrictions on the molecules disappear alongwith the disappearance of one dimensional density wave characterizing the layered structure of the S_A phase along the director. This leads to a more liquid like nematic phase with retention of a small degree of orientational order. It has been reported that the S_A—N transition in the compound 5O.5 is a second order transition with large pre-transitional effects, predominantly on the nematic side, using density, ultrasonic velocity and X-ray diffraction studies [15,16,17]. The formation of the cybotactic clusters in the nematic phase just above the S_A—N transition explains the pre-transitional effects. Also the smectic like ordering (cybotactic clusters) in the nematic phase itself may be the reason for second order S_A—N transition. Accordingly in our present results only a noticeable

change is observed in the integrated intensity for all the peaks at the S_A—N transition which may be attributed to the disappearance of positional ordering altogether. No changes are observed in the peak positions and the linewidths indicating that there is no change in the molecular configuration at the transition and that the orientational order among the molecules is still retained in the nematic phase.

3.3.5. The Nematic (N)—Isotropic (I) phase transition.

While cooling an isotropic liquid the infinite rotational symmetry of the isotropic phase breaks down at the I-N transition. Therefore the N-I transition marks the complete loss of orientational order present in the nematic phase and is expected to be a first order transition. The N—I transition is marked by a simultaneous coexistence of two phase in a range of about 2 ^{0}C which is a signature of a first order transition as is evident by the irregular behaviour observed in the peak positions, integrated intensities and linewidths of all the bands monitored.

3.4. CONCLUSION.

The main conclusions that we could arrive at from our studies are emphasized in this section. From the results obtained we find that the crystal—G phase transition in 5O.5 is a first order transition between two well-defined three dimensional structures. We also see that at the melting process, the alkyl chains attain a higher degree of orientational and vibrational freedom whereas the core portion remains almost rigid. The lateral gap among the pseudo- hexagonal clusters enable the alkyl chains to move freely, putting strain on the core part and resulting in

softening of the -ϕ-N= bond. The G—S_F transition is characterized by a subtle increase in the peak positions and the linewidths indicating higher freedom of the molecules in the S_F phase. The fact that the integrated intensity remains almost constant points to the fact that there is only a loss of intermolecular ordering during this transition. The S_F—S_C phase transition shows sharp changes in all the spectral parameters indicating the first order nature of this transition. There is also a high degree of positional and orientational freedom of the molecules. The S_A—N phase transition is a second order transition marked by gradual changes in peak positions, linewidths and integrated intensities. Some pre-transitional effects are also observed which are attributed to the formation of cybotactic clusters.

REFERENCES

1. Bulkin, B. J., and. Prochaska, F. T., *J. Chem. Phys.*, **54**, 635, 1971.

2. Borer, W. J., Mitra, S. S., and Brown, C. W., *Phys. Rev. Lett.*, **27**, 379, 1971.

3. Fontana, M., and Bini, S., *Phys. Rev. A* **14**, 1555, 1976.

4. Amer, N. M., and Shen, Y. R., *Solid State Comm.*, **12**, 263, 1973.

5. Amer, N. M., Shen, Y. R., and Rosen, H., *Phys. Rev. Lett.*, **24**, 718, 1970.

6. Dvorjetski, D., Volterra, V., and Wiener-Avnear, E., *Phys. Rev. A* **12**, 681, 1975.

7. Amer, N. M., and Shen, Y. R., *J. Chem. Phys.*, **56**, 2654, 1972.

8. Schnur, J. M., *Phys. Rev. Lett.*, **29**, 1141, 1972.

9. Amer, N. M., and Shen, Y. R., *J. Chem. Phys.*, **56**, 2654, 1972.

10. Dash, S. K., Singh, R. K., Alapati, P. R., and Verma, A. L., *Mol. Cryst. Liq.Cryst.*, **319**, 147, 1997.

11. Dash, S. K, Singh, R. K., Alapati, P. R., and Verma, A. L., *J. Phys. Condensed Matter*, **9**, 7809, 1997.

12. Dash, S. K., Singh, R. K., Alapati, P. R., and Verma, A. L., *Liq. Cryst.*, **25**, 459, 1998.

13. Dash, S. K., Singh, R. K., Asthana, B. P., Alapati, P. R. and Verma, A. L., *J. Raman. Specstrosc.*, **7**, 302, 1999.

14. Dash, S. K., Singh, R. K., Alapati, P. R., and Verma, A. L., *Liquid Cryst.*, **26**,1479, 1999.

15. Pisipati, V. G. K. M., Rao, N. V. S., Pisipati, D. M., Alapati, P. R., and Rao, P. B., *Liq. Cryst.*, **167**, 167, 1989.

16. Alapati, P. R., Pisipati, D. M., Rao, N. V. S., Pisipati, V.G. K. M., Paranjpe A.S., and Rao, U. R. K., *Liq. Cryst.*, **3**, 1461, 1988.

17. Alapati, P. R., Pisipati, D. M., Rao, P. B., Rao, N. V. S., Pisipati, V.G. K. M., and Paranjpe, A.S., *Liq. Cryst.*, **5**, 545, 1989.

18. Asthana, B. P., and Kiefer, W., *Vibrational Spectra and Structure,* Elsevier; Amsterdam, ed., Durig, J. R., **20**, 67, 1993.

19. Singh, R. K., Singh, S. N, Asthana, B. P., and Pathak, C. M., *J. Raman Spectrosc,* **24**, 423, 1994.

20. Colthup, N.B., Daly, L.H., and Wiberley, S.E., *Introduction to Infrared and Raman Spectroscopy*, Academic, New York, 1975. Chapters 4 and 8.

21. Gray, G. W., and Goodby, J. W., *Smectic Liquid Crystals*, Leonard Hill, London, 1984.

22. Priestley, E. B., Wojtowicz, P. J., and Sheng, P, *Introduction to Liquid Crystals*, Plenum Press, London, 1975.

23. de Gennes P. G., *The Physics of Liquid Crystals*, Oxford University Press, London, 1974.

24. Hergberg G., "*Infrared and Raman spectra of polyatomic molecules*", Van Nostrand Reinhold Co : N. Y. **2**, 1945.

25. Rao, N. V. S., Pisipati, V.G. K. M., Murthy, J. S. R., Rao, P. B., and Alapati, P. R., *Liq. Cryst*, **5**(2), 539, 1989.

Table 3.1. Assignment of the various core-related and other modes of the 5O5 molecule.

Serial No.	Band Position. (cm^{-1})	Assignment.
1.	629	In plane C=C quadrant bending.
2.	643	In plane C=C quadrant bending.
3.	726	Out of plane ring bending by sextent
4.	802	In phase out of plane aromatic CH wagging mode.
5.	834	In phase out of plane aromatic CH wagging mode.
6.	846	In phase out of plane aromatic CH wagging mode.
7.	897	In phase out of plane aromatic CH wagging mode.
8.	937	In phase out of plane aromatic CH wagging mode.
9.	976	C=C breathing modes.
10.	981	C=C breathing modes.
11.	1162	Aromatic C-H in plane bending mode.
12.	1167	Aromatic C-H in plane bending mode.
13.	1171	C-O stretch.
14.	1194	Aromatic C-N stretching mode.
15.	1311	CH_2 twist.
16.	1373	CH_2 deformation.
17.	1509	Semi-circle stretching mode.
18.	1572	Quadrant stretching mode of the aromatic ring.
19.	1575	Quadrant stretching mode of the aromatic ring.
20.	1594	Quadrant stretching mode of the aromatic ring.
21.	1598	Quadrant stretching mode of the aromatic ring.
22.	1627	C=N stretching mode.
23.	2876	CH_3 stretching mode.
24.	3060	CH_3 stretching mode.

Table 3.2a The variation of peak positions of the various bands as a function of temperature.

Temperature (°C)	Liquid Crystal Phases	1161 (cm^{-1})	1167 (cm^{-1})	1171 (cm^{-1})	1195 (cm^{-1})	1573 (cm^{-1})	1578 (cm^{-1})	1592 (cm^{-1})	1598 (cm^{-1})	1627 (cm^{-1})
22	K	1162.72	1165.69	1171.24	1194.93	1572.28	1575.37	1592.57	1598.10	1627
24	K	1162.65	1165.43	1171.48	1195.05	1572.33	1575.36	1592.51	1598.08	1627
27	K	1162.61	1165.33	1171.21	1194.88	1572.66	1575.42	1592.54	1598.19	1627.20
29	G	1163.83	1167.21	1172.75	1192.26	1573.69	1577.31	1594.41	1599.67	1628.66
32	G	1164.01	1167.62	1172.38	1192.33	1573.76	1577.40	1594.30	1599.52	1628.61
38	G	1163.68	1167.72	1172.42	1192.19	1573.81	1577.27	1594.29	1599.48	1628.46
42	G	1163.71	1167.55	1172.39	1192.45	1573.56	1577.51	1594.37	1599.53	1628.57
44	G	1163.63	1167.42	1172.56	1192.57	1573.87	1577.62	1594.68	1599.32	1628.63
45.8	G	1163.75	1167.66	1172.53	1192.46	1573.85	1577.57	1594.72	1599.36	1628.72
46.5	G	1163.55	1167.46	1172.45	1192.49	1573.67	1577.62	1594.92	1599.59	1628.77
47.3	S_F	1164.83	1168.09	1174.61	1195.27	1574.72	1578.82	1596.51	1601.27	1630.48
48	S_F	1164.34	1167.42	1174.42	1194.79	1574.32	1578.80	1596.09	1601.07	1630.23
48.7	S_F	1164.21	1167.46	1173.36	1194.47	1574.02	1578.49	1595.98	1599.89	1630.07
49.5	S_C	1163.59	1166.76	1171.56	1193.08	1574.13	1578.70	1595.72	1599.44	1630.22
50.8	S_C	1163.14	1166.21	1171.43	1192.52	1574.10	1578.27	1595.89	1599.64	1629.02
52	S_C	1163.23	1166.59	1171.34	1192.73	1573.78	1578.02	1594.82	1599.73	1629.12
53.5	S_A	1163.17	1166.45	1171.40	1192.67	1573.60	1577.89	1594.67	1599.66	1629.15
54.8	N	1163.08	1166.18	1171.39	1192.61	1573.42	1577.67	1594.57	1599.54	1629.11
58	N	1162.66	1165.96	1171.06	1192.58	1573.36	1577.42	1594.47	1599.52	1628.89
59	N	1162.51	1165.88	1171.51	1192.46	1573.38	1577.34	1594.68	1599.38	1629.03
62	N	1162.46	1165.56	1171.28	1192.57	1573.22	1577.44	1594.42	1599.46	1628.78
66.6	N	1162.55	1165.48	1171.63	1192.28	1573.46	1577.52	1594.58	1599.47	1628.83
70	N	1163.01	1166.01	1172.08	1192.63	1573.41	1577.66	1594.55	1599.49	1629.12
72	N	1163.17	1166.67	1172.19	1192.46	1573.52	1577.62	1594.53	1599.32	1628.88
73	N	1163.38	1166.72	1172.32	1192.53	1573.56	1577.54	1594.63	1599.51	1628.92
75.6	N	1163.22	1167.11	1172.43	1192.53	1573.62	1577.61	1594.72	1599.66	1628.87
78	Iso	1163.87	1167.88	1173.61	1191.20	1574.88	1579.06	1596.31	1601.89	1630.44
80	Iso	1163.81	1167.72	1173.77	1191.06	1574.98	1579.66	1596.20	1602.01	1630.56

Table 3.2b The variation of linewidths of the various bands as a function of temperature.

Temperature (°C)	Liquid Crystal Phases	1161 (cm^{-1})	1167 (cm^{-1})	1171 (cm^{-1})	1194 (cm^{-1})	1573 (cm^{-1})	1578 (cm^{-1})	1594 (cm^{-1})	1598 (cm^{-1})	1627 (cm^{-1})
22	K	5.34	5.26	7.26	8.17	3.91	3.78	8.88	6.22	7.36
24	K	5.37	5.37	7.38	8.22	3.87	3.7	8.94	6.22	7.72
27	K	5.22	5.22	7.45	8.27	4.08	3.24	8.97	6.9	7.70
29	G	6.42	6.78	9.44	9.68	4.44	4.3	11.78	7.72	9.76
32	G	6.56	6.88	9.54	9.78	4.47	3.98	11.62	7.32	9.63
38	G	6.34	6.93	9.62	9.72	4.74	4.22	11.82	7.62	9.64
42	G	6.36	6.80	9.74	9.81	4.56	4.00	11.74	7.14	9.96
44	G	6.43	6.82	9.76	9.86	4.71	4.12	11.88	7.66	10.28
45.8	G	6.47	6.92	9.82	9.68	4.86	4.24	11.83	7.78	10.36
46.5	G	6.54	6.96	9.96	9.94	4.68	4.3	11.84	7.76	10.54
47.3	S_F	6.78	7.32	9.86	9.83	5.18	4.04	11.87	7.76	10.56
48	S_F	6.81	6.10	9.94	9.92	5.24	4.06	11.81	7.82	10.93
48.7	S_F	6.92	7.14	10.05	9.96	5.58	5.20	11.96	8.04	11.07
49.5	S_C	5.02	4.02	5.13	6.21	4.02	3.98	12.07	6.78	5.26
50.8	S_C	6.12	5.84	8.02	8.94	4.44	4.18	12.41	7.56	7.78
52	S_C	5.96	6.14	8.64	9.52	4.57	4.32	12.57	8.02	9.86
53.5	S_A	6.42	8.74	10.87	11.68	5.69	3.52	13.91	8.36	12.84
54.8	N	7.16	6.28	9.73	9.76	5.48	3.92	12.48	8.41	11.52
58	N	6.56	5.94	9.07	9.63	5.23	3.98	12.26	7.64	11.38
59	N	6.71	5.68	8.51	9.50	4.74	4.98	11.92	7.94	11.51
62	N	6.77	5.98	8.02	9.57	4.34	4.61	11.54	7.72	11.04
66.6	N	6.92	5.84	7.66	9.66	4.68	3.64	11.32	7.78	10.28
70	N	6.82	5.87	7.91	9.38	3.82	3.94	11.57	7.88	10.52
72	N	6.76	5.96	8.16	9.72	4.61	3.72	11.76	7.52	10.46
73	N	6.87	5.92	8.52	9.66	4.72	4.04	11.72	7.28	10.28
75.6	N	6.98	5.88	8.56	9.78	4.62	3.88	11.22	7.24	10.77
78	Iso	7.32	8.08	10.78	11.49	5.61	5.56	13.97	8.34	10.78
80	Iso	7.47	8.16	10.63	11.60	5.67	5.62	13.89	8.52	12.96

Table 3.2c The variation of integrated intensities of the various bands as a function of temperature.

Temperature (°C)	Liquid Crystal Phases	1161 (cm^{-1})	1167 (cm^{-1})	1171 (cm^{-1})	1195 (cm^{-1})	1573 (cm^{-1})	1578 (cm^{-1})	1592 (cm^{-1})	1598 (cm^{-1})	1627 (cm^{-1})
22	K	24.0	27.2	29.1	23.7	11.9	12.1	17.3	27.8	14.1
24	K	23.8	27.4	29.4	23.6	12.01	12.1	17.4	28.1	14.4
27	K	23.8	27.1	29.3	23.4	12.2	11.8	17.1	28.01	14.2
29	G	28.3	30.6	36.7	26.5	14.4	13.8	21.6	33.9	15.2
32	G	28.4	30.3	36.8	27.6	14.2	13.8	21.9	35.1	15.6
38	G	28.4	30.4	36.2	27.7	14.2	14.6	22.2	35.01	15.9
42	G	28.4	30.2	36.4	27.2	14.1	13.7	23.7	33.8	15.6
44	G	28.1	30.6	36.5	27.9	13.1	13.6	23.7	34.6	16.1
45.8	G	28.3	30.7	36.1	27.6	13.4	13.6	23.4	34.8	16.2
46.5	G	28.4	30.5	35.9	27.5	14.5	13.7	23.1	35.4	16.5
47.3	S_F	28.8	30.8	36.4	27.5	15.5	13.8	24.5	33.6	17.5
48	S_F	28.8	31.7	36.8	27.5	14.9	12.8	24.6	33.5	17.6
48.7	S_F	28.7	31.8	36.9	24.3	14.8	13.1	25.7	32.9	17.5
49.5	S_C	31.4	28.7	33.5	26.4	13.1	13.2	25.1	34.2	16.7
50.8	S_C	30.2	29.1	32.8	28.8	12.8	13.3	19.6	31.8	16.6
52	S_C	30.3	29.2	33.4	27.9	12.8	13.2	20.1	31.7	16.7
53.5	S_A	27.1	32.6	34.7	26.8	16.1	18.1	20.0	37.9	15.9
54.8	N	29.2	31.2	34.1	26.3	16.2	15.4	23.1	39.4	15.8
58	N	28.4	31.4	34.5	26.2	15.8	14.3	22.4	31.2	16.2
59	N	27.6	31.3	34.1	25.5	16.4	13.5	22.6	34.3	15.5
62	N	28.0	30.1	34.0	25.5	15.8	14.4	22.7	33.2	15.7
66.6	N	28.1	30.5	35.1	25.4	15.7	15.1	22.4	33.5	15.8
70	N	28.2	31.1	34.1	25.6	15.6	16.0	22.1	31.2	14.2
72	N	27.8	31.0	35.2	25.7	16.3	13.9	22.5	32.3	16.2
73	N	27.9	31.0	34.0	25.5	15.8	13.8	22.6	31.9	15.3
75.6	N	28.1	31.1	34.0	25.5	15.6	13.2	22.4	32.6	16.2
78	Iso	31.6	34.2	38.6	31.8	18.9	18.0	30.5	33.2	19.2
80	Iso	31.8	34.6	41.7	32.1	18.6	18.6	30.6	33.6	19.5

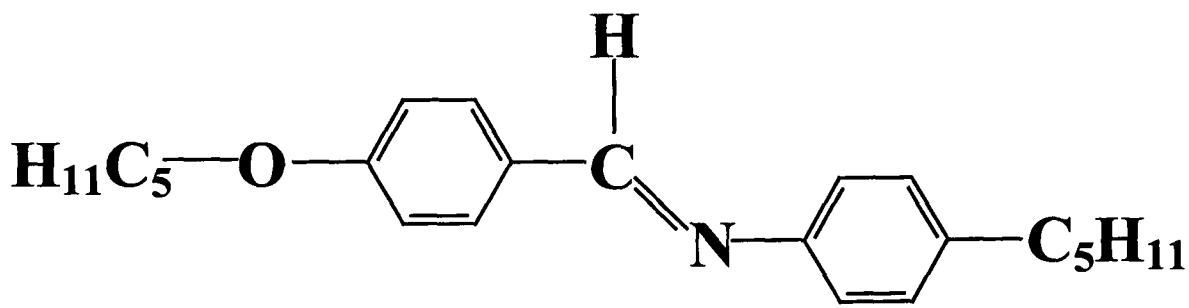

Fig 3.1. Structure and phase transition sequence of liquid crystalline compound N-(4-n- Pentyloxy benzylidene)- 4'-n-pentylaniline, (5O.5).

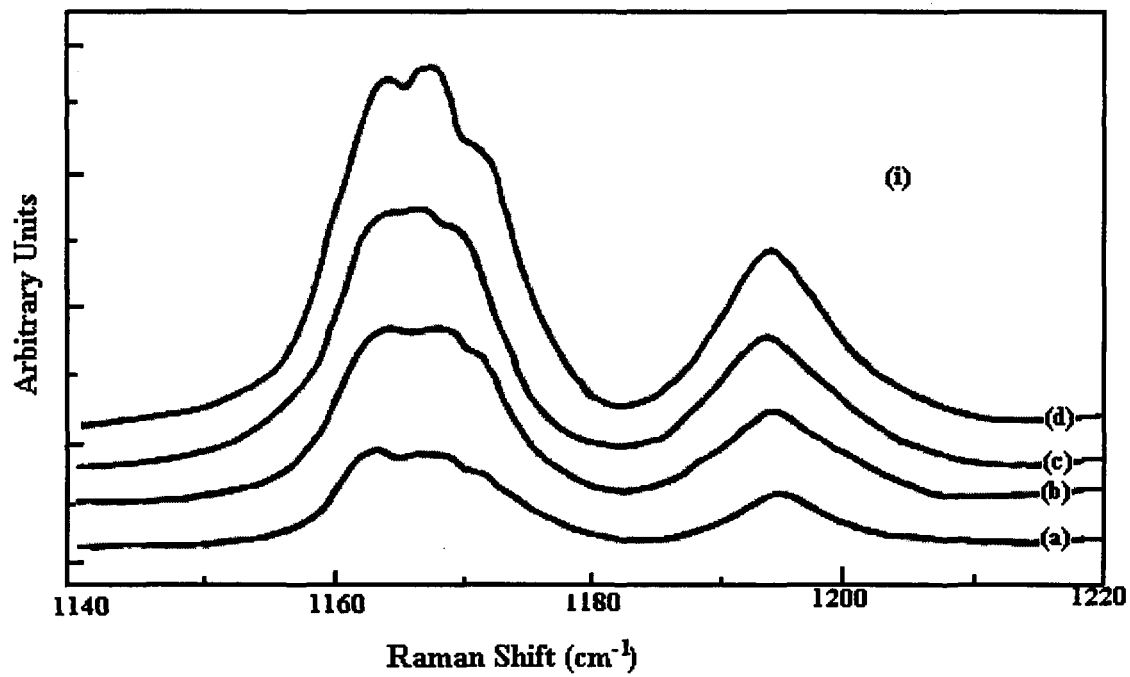

Fig.3.2.a (i). Raman spectra of 5O.5 in 1140-1220 cm^{-1} region at different phases. (a) Crystalline (K) phase, (b) Smectic G (S_G) phase, (c) Smectic C (S_C) phase, (d) Smectic A (S_A) phase.

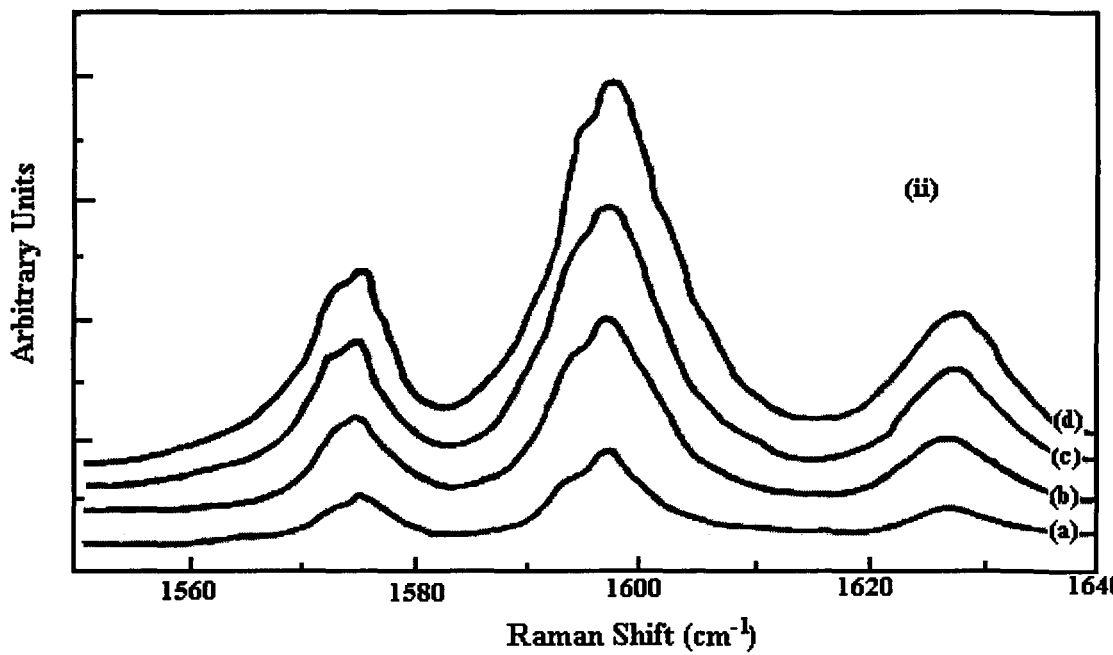

Fig.3.2.a(ii). Raman spectra of 5O.5 in 1550-1640 cm^{-1} region at different phases. (a) Crystalline (K) phase, (b) Smectic G (S_G) phase, (c) Smectic C (S_C) phase, (d) Smectic A (S_A) phase.

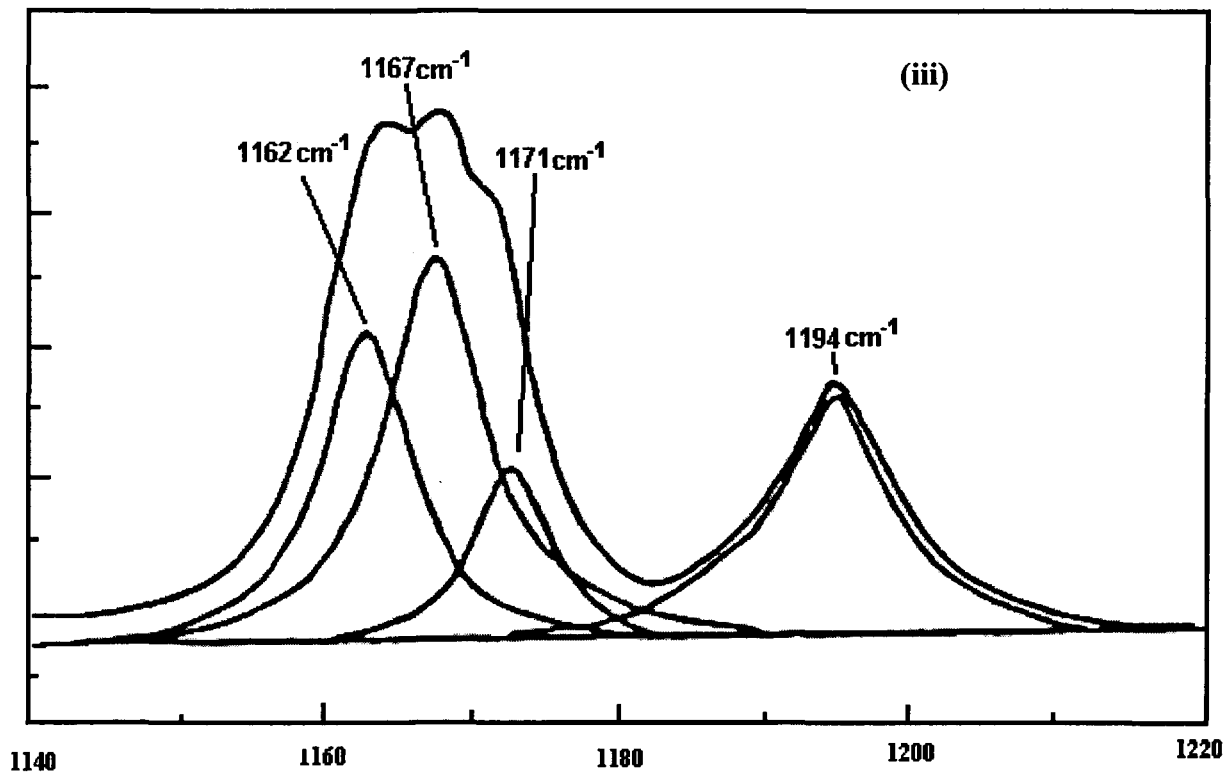

Fig.3.2a (iii) The deconvoluted spectra in (i) 1140-1220 cm^{-1} region of the Raman spectra in the Smectic A phase of 5O.5.

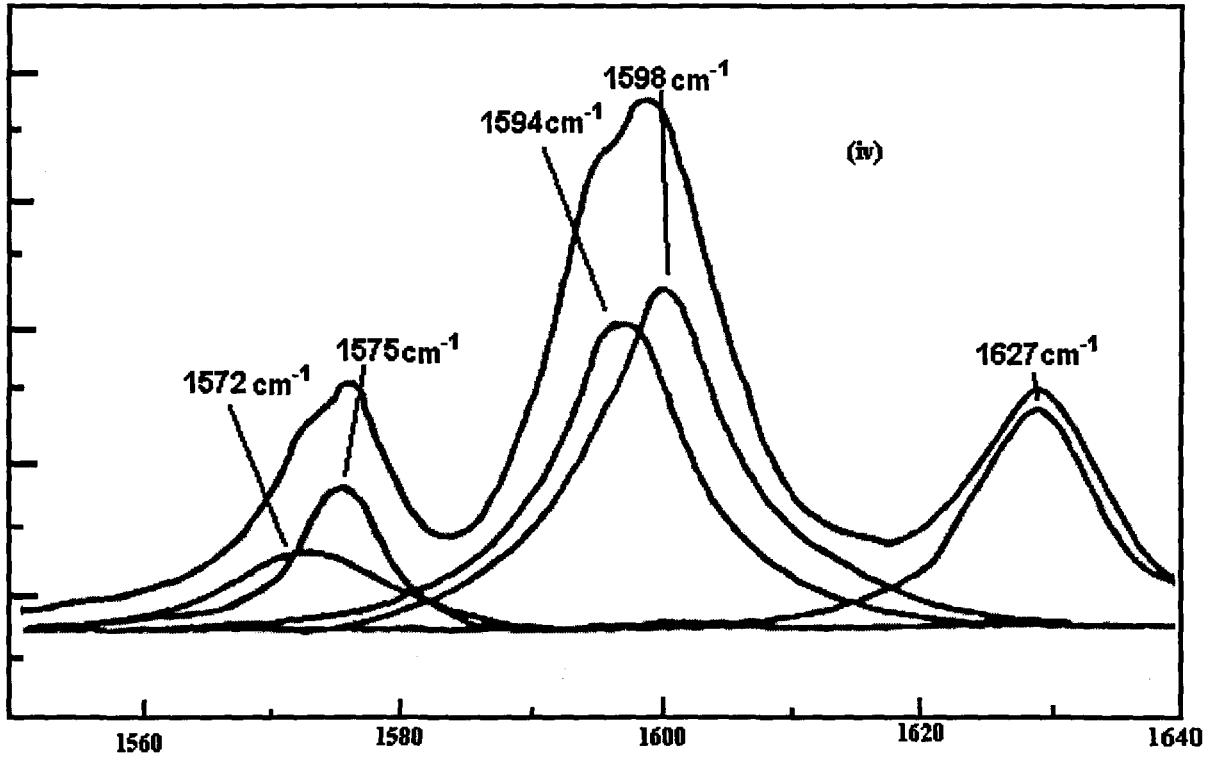

Fig.3.2a (iv). The deconvoluted spectra in 1550-1640 cm^{-1} region of the Raman spectra in the Smectic A phase of 5O.5.

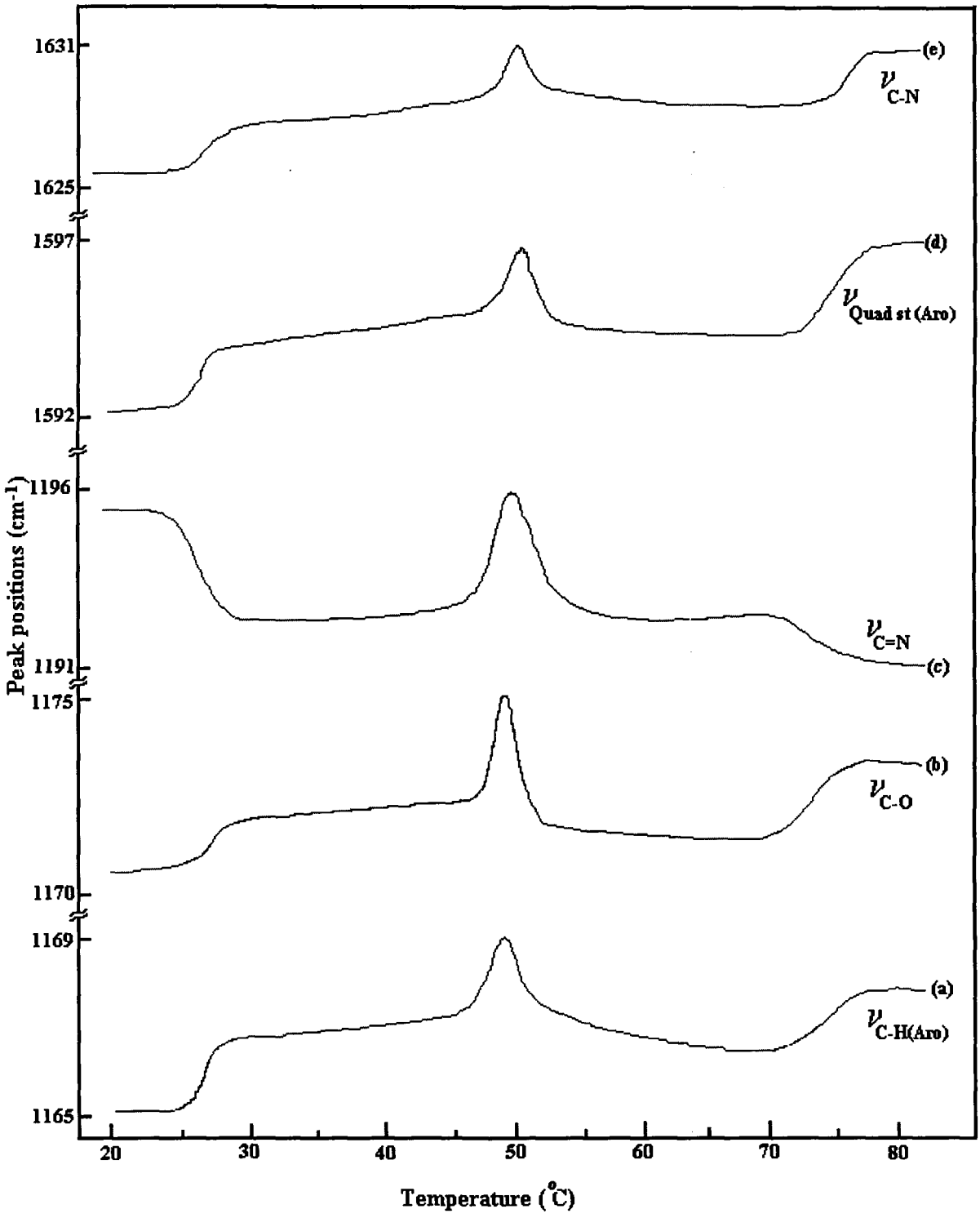

Fig.3.3. Variation of peak positions of the individual bands as a function of temperature. (a) 1167 cm^{-1}, (b) 1171 cm^{-1}, (c) 1194 cm^{-1}, (d) 1594 cm^{-1}, (e) 1627 cm^{-1}. (Uncertainty within ± 0.2 cm^{-1})

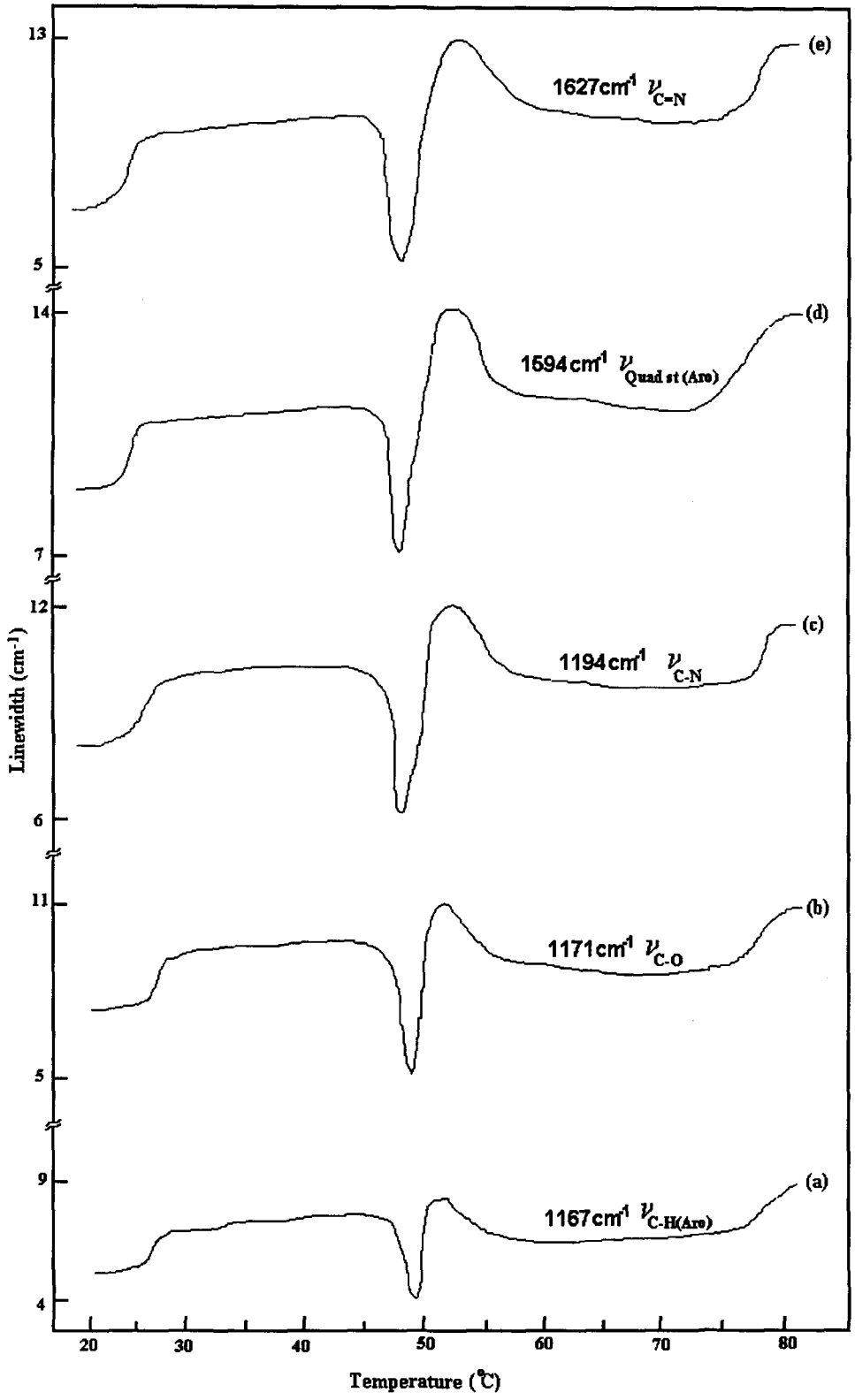

Fig.3.4. Variation of linewidths of the individual bands as a function of temperature. (a) 1167 cm^{-1}, (b) 1171 cm^{-1}, (c) 1194 cm^{-1}, (d) 1594 cm^{-1}, (e) 1627 cm^{-1}. (Uncertainty within ± 2 %)

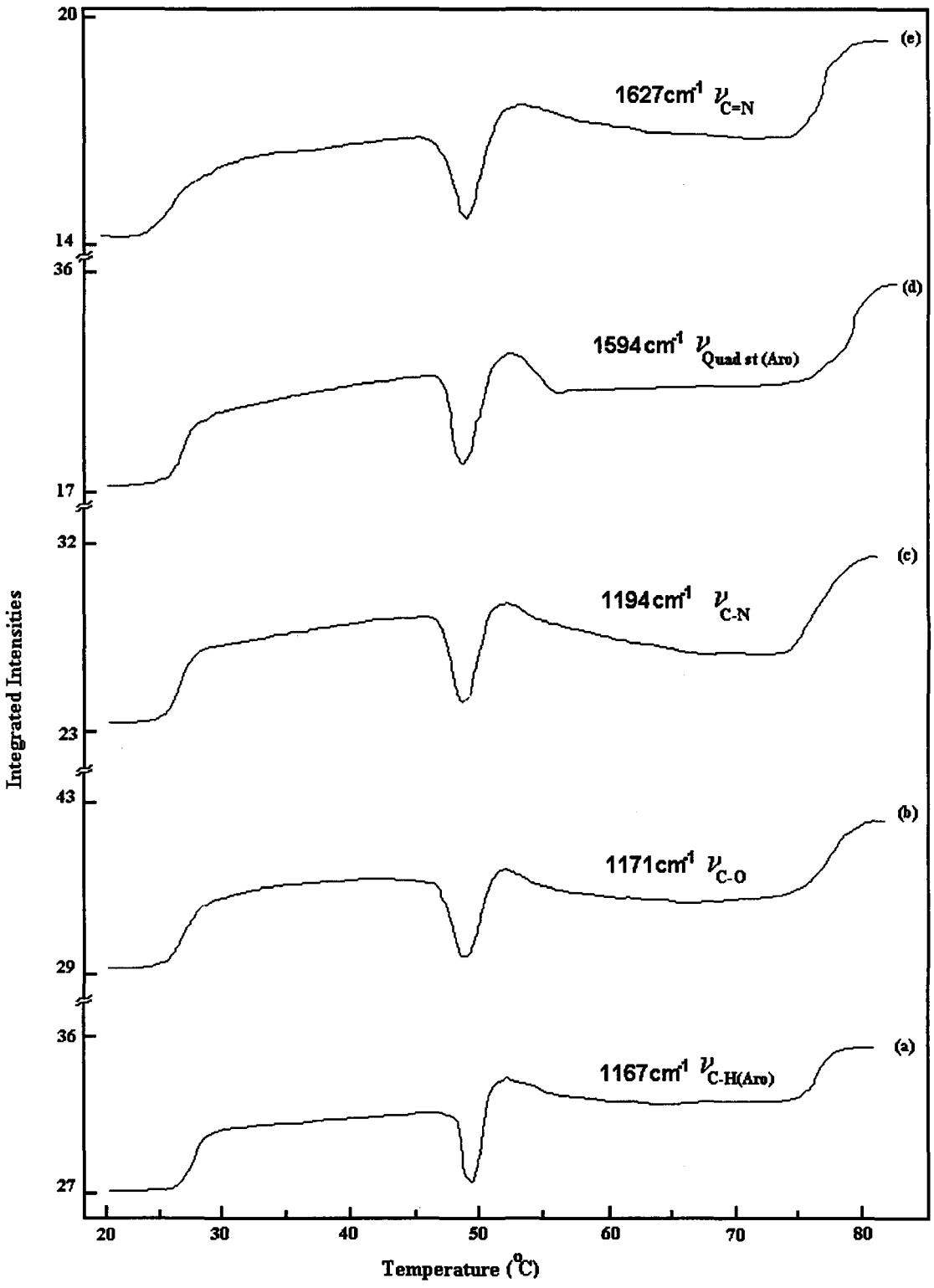

Fig.3.5. Variation of integrated intensities of the individual bands as a function of temperature. (a) 1167 cm^{-1}, (b) 1171 cm^{-1}, (c) 1194 cm^{-1}, (d) 1594 cm^{-1}, (e) 1627 cm^{-1}. (Uncertainty within ± 2 %)

Chapter 4

A COMPARATIVE STUDY OF THE PROPERTIES OF LIQUID CRYSTALLINE COMPOUNDS 5O.5 AND 5O.6 IN SOLID, SOLUTION AND THIN FILM FORMS BY LASER RAMAN SPECTROSCOPY.

Comparative Raman studies of a higher homologue 5O.6 with 5O.5 as well as between bulk state and thin film form of the compound 5O.6, is reported in this chapter. Raman spectroscopic studies of liquid crystalline compounds 5O.5 and 5O.6 revealed that the two aromatic rings in the core are in different environments with distorted electron cloud distribution and the behaviour of each of these rings is independent of the other. Increased chain length results in the development of strains on the molecule. At the S_F — S_B phase transition there is a slight transfer of charge along with an increase in the freedom of the individual molecules. Our experiments also reveal that the molecules are strained in the crystalline state and take up some preferred orientations in free-standing films. There is also a tendency towards the straightening of the molecules along the C=N- linkage in the solution for the liquid crystal 5O.6. Raman spectra of 5O.6 in free-standing film form have shown drastic changes compared to the spectra in the bulk form.

4.1 INTRODUCTION

The orientational and translational ordering of the molecules in liquid crystals gives rise to a rich variety of mesophases. One of the most interesting group of liquid crystalline compounds is the N (p-n-alkyloxy benzylidene) p-n alkylanilines which consist of compounds containing Schiff base central linkages and is popularly known as the nO.m series [1-3]. Of these nO.m's, the N (p-n-pentyloxy benzylidene) p-n alkylanilines (5O.m's) are a fascinating group as the intermediate compounds of this group viz., 5O.5 and 5O.6 exhibit a rich variety of smectic mesomorphism in addition to the presence of nematic phase. The lower homologues of the series such as 5O.2 exhibit nematic and smectic G phases while the higher homologues show the nematic, smectic A and smectic B phases. The phase sequence of the compounds 5O.5 and 5O.6 is N-S_A-S_C-S_F-G and N-S_A-S_C-S_B-S_F-G respectively. This particular series of compounds attracts more attention also since the smectic A- nematic tricritical point among nO.m compounds is found to exist in 5O.m series [4]. Further curiosity is aroused in this series as a large variation of tilt angle (0° to 23° within a temperature range of 4 °C) in smectic C phase of 5O.5 [5] is observed along with the existence of smectic F phase in 5O.5 and 5O.6 (besides 9O.4), which is an extremely rare phase in the nO.m series of compounds. Although the phase transitions and structural changes in the nO.m compounds have been studied extensively using various experimental techniques, a detailed spectroscopic analysis to probe the

microscopic details of the different phases exhibited by nO.m compounds has not been reported so far, to the best of the author's knowledge.

Raman spectroscopy has proved to be a very powerful technique in the investigation of the vibrational dynamics of liquid crystalline compounds. The spectra-structure correlation, as well as the connection between structural changes during phase transitions and the corresponding changes in the Raman spectra, is of particular interest. These relationships have been used [6-13] to obtain information on the liquid crystals at the molecular level such as molecular orientation / rotation [14], inter / intra-molecular interactions [15,16] etc.

Raman spectroscopic studies on 5O.5 provide evidence for the existence of a lateral dipole moment at the core part of the molecule as was demonstrated in the previous chapter [17]. Secondly, the compounds 5O.5 and 5O.6 are N-S_A-S_C-S_F-G and N-S_A-S_C-S_B-S_F-G phase variants respectively. It must be noted that the increase of just one CH_2 group in the end alkyl chain of the molecule 5O.5 induces an orthogonal phase (smectic B) in between two tilted phases (smectic C and smectic F). In an attempt to understand the origin of this behaviour at molecular level we have undertaken a comparative study of the properties of 5O.5 and 5O.6 compounds using Laser Raman Spectroscopy. We also report here the results of Raman studies in solution state of 5O.6. Some preliminary results on free-standing films of the compound 5O.6 are also discussed.

4.2 Experimental Details

The Raman spectra of the sample were recorded using a Spex Ramalog 1403 double monochromator equipped with an RCA-31034 photomultiplier tube and a

CCD detector, in the 1100—1250 cm^{-1} and 1550—1650 cm^{-1} regions. The spectrometer control and data acquisition was done using DM3000 software and also with Spex Datamate, which is an 8-bit dedicated microcomputer. As the changes in wavenumbers of bands for different samples were small, we took extra precaution to estimate the shifts by superimposing the different Raman spectra. The reported relative frequency shifts are accurate to within ± 0.2 cm^{-1}. Spectra-Physics Model 165-09 Ar^+ laser provided the excitation line at 4880 Å. For obtaining the spectra in the bulk form the sample was confined in a quartz capillary tube of 0.8 mm diameter and was sealed at both ends. Temperature resolution of the measurements was ± 0.5 °C. Molar solution of the sample in CS_2 was prepared to record the spectra in solution. Thin film studies were carried out on free-standing films of the sample 5O.6. The free-standing films were drawn across a conical hole made in a slab of hylam as well as in glass slab. Free-standing films of the liquid crystal were drawn on the surface of the hylam by using a spreader in smectic A phase of the sample and were allowed to stabilize for some time. It is a known fact that the molecular alignment in such films is homeotropic [18]. The construction details of the thin film cell have been described in chapter 2 of this thesis. To the best of our knowledge, no report of free-standing films drawn using hylam slab (a kind of composite laminate used in electrical printed circuit boards) are available in literature. We found that, with a hylam surface not only drawing the films was easier, the stability of these films was found to be excellent. Once properly drawn these films on a hylam surface could remain stable for a long time. The thickness of the films was roughly estimated using interference pattern from the transmitted portion of the laser beam.

4.3 RESULTS AND DISCUSSIONS

The molecular structure of the compounds 5O.5 and 5O.6, phase sequence and transition temperatures are given in Figure 4.1. As is obvious from the figure, both of the molecules are composed of two portions. The two phenyl rings along with the —C(H)=N— linkage forms the mesogen (core part) whereas the two alkyl chains at the two ends of the core forms the zigzag tails. Raman spectra were obtained in the 1100-1250 cm^{-1} and 1550-1650 cm^{-1} regions as both these regions contain the bands related to the core whose behaviour is the subject of our interest.

4.3.1 Comparison of Raman Spectra of 5O.5 and 5O.6 in the Crystalline State

It was already observed in 5O.5 that the oxygen present in this molecule severely distorts the electron clouds in various parts of the molecule and this distortion is dependent on the molecular configurations as well as the type of phase. The analysis of the spectra recorded in the 1140-1220 cm^{-1} and 1550-1650 cm^{-1} regions for the 5O.5 system has already been reported [17]. Raman spectra of bulk sample of 5O.6 at different temperatures were recorded in the 1100-1250 cm^{-1} and 1550-1650 cm^{-1} regions for comparative studies in the entire mesophase region.

In the crystalline state, both the 5O.5 as well as 5O.6 compounds crystallize in a c-centered monoclinic lattice [16,18,19] with a two-fold axis along the b-axis and molecular orientation along the c-axis. The c-axis is approximately half the molecular length. Therefore the molecular length stretches towards the c-axis and a layer forms along the b-axis. The b-axis being two-fold and the molecule being staggered, the most probable conformation is that in which the phenyl rings are

oriented along the a-c plane. So we can easily visualize that the alkyl chains of the adjacent rings will be closer along the c-axis and the phenyl rings will be closer along the b-axis.

As in a homologue 5O.5 that we had investigated earlier, the Raman spectrum of the bulk sample of 5O.6 also showed a triplet in the 1155–1170 cm^{-1} region. Similarly the doublets in the 1570–1580 and 1594–1600 cm^{-1} regions as observed in the 5O.5 sample were also seen in the 5O.6 sample. But in 5O.6 the doublets and triplets are more clearly visible and the splittings became sharper. {Figure 2, spectra (a) and (b)}

The origin of these triplets and doublets has been discussed in details in the previous chapter. A tentative assignment of all the peak positions made on the basis of the expected group frequencies and reported assignments for similar schiff base compounds in bulk samples, solutions state and free-standing films for the compound 5O.6 are given in Table 4.1 [16,20,21]. The spectral data for the compound 5O.5 is also included in the Table 4.1 for comparison. On a closer look at the structures of the 5O.5 and the 5O.6 molecules, one finds that the only difference between them is an extra CH_2 group in one of the alkyl chains of the 5O.6 molecule. It should be noted that both the alkyl chains in the earlier sample were equal whereas in the present sample the alkyl chain adjacent to the oxygen atom is shorter than the one at the other end. This subtle change in the case of 5O.6 molecule results in the effect of the oxygen atom becoming more dominant, as the π-electron cloud is now more severely distorted and as a result it affects the charge distribution of the phenyl rings adjacent to it. These changes are also accompanied by small but definite relative shift in the peak positions of all the representative bands towards lower

wavenumber side by few wavenumbers (Table 4.1) indicating a decrease in the energy of the respective bond undergoing vibration (loosening of bond). This is expected due to the increased orientational freedom of the long alkyl chain due to decrease in intermolecular interactions which may put strain (by increased stretching along the molecular axis) on the whole core part. Apart from frequency shift, the change in the bandwidth of certain Raman bands also indicate the magnitude of disorder in the system. We have analyzed our results by taking into account the shift in band position as well as changes in the linewidth of Raman bands. Given the accuracy of the measurements of peak positions in our experiments and our previous experience, the expected shift in peak positions due to increase or decrease of methylene units in the end alkyl chains is only of the order of few wavenumbers [15]. Therefore, the changes observed in the modes associated with the core part suggest that the core is also affected by the increased chain length. One can rationalize these observations in the following way: as the chain length increases, the CH_2 groups will come closer along the c-axis and will be stabilized in a minimum energy configuration due to steric hindrance, whatever be the conformation i.e., trans or gauche. Moreover, as a result of the increased stress imposed by the long alkyl chains upon the backbone, the σ electron cloud over the -Φ–C– (Φ = phenyl ring) bond may also distort significantly. With such constraints the two benzene rings are not able to orient themselves in a single plane but there is a possibility that rotation occurs along the C – N single bond and the molecule is stabilized in a minimum energy configuration.

4.3.2 Solution state

In order to find whether there is any appreciable change in intermolecular interactions in solid and liquid crystalline states by increasing the chain length by one methylene unit we have measured the spectra of 5O.6 in solution state by dissolving it in carbon disulphide. The solution state spectrum is marked by some very interesting changes. Previous studies of similar Schiff based compounds [24] without an oxygen atom (such as TBBA, TBDA, etc.,) had shown that the peak positions of all the core related bands shift to the lower side as compared to their counterparts in the solid state (Fig 4.2). But the reverse is observed in 5O.6. The bands arising due to the C-O stretch and the aromatic C-N stretching modes show an upward shift of peak positions when compared to the crystalline state. The bands arising due to the phenyl ring modes, however, almost maintain their position. The band arising due to the C=N stretching mode shifts to a lower wavenumber. This shows that the major change that occurs in the solution state is that the strains on the alkyl chains and on the inter-linking bonds of the phenyl rings are relaxed and there is a tendency towards the straightening of the individual molecules. But as the straightening of the molecule occurs there is increased strain on the C=N bond resulting in the redistribution of the charges around this region. Also accompanying this change is in peak position of the C=N mode (4 wavenumbers) and the peak position of one of the aromatic in-plane bending modes also shows a shift towards higher wavenumber side. This is possible since the change in peak position is observed in the mode related to the phenyl ring adjacent to the oxygen atom, which should be gaining in charge density. In the solution state, it may be noted that the restrictions on movement of molecules are lifted because now the molecule need

not to be confined to a lattice. Secondly, intermolecular interactions being almost negligible in solution each segment of the molecule now has more rotational and orientational freedom. The red shift of the representative bands from solid to solution state along with the increase in linewidth of these bands indicate that the strain imposed in the crystalline state is eased making the respective bonds stronger at the same time increasing the orientational disorder.

4.3.3 The Smectic F (S_F) – Smetic B (S_B) Phase Transition

The changes in Raman spectral parameters viz. peak positions, linewidths and integrated intensities of various core related modes of the compound 5O.6 are found to be almost similar to those of the compound 5O.5 at the smectic G- smectic F, smectic A- nematic and nematic-isotropic phase transitions (Figures 4.3,4.4,4.5). As the temperature range of the smectic C is very small, the spectral changes at the S_C-S_B transition could not be monitored. Therefore, we discuss here the spectral changes at the smectic F – smectic B transition only.

The S_F—S_B phase transition takes place when the sample is heated through a temperature of 42.4 °C. The S_F phase has a c- centered monoclinic lattice with a strong in-plane short range positional correlation and almost negligible inter-layer positional correlation. The molecules in this phase are tilted with respect to the layer planes and are packed in pseudo-hexagonal clusters. In the S_B phase the molecules form stacks of interacting hexatic layers with strong in–plane short range positional correlation. The interlayer positional correlation is almost non-existent in this phase. In this phase, the molecules are not tilted but are orthogonal to the layer planes. So the only difference between the S_F and the S_B phases is that the molecules are tilted

in the S_F phase whereas they are orthogonal in the S_B phase. When the transition from the S_F to the S_B phase takes place the molecules in a hexatic packing order which are tilted in the S_F phase become orthogonal in the S_B phase. Peak positions, linewidths and the integrated intensities of various core related Raman modes of 5O.6 in smectic F and smectic B phase are compared in Table 4.2. A close look at Table.4.2 suggests that there is no major change in either the peak positions or in the linewidths of any of the bands. Very subtle increase in the peak position and linewidths of almost all the bands indicate a slight increase in the freedom of the individual molecules in the S_B phase. Integrated intensity on the other hand, shows considerable increase for those bands which are related to the phenyl ring adjacent to the oxygen atom. Similarly, a decrease is observed in the integrated intensity for the bands related to the C—N stretch. This indicates that due to the change in the alignment of the molecules from a tilted position in the S_F phase to the orthogonal position in the S_B phase, some conformational changes of the phenyl ring around the single bond occur resulting in charge transfer from the nitrogen atom towards the phenyl ring adjacent to the oxygen atom. This charge transfer is possible due to lower electro negativity of nitrogen (2.5) compared to that of oxygen (3.5) permitting the mesomeric delocalization of the π-electron cloud.

4.3.4 Thin Film Form

Free-standing homeotropically aligned thin films of 5O.6 in the S_A phase were obtained on a surface of hylam using a indigenously made high temperature cell. In free-standing films the molecules align parallel to the direction of the incident radiation. In the absence of an applied electric field, molecular orientation

varies continuously over the film surface in 'swirl patterns' [25]. These patterns are interrupted by a small number of point defects which was observed by focussing the transmitted portion of the laser beam to a screen. These patterns stabilized after an interval of 15-20 minutes. In the S_A phase the molecules are arranged in equidistant layers and form a one-dimensional periodic structure in a direction perpendicular to the layers. There is no translational order within the layers, which is a case similar to that of the two-dimensional fluids. But, an orientational order is certainly found to exist and the molecular long axes are on an average oriented perpendicular to the layers. In the films that we have drawn in the S_A phase, the probability that the average long molecular axes are perpendicular to the respective layers is further enhanced. But as stated earlier, these molecules are found to possess a lateral dipole moment. In the absence of an electric field, these dipoles can be assumed to be oriented randomly in two configurations which we may name as the up and the down states for convenience. Due to this random orientation no spontaneous polarization is observed. When the Raman spectra of these molecules in the thin films were recorded, drastic variations were noticed. The peak position of the bands related to the phenyl rings, both the in-plane C–H stretching modes as well as the quadrant stretching modes showed a shift in the peak positions towards lower wavenumber (Figure 4.6). The C—O stretching mode at 1169 cm^{-1} and the C—N stretching mode at 1192 cm^{-1} showed large shift in the peak positions towards the higher wavenumber side. But surprisingly, the C=N stretching mode at 1626 cm^{-1} showed only a subtle shift of peak position to the higher wavenumber side. Figure 4.6 gives a comparison of the Raman spectra in bulk and thin film forms for 5O.6 for clarity. These changes indicate that the central linkage of the core remains

almost unaffected during the formation of the free-standing thin films. There is a transfer of charge from the phenyl rings towards the alkyl chains. Such changes are possible since there are conformational changes in the alkyl chains and also twisting of the whole core around the single bonds at the ends of the core which is facilitated by the attainment of the ordered layered structure in the homeotropic free-standing thin films [26]

4.4 CONCLUSIONS

Our comparative studies on 5O.5 and 5O.6 compounds suggest that the strain on the various segments increases with increase in end chain length of the molecule (i.e., the alkyl chain) as is evident from the decrease of the peak positions in case of the higher homologue 5O.6. In the solution state, though the strain on the molecule due to the lattice is reduced, there is a tendency towards the straightening of the molecule resulting in the increase in strength of all bonds except the weakening of the C=N bond. In the thin film form, the molecules are aligned perpendicular to the layers in a random bipolar orientation without affecting the core much.

REFERENCES

1. Smith, G. W., and Gardlung, Z. G., *J. Chem. Phys.*, **59**, 3214, 1973.

2. Wiegeleben, A., Richter, L., Deresch, J., and Demus, D., *Mol.Cryst. Liq.Cryst.*, **59**, 329, 1980.

3. Goodby, J. W., Gray, G. W., Leadbetter, A. J., and Mazid, M. A., *Liq. Cryst. of one-and two-dimensional order edited by W. Helfrich and G. Heppke* (Springer Verlag) p.3.

4. Pisipati, V. G. K. M., Rao, N. V. S., Potukuchi, D. M., Alapati, P. R., and Rao, P.B., *Mol. Cryst. Liq. Cryst.*, **167**, 167, 1989.

5. Alapati, P. R., Potukuchi, D. M., Rao, P. B., Rao, N. V. S., Pisipati, V.G.K.M., and Paranjpe, A. S., *Liq. Cryst.*, **5**, 545, 1989.

6. Fontana, M., and Bini, S., *Phys.Rev.A*, **14**, 1555, 1976.

7. Dvorjetski, D., Volterra, J. P., and Wiener-Avnear, E., *Phys. Rev. A*, **12**, 681, 1975.

8. Schnur, J. M., Sheridan, J. P., and Fontana, M., in *Proc of Intl. Liq. Cryst. Conference*(Pramana, suppl. No.1) edited by S. Chandrasekhar, 175, 1973.

9. Schnur, J. M., and Fontana, M., *J. Phys (Fr)*, **35**, L-53, 1974.

10. Bulkin, B. J., Grunbaum, D., Kenneley, T., and Lok, W. B., in *Proc. of Intl. Liq. Cryst. Conf.* (Pramana.suppl.no.1) edited by S.Chandrasekhar, 155, 1973.

11. Schnur, J. M., *Mol. Cryst. Liq. Cryst.*, **23**, 155, 1973.

12. Amer, N. M., and Shen, Y. R., *Solid State Commn,*. **12**, 263, 1973.

13. Amer, N. M., and Shen, Y. R., *J. Chem. Phys.*, **56**, 2654, 1972.

14. Sakamoto, A., Yosino, K., Kubo, U., and Inuishi, Y., *Jpn .J. Appl. Phys.*, **13**, 1691, 1974.

15. Dash, S. K., Singh, R. K., Alapati, P. R., and Verma, A. L., *Mol. Cryst. Liq. Cryst.*, **319**, 147, 1998.,

16. Dash, S. K., Singh, R. K., Alapati, P. R., and Verma, A. L., *J.Phys., Cond. Matter,* **9**, 7809, 1997.

17. Bhattacharjee, A., Alapati, P.R., and Verma, A.L., *Liq. Cryst.*, **28**, 1315, 2001.

18. Goodby, J. W., and Gray, G. W, in *Smectic Liquid Crystals,* Leonard Hill, Heyden and Son Inc., Philadelphia, 1987.

19. Alapati, P. R., Pisipati, D. M., Rao, N. V. S., Pisipati, V.G. K. M., Paranjpe, A. S., and Rao, U. R. K., *Liq. Cryst.*, **3**, 1461, 1988.

20. Colthup, N. B., Daly, L. H., and Wiberley, S. E., *Introduction to Infrared and Raman Spectroscopy*, Academic, New York, 1975.

21. Cotton, F. A., *Chemical Applications of Group Theory,* Wiley Eastern Limited, 2ed, 1971.

22. Doucet, J., Levelut, A. M., and Lambert, M., *Phys Rev Lett.*, **32**,301, 1972.

23. Benattar, J. J., Doucet, J., Lambert, M., and Levelut, A. M., *Phys Rev A*, **20**, 2505, 1979.

24. Leadbetter, A. J., Chauhan, J. P., Kelly, B., Gray, G. W. and Goodby, J. W., *J. Phys(Fr)*, **40**, C3-178, 1979.

25. Pindak, R., Young, C. Y., Meyer, R. B. and Clark, N. A., *Phys Rev Lett.*, **45**,1193, 1980.

26. Bahr, Ch., and Fliegner, D., *Phys Rev A*, **46**, 7657 1992.

Table 4.1. Peak positions (cm^{-1}) and linewidths (cm^{-1}) of the various core-related modes of the 5O.5 and 5O.6 molecules along with assignments in the crystalline state, solution and in bulk.

Assignments.	5O.5 (Bulk)		5O.6 (Bulk)		5O.6(Solution)		5O.6 Thin films)	
	P P	L W	P P	L W	P P	L W	P P	L W
Aromatic C-H in plane bending mode.	1162	8.9	1160	8	1161	9.4	1158	9
Aromatic C-H in plane bending mode.	1167	5.5	1165	5.0	1165	6.5	1164	5.7
C-O stretch.	1171	5.9	1169	6.8	1172	6.9	1178	6.0
Aromatic C-N stretching mode.	1194	7. 4	1192	8.4	1195	8.2	1201	8.0
Quadrant stretching mode of the aromatic ring.	1572	7.8	1571	6.53	1573	10.3	1569	9.8
Quadrant stretching mode of the aromatic ring.	1575	7.3	1574	6.8	1576	10.0	1572	9.1
Quadrant stretching mode of the aromatic ring.	1594	6.2	1593	9.0	1595	9.5	1592	8.7
Quadrant stretching mode of the aromatic ring.	1598	7. 7	1597	8. 6	1599	8.7	1596	10.1
C=N stretching mode.	1627	7.3	1626	8.4	1622	8.6	1628	9.3

PP = Peak position, LW = Linewidth

Table 4.2. Comparison of the various Raman parameters of the core-related modes of the 5O.6 molecules in the S_F and the S_B state.

Sr. No	Smectic F state			Smectic B state		
	P P	**LW**	**I I**	**P P**	**LW**	**I I**
1.	1161 cm^{-1}	6.96	29.77	1161 cm^{-1}	6.08	28.82
2.	1166 cm^{-1}	6.73	18.07	1166 cm^{-1}	6.23	23.80
3.	1169 cm^{-1}	5.73	24.67	1170 cm^{-1}	6.20	24.31
4.	1193 cm^{-1}	9.43	27.48	1194 cm^{-1}	9.15	23.06
5.	1570 cm^{-1}	7.18	19.98	1571 cm^{-1}	7.60	19.34
6.	1574 cm^{-1}	5.13	42.06	1574 cm^{-1}	4.70	38.85
7.	1592 cm^{-1}	7.45	17.27	1593 cm^{-1}	7.50	20.96
8.	1596 cm^{-1}	9.66	7.41	1597 cm^{-1}	9.10	5.98
9.	1625 cm^{-1}	10.40	13.26	1626 cm^{-1}	10.60	14.87

PP = Peak position, LW = Linewidth, II = Integrated Intensity

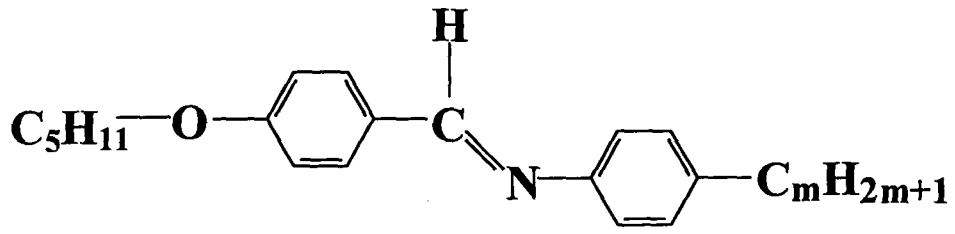

m= 5 and 6

(a) 5O.5

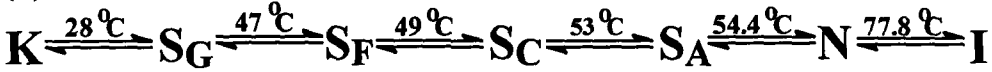

(b) 5O.6

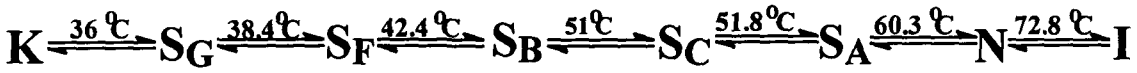

Fig. 4.1. Structure of liquid crystalline compounds 5O.5 and 5O.6 and their respective phase transition sequences. (a) 5O.5 and (b) 5O.6

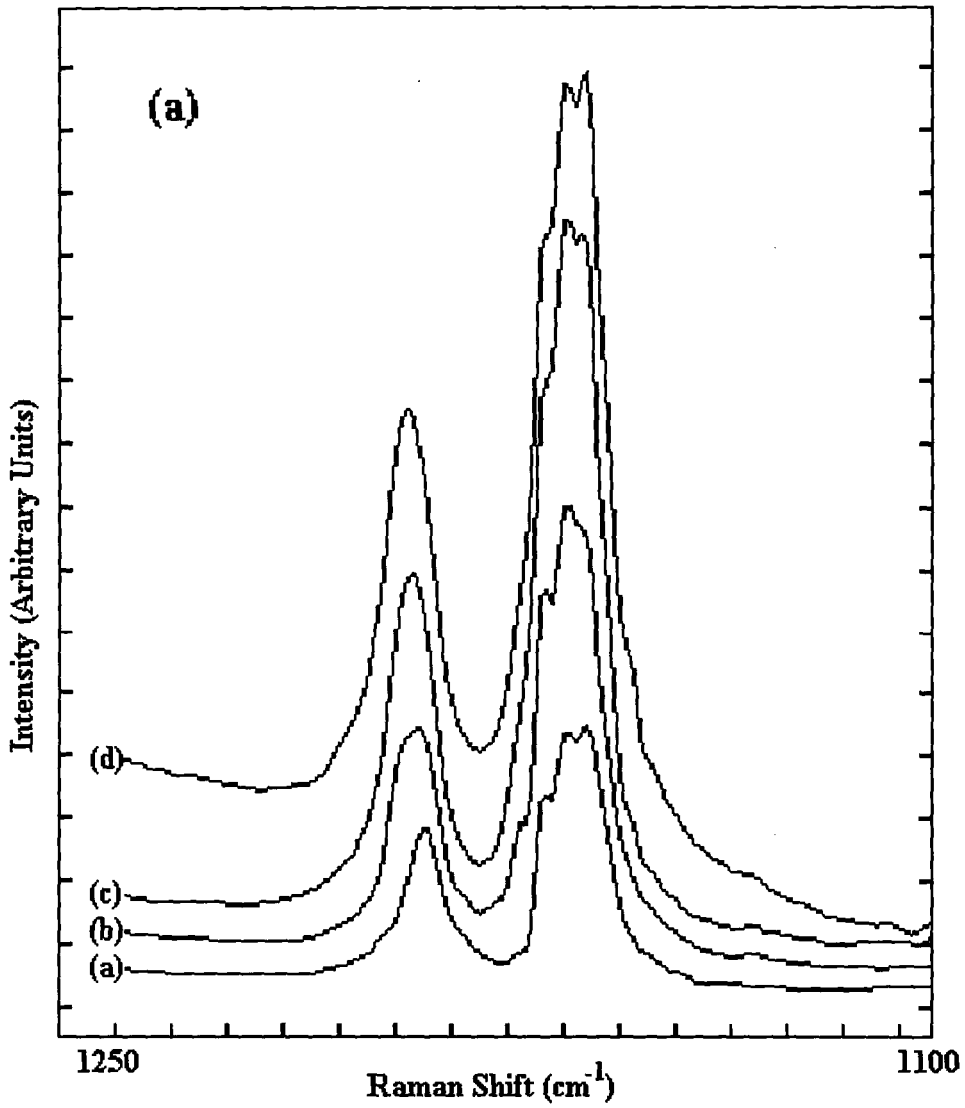

Fig. 4.2a. Raman spectra in the 1100-1250 cm^{-1} region at different phases. (a) 5O.5 Crystalline (K) phase in bulk, (b) 5O.6 Crystalline (K) phase in bulk, (c) 5O.6 liquid crystals in CS_2 solution, (d) 5O.6 liquid crystals in free standing thin films.

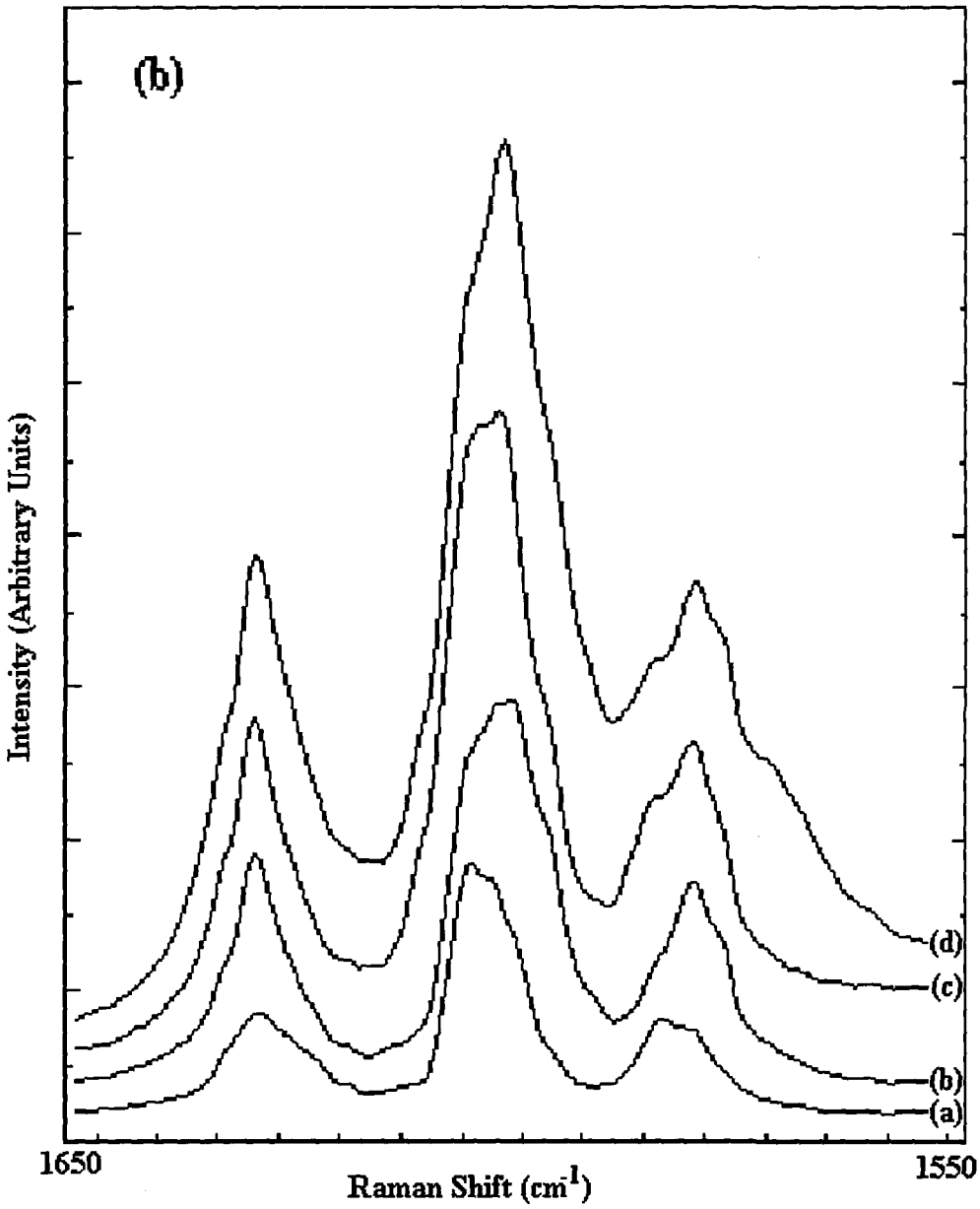

Fig. 4.2b. Raman spectra in the 1550-1650 cm^{-1} region at different phases. (a) 5O.5 Crystalline (K) phase in bulk, (b) 5O.6 Crystalline (K) phase in bulk, (c) 5O.6 liquid crystals in CS_2 solution, (d) 5O.6 liquid crystals in free standing thin films.

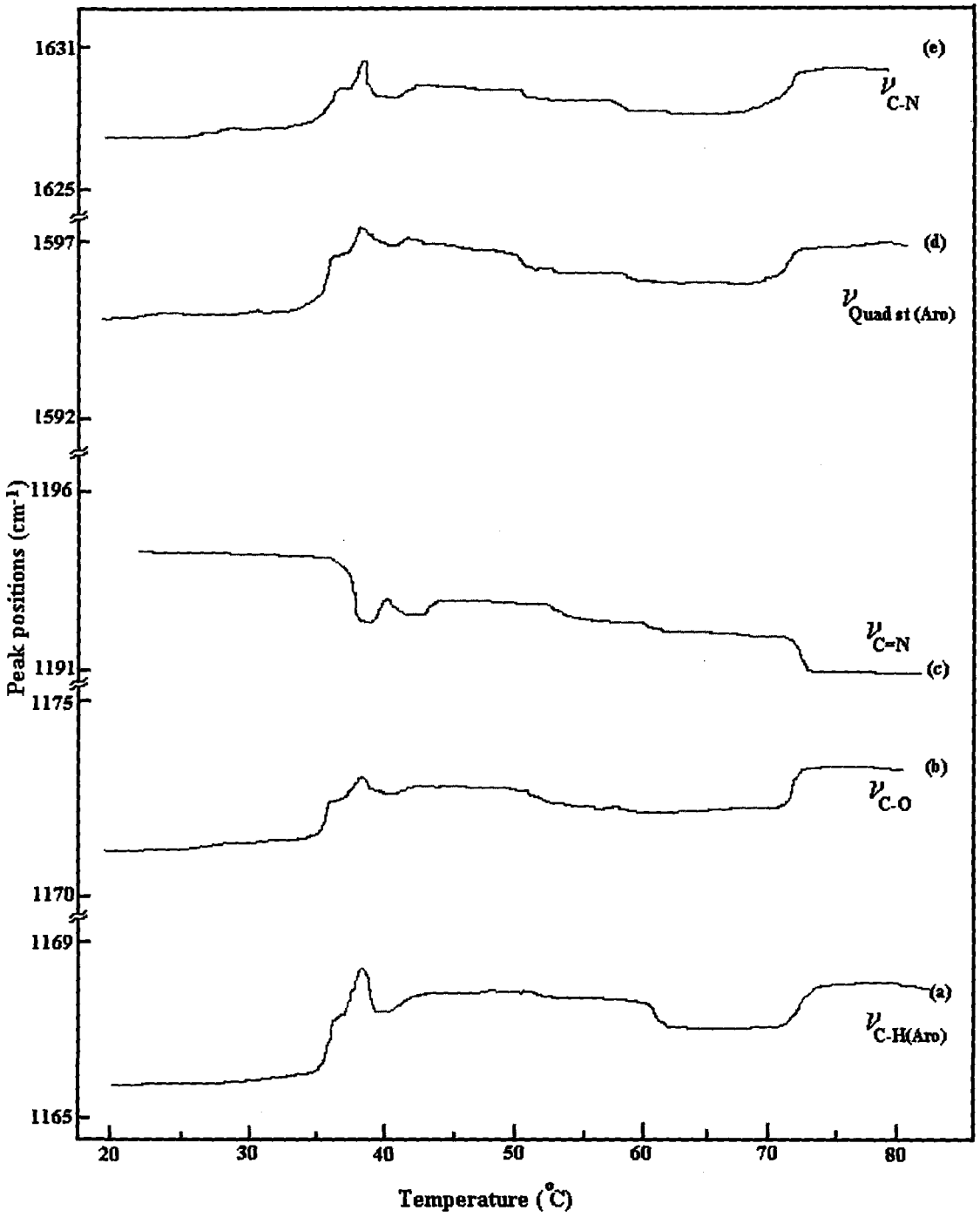

Fig.4.3. Variation of peak positions of the individual bands as a function of temperature. (a) 1165 cm^{-1}, (b) 1169 cm^{-1}, (c) 1192 cm^{-1}, (d) 1593 cm^{-1}, (e) 1626 cm^{-1}. (Uncertainty within ± 0.2 cm^{-1})

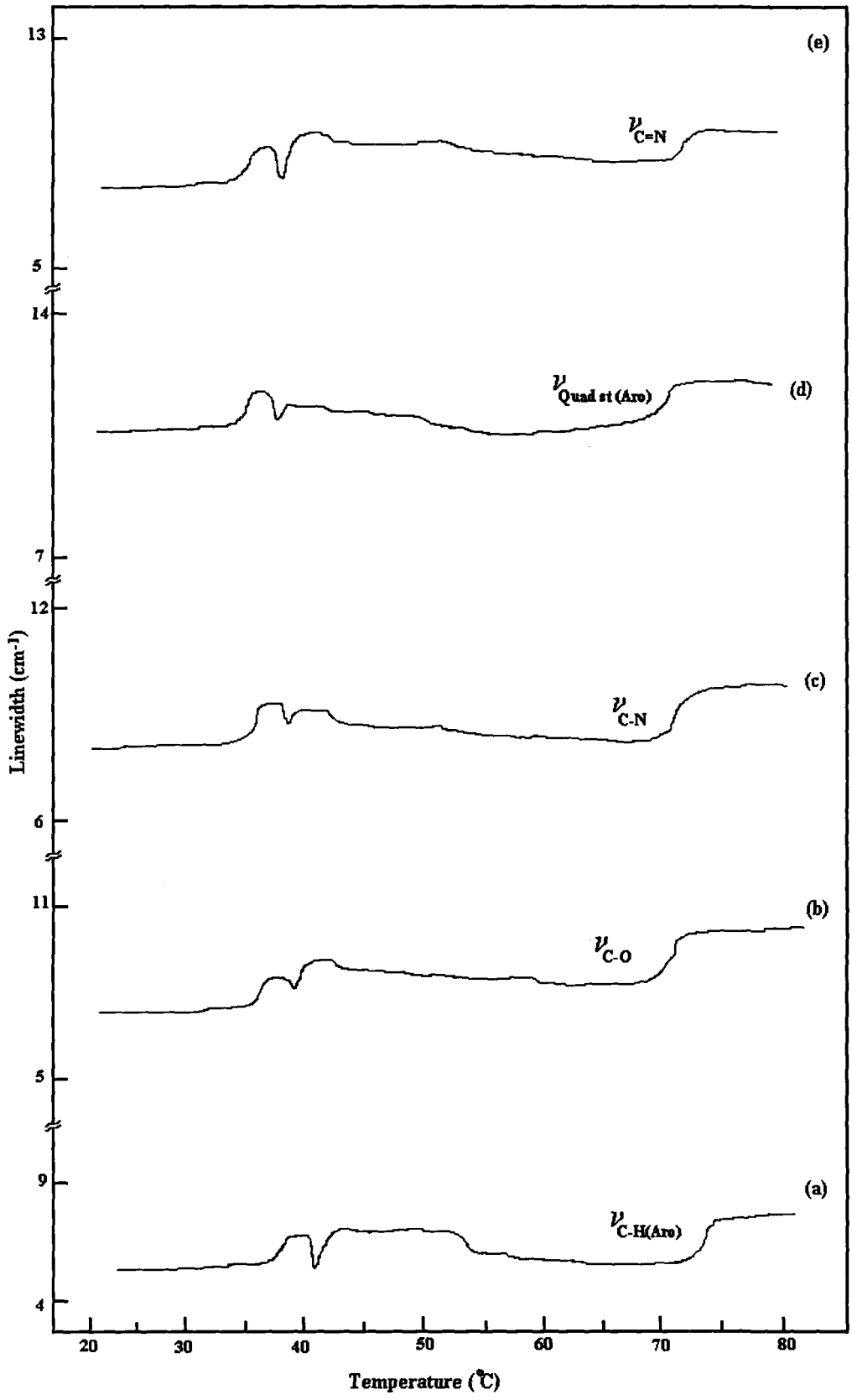

Fig.4.4. Variation of linewidths of the individual bands as a function of temperature. (. (a) 1165 cm^{-1}, (b) 1169 cm^{-1}, (c) 1192 cm^{-1}, (d) 1593 cm^{-1}, (e) 1626 cm^{-1}. (Uncertainty within 2 %)

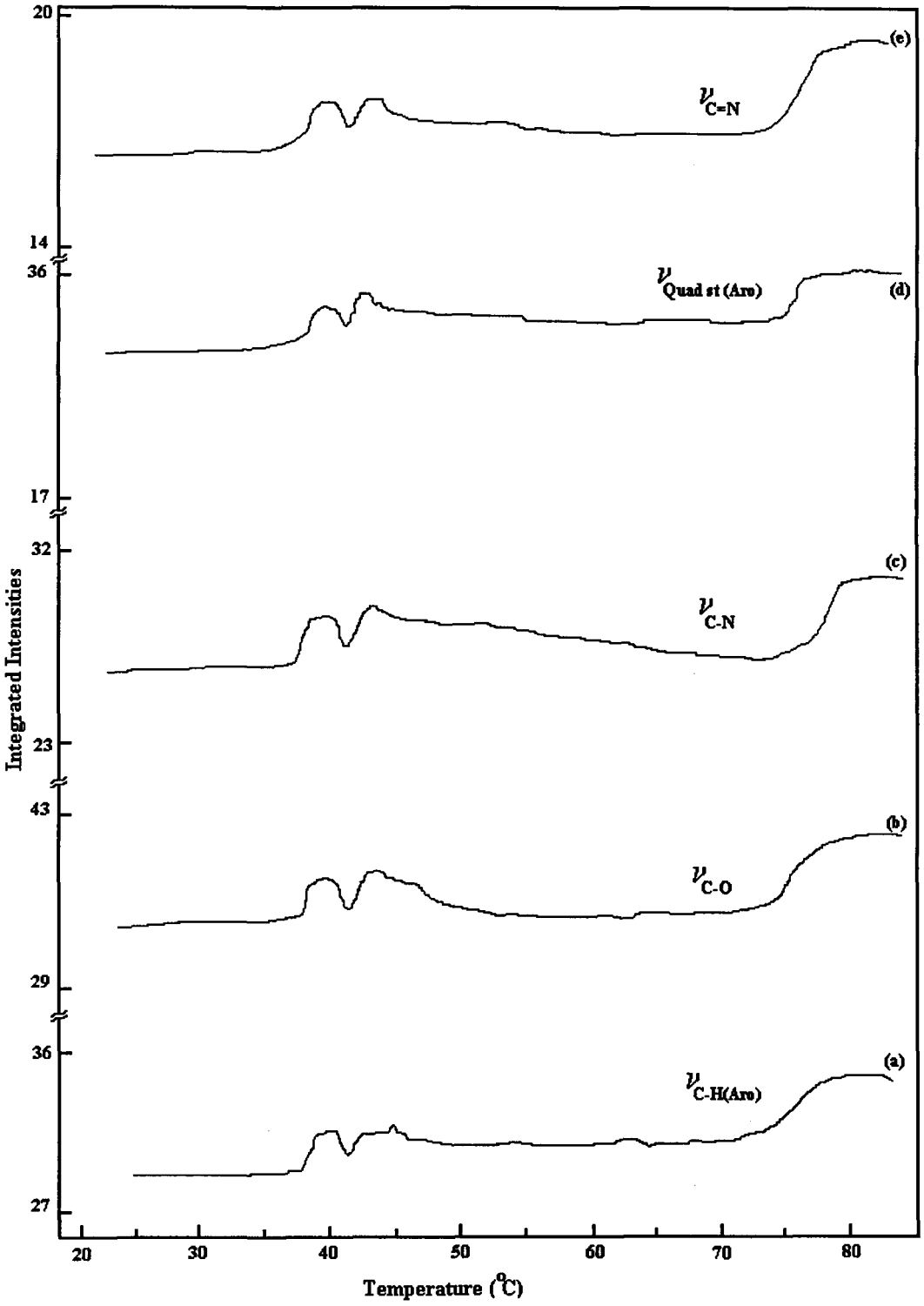

Fig.4.5. Variation of integrated intensities of the individual bands as a function of temperature. (a) 1165 cm^{-1}, (b) 1169 cm^{-1}, (c) 1192 cm^{-1}, (d) 1593 cm^{-1}, (e) 1626 cm^{-1}. (Uncertainty within 2 %)

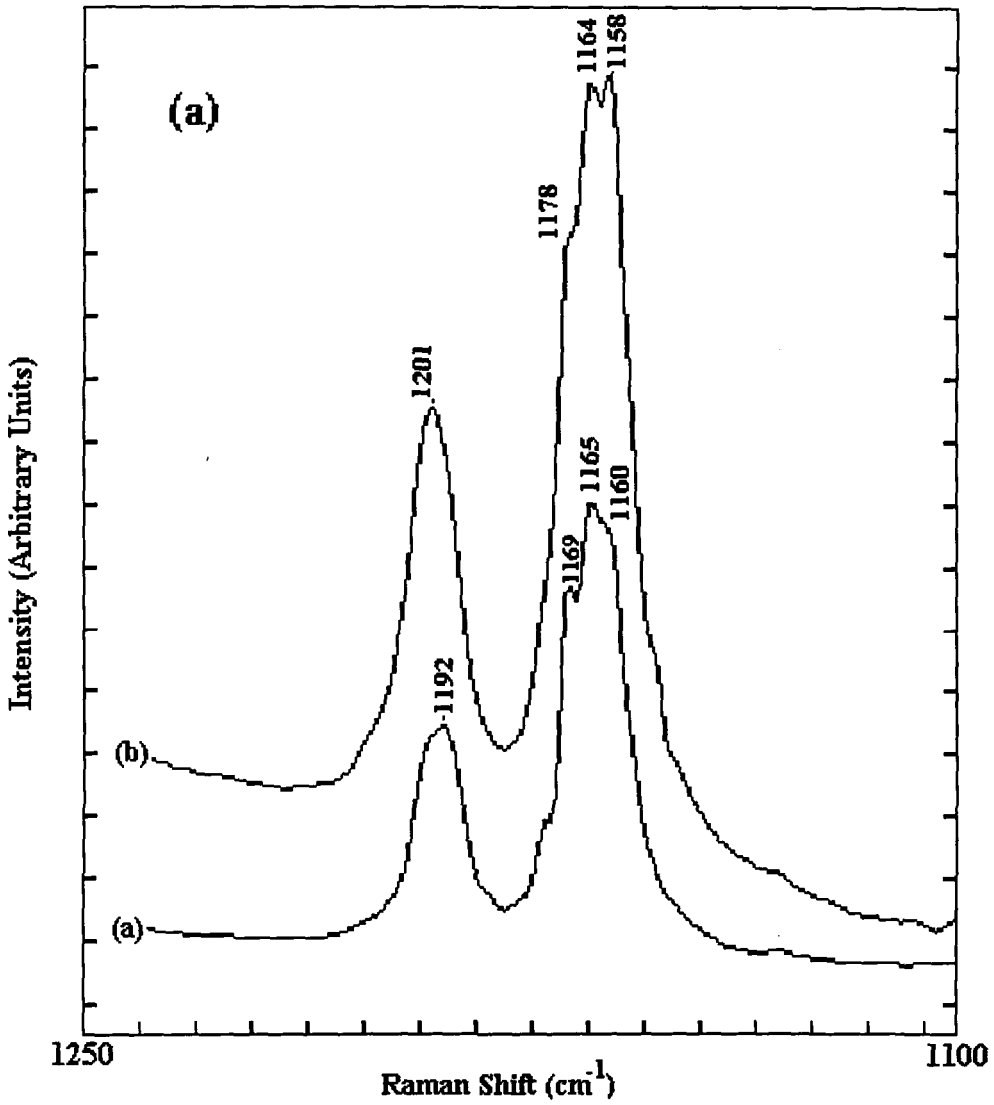

Figure 4.6a Comparative Raman spectra in the 1100-1250 cm^{-1} region in different forms. (a) 5O.6 in bulk and (b) 5O.6 liquid crystals in free standing thin films.

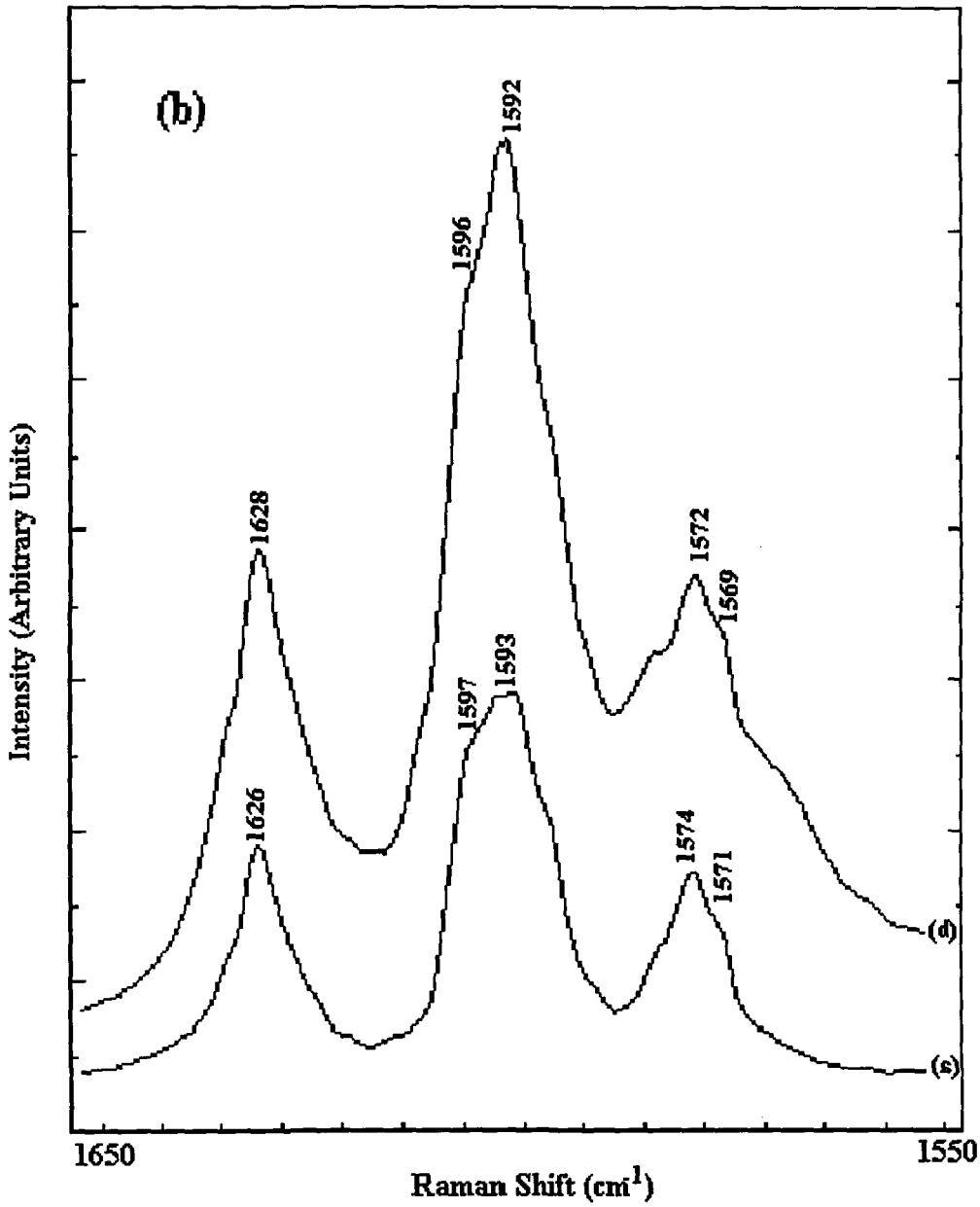

Figure 4.6b **Comparative Raman spectra in the 1550-1650 cm^{-1} region in different forms. (a) 5O.6 in bulk and (b) 5O.6 liquid crystal in free standing thin films.**

Chapter 5

DYNAMICS OF ELECTRIC FIELD INDUCED MOLECULAR REORIENTATION OF A SURFACE-STABILIZED ANTI-FERROELECTRIC LIQUID CRYSTAL IN THE SMECTIC-C* PHASE PROBED BY TIME-RESOLVED INFRARED SPECTROSCOPY.

In this chapter we report polarization dependent and time-resolved Fourier transform infrared (FTIR) studies carried out on the electric field induced ferroelectric phase (S_C^*) of a chiral, anti-ferroelectric liquid crystal at different temperatures. Polarization dependent infrared spectra under dc electric field reveal that the average alkyl chain axis does not coincide with the mesogen axis and is less tilted with respect to the layer normal than the mesogen. The analysis of the various absorbance profiles obtained from temporal response of absorption changes of infrared bands at different time delays provides clear evidence for biased orientation and hindered rotation of almost all the molecular segments around the average molecular long axis and the rotation of the whole molecule around its axis is also hindered. It is further inferred that the mesogen, the chiral segment and the alkyl chains reach their equilibrium orientations at nearly the same time on switching the polarity of the ac electric field but the different molecular segments reorient through different angles.

5.1. INTRODUCTION

The combination of application potentials of the ferroelectric liquid crystals and the advantages of vibrational spectroscopy have been the important considerations for our studies in this chapter. The surface stabilized ferroelectric liquid crystals (SSFLC) are some of the most important liquid crystals with very interesting properties, leading to their applications in high resolution flat panel displays, fast electro-optic devices and many other fields. [1-6]. Generally, the molecules forming the liquid crystalline phases have a number of conformational and orientational states and their statistical distribution and equilibrium populations strongly influence the physical and electro-optical properties [7,8]. The conformation and orientation of the alkyl chains with respect to the average long molecular axis, flexibility of the core and hindered rotation of the molecular segments like carbonyl groups located near the chiral carbon are expected to play dominant role in influencing the dynamical behavior of the system.

Ever since the discovery of antiferroelectric modification of the chiral smectic C_A (S_{CA}*) phase of 4-(1-methylheptyloxycarbonyl) phenyl 4'octygloxyhiphenyl-4-carboxylate (MHPOBC) by Chandani et al [9], considerable effort is being made to understand the role of he different molecular segments in the emergence of ferroelectric/ antiferroelectric states, and mechanism of electric field induced phase transition from S_{CA}* to the ferroelectric S_C* phase during tristable switching [10-13]. In both chiral S_C* and S_{CA}* phases, the molecular director tilts uniformly relative to the layer normal in any smectic layer; the tilt of the neighbouring

molecules is the same in the usual ferroelectric S_C^* phase, while it is equal but opposite in sign in the antiferroelectric S_{CA}^* phase [14].

When an antiferroelctric liquid crystal in the S_{CA}^* phase is placed inside a cell of few μm thickness, the application of electric field higher than a threshold value produces a field induced phase transition from the helicoidal S_{CA}^* to the unbound, uniform S_C^* phase. The average long axis then aligns along the two directions at temperature dependent angles forming surface stabilized states [7,14]. By reversing the polarity of the electric field, the molecules can be switched back and forth from one state to the other state at a fast speed in the microsecond range. The electric field interacts with the polarization and the dielectric anisotropy of the molecules in the process of electro-optical switching, which depends strongly on the molecular conformation and orientational freedom of the different segments about the long molecular axis.

In spite of the great promise of the ferroelectric liquid crystals having fast response and excellent electro-optic properties, the detailed mechanism of field-induced reorientation of different segments of ferroelectric liquid crystals is not yet fully understood. One major hurdle has been the non-availability of suitable time-resolved experimental techniques to probe the structural details at molecular level. As the vibrational frequencies are very sensitive to small changes in the bonding and geometrical arrangement of the atoms in molecules, IR absorption and Raman scattering techniques can provide very useful information about the conformation and hindered rotational motions of individual segments of liquid crystal molecules.

In recent years, time-resolved FTIR spectroscopy has been one of the most extensively employed and powerful technique for probing the switching dynamics

of different molecular segments in liquid crystals [15-25]. By this technique, one can probe the mobility and switching behaviour of each segment of a liquid crystal molecule separately as infrared spectroscopy has the advantage of being bond specific. Two broad ideas have emerged from previous studies. Earlier workers believed that the whole molecule behaves as a rigid unit and all the molecular segments reorient nearly simultaneously [15-18] whereas others have shown that the different molecular segments respond and reorient at different times [19-25]. However, the switching dynamics of ferroelectric liquid crystals at molecular segmental level is a very complicated process and many basic aspects of dynamical behaviour of FLC's have yet to be clarified.

To explore the mechanism of electric-field induced reorientation of different segments of the surface stabilized ferroelectric liquid crystals (SSFLC) in the smectic C^* phase, we report in this study a time-resolved Fourier-Transform infrared (FTIR) study on a chiral, anti-ferroelectric liquid crystal (Chisso-2061) to monitor the response of different molecular segments under pulsed electric field. From detailed analysis of the temporal responses of absorption changes of selected IR bands over a range of polarizer orientations, we have found clear evidence for hindered rotation of all the molecular segments around the long molecular axis. It is also inferred that both the mesogen and alkyl chains start reorienting immediately on application of the electric field and that the mesogen as well as the alkyl side chains reorient at almost the same rate during the process of electro-optical switching. In contrast to previous results [15-25], our studies also indicate that the rotation of the whole molecule is not free but is biased around the long molecular axis.

5.2. EXPERIMENTAL DETAILS

Chiral antiferroelectric liquid crystal (AFLC), 4-(1-methylheptyloxy carbonyl) phenyl 4-(4'-octyloxy benzoylxy) benzoate, named as Chisso 2061, was obtained from the Chisso Company, Japan. The structure and the phase transition sequence of this sample are shown in Figure. (5.1). The pure sample was directly used for our experiments. The details regarding its synthesis are given in reference [26].

A sample cell was constructed using two BaF_2 plates coated with a conducting layer of indium tin oxide (ITO) and polyvinyl alcohol rubbed in one direction. The cell was filled with the melted sample by capillary action. Monodomains of the sample inside the cell were obtained by employing cyclic and slow temperature treatment under an electric field of ±15 V. A JOEL JIR-6500 Fourier transform infrared spectrometer equipped with a micro-attachment (JEOL IR-MAU 110) and a mercury-cadmium-telluride (MCT) detector was used for obtaining the data. A wire grid polarizer was rotated about the direction of the IR radiation for making polarization dependent studies.

The measurement geometry is schematically shown in Fig 5.2, where the horizontal dashed line along the Y-axis indicates the projection of the smectic layer normal in the plane of the cell windows. The two surface stabilized states are indicated by arrows I and II, which are the projections of the long molecular axes in the plane of the cell windows in states I and II. The polarization direction was fixed at 45° to the rubbing direction. In order to make time-resolved measurements the same instrument equipped with a boxcar integrator (SRS Model-250) was used. Rectangular wave electric field of ±15 V at 5 kHz repetition rate was applied

between the electrodes of the cell from a function generator (Kenwood FG-273). The time-resolved polarized spectra were measured from 0 to 100 μs with a resolution of 4 cm^{-1} and 100 scans were accumulated in each case. Baseline corrections of the spectra were made using a non-linear spline function and curve fitting was done using GRAMS software. As the different spectral regions show many overlapping components, we have deconvoluted the relevant bands and have used the peak heights of the deconvoluted components as a measure of absorbance.

5.3. Results and Discussion

5.3.1 Static switching behaviour

Fig.5.3 shows polarized IR spectra as a function of the polarization angle ω for a monodomain of the sample in the smectic C_A* phase at ω = 0 and 90°. The polarization angle ω is the angle between the direction of rubbing (i.e., the smectic layer normal) and the polarization direction of the incident IR radiation; and is taken to be zero when these two directions coincide. From these spectra the dichroic ratio D, defined as the ratio of absorbances for the parallel and perpendicular polarizations of light, were calculated for different bands. Table 5.1 lists the assignment of the bands based on expected group frequency considerations and previous works [27-28] with their dichroic ratios. It is to be noted that due to the presence of $-CH_2$ and $-CH_3$ groups in both the achiral and the chiral chains, only averaged information can be obtained from the C-H stretching modes. A noticeable feature observed is that the dichroic ratios for the alkyl chain modes are $\leq$1, which can be ascribed to the disordering of the chains. For the bands related to the

mesogen segments, the dichroic ratio is found to vary widely (≈2.3 to 7.6) suggesting that there is substantial disorder in the core and also that the benzene rings may be skewed with respect to each other in the smectic C_A* phase. An interesting feature in the IR spectrum is the observation of two components in the C=O stretching mode region at 1741 and 1720 cm^{-1}. The origin of the former is attributed to the C=O groups between the phenyl rings and that of the latter is ascribed to the C=O groups adjacent to the chiral part.

For detailed study on the behavior of different molecular segments, few relevant and comparatively isolated bands were chosen. The band at 2930 cm^{-1} (CH_2 antiymmetric stretch) provides information that is exclusive to the alkyl chain portion. The bands observed at 1741 ($\nu_{C=O}$), 1510 ($\nu_{C=C}$), 1603 ($\nu_{C=C}$) and 1160 cm^{-1} (phenyl ring C-H in plane deformation) are all related to the mesogen portion while one clear band at 1720 ($\nu_{C=O}$) cm^{-1} is related to the chiral portion of the molecule. At zero applied voltage the mesogen bands show parallel dichroism with their maximum intensity (I_{max}) at $\omega = 0^{\circ}$ and 180° while the alkyl chain bands exhibit perpendicular dichroism with their I_{max} at $\omega = 90^{\circ}$ and 270°. For monitoring the relative orientation of the alkyl chain, mesogen, and the chiral segments, polarization-dependent IR spectra of the sample in the electric field induced smectic -C* phase were measured at 75 ^{0}C under dc voltages of 0 and ± 15 volts. The polarization dependence of absorption peaks can be conveniently described by the plots in Figures. 5.4a, b, c and b where the peak absorbance $A(\omega)$ at a particular polarization angle ω is plotted as a function of ω. It is clear from this figure that the absorbance of the bands for all the three segments attain their maxima at different

angles of polarization. Another very interesting observation in this study is that the absorbances for the bands associated with the different segments maximize at different angles for negative and positive bias voltages. For example, the mesogen bands at 1510 and 1603 cm^{-1} at 75 °C show absorbance maxima at $\omega = -18^{o}$ at +15 V whereas the absorbance maxima occurs at $\omega = +10^{o}$ at –15 V. Similar variations in the angular shifts of the peak profiles for the bands associated with the other segments of the molecule have been observed, the details of which are given in Table. 5.2. Also one can see that the observed rotation of the absorbance maxima for positive and negative polarity $\Delta\omega$ is distinctly different for the bands related to the different segments. The maximum tilt angle $\Delta\omega$ for the bands due to the mesogen is 28^{o}, that for the alkyl chains is 23^{o} whereas for the modes related to the chiral part it is 21^{o}. As the estimated uncertainty in the measurement of the polarization angles is not more than $\pm 1^{o}$, these differences in the value of ω for positive and negative biasing are very significant. Qualitatively, one can understand the different values of the maximal tilt angles $\Delta\omega$ for the mesogen and alkyl chains modes in terms of a steric and zigzag model of the molecules arranged in smectic layers where the aromatic cores may be packed up in a higher tilted orientation in the smectic layers than the molecule as a whole. On the other hand, the inconsistency in the angular shifts in the peak positions for the positive and negative polarity of the applied electric field provides strong evidence that the rotation of the molecule along the long molecular axis is not free and is a clear manifestation of the hindered rotation. In other words, it appears that the rotation of the whole molecule is biased around its long molecular axis with the molecule adopting some

preferential orientation. This important finding is also supported by our time-resolved studies (see later). Although the interface-induced electroclinic effect may play some role for the observed inconsistencies in the orientations of different segments of the molecule, this effect alone can not explain the different values of maximal tilt angles $\Delta\omega$ for the mesogen and alkyl chains modes and other effects observed during dynamical switching.

In order to understand the behaviour of the system in details, we consider a vibrational mode N of the molecule confined in a laboratory frame of reference with its transition dipole moment **p** oriented along a fixed angle α_N with respect to the molecular axis M. The molecular axis M is, in turn, oriented with respect to the mean orientation direction **n** by an angle θ.

Then the long axis order parameter about **n** is given by [27].

$$S = \langle P_2(\cos\theta) \rangle = \frac{1}{2}\langle (3\cos^2\theta - 1) \rangle \qquad (5.1)$$

where P_2 is a Legendre polynomial of order 2. The dichroic ratio is related to the average $\langle\cos^2\theta\rangle$ for a particular band whose transition dipole moment is oriented at an angle α_N relative to the long molecular axis by the relation given below [29]:

$$D(S,\alpha_N) = \frac{A_Z}{A_Y} \qquad (5.2)$$

$$= \frac{[1+2P_2(\cos\alpha_N)S]}{[1-2P_2(\cos\alpha_N)S]}$$

$$= \frac{\left\{\frac{1}{2}\sin^2\alpha_N\cos^2\theta\left[1-\langle\cos^2\theta\rangle S\right]+\cos^2\theta\langle\cos^2\alpha_N\rangle\right\}}{\left\{\frac{1}{2}\sin^2\alpha_N\cos^2\theta\left[1-\langle\cos^2\theta\rangle S\right]-\cos^2\theta\langle\cos^2\alpha_N\rangle\right\}}$$

The mean orientation of the transition dipole moment with respect to the average long molecular axis is obtained as,

$$\cos^2\alpha_N = \frac{1}{3}\left[\frac{2(D-1)}{S(D+2)}+1\right] \qquad (5.3)$$

As the value of the dichroic ratio for the C-O stretches observed at 1265 and 1237 cm^{-1} are relatively large (>4), therefore we can assume that the transition dipole moment for these bands lie along the long molecular axis, i.e. θ =0 in these cases. Using this in equation (5.1) we obtain the value of S to be 0.92. This value of S along with the value of D measured from our experiments is used to calculate the mean orientation α_N of the transition dipole moments. The average values of α_N are obtained as 24°, 36°, 24, 61°, 62° and 64° for the bands observed at 1160, 1510, 1603, 1720, 1741 and 2930 cm^{-1}, respectively. These values of α_N indicate that the deviations from isotropic averaging of different functional groups about the long molecular axis are not negligible.

As stated earlier we have found that the dichroic ratio of the C=C stretching mode at 1603 cm^{-1} is 7.66 while for the other phenyl ring modes it varies from 2.7 to 7.3. A magnified view of the spectrum shows presence of fine structures in the bands which may originate from the combined effects of non-planarity of the benzene rings having different environments and conformational isomers of the core. In similar type of compounds, the para-benzene ring axis is found to be tilted from the long molecular axis by more than 20° [28-30]. The torsional angle $\angle C_{C=O}—O—C_{Ph}—C_{Ph}$ is reported to be around 55° whereas the torsional angle $\angle C_{Ph}—C_{Ph}—C_h—O$ is only about 5°. Hence the core of the molecule is non-planar with the benzene rings skewed with respect to each other by about 50° to 60°.

Similar results have also been obtained using quantum orbital calculations on related molecules [28,31,32]. Due to the non-planar structure and hindered rotation of the molecule around its long molecular axis, it will not reorient to mirror symmetric position on changing the polarity of the electric field. The electrostatic and quadrupolar interactions between the chiral centre and the non-symmetrically distributed highly polarizable groups like carbonyl groups are likely to contribute significantly to the molecular anchoring strength which will influence the rotational freedom of the molecules. As a result of these interactions, the molecule may not reorient freely with change in the electric field bias but may adopt some privileged orientation.

On the basis of these findings it is inferred that in the Chisso-2061 sample in the smectic C_A* phase, the alkyl chains are tilted at different angles with respect to the smectic layer normal in the equilibrium state. In this static arrangement the magnitude of the tilt angle for the various segments depends on the polarity of the applied voltage. There is a substantial disorder in the alkyl chains due to the presence of gauche conformations. The benzene rings are also skewed with respect to each other. When the polarity is reversed, the applied electric field rotates the different segments of the molecule to new positions which are not mirror symmetric about the layer normal.

5.3.2 Dynamical Switching Behavior

In order to probe the dynamical switching behavior from one surface stabilized state to another on application of ac electric field, time-resolved infrared measurements were carried out. FTIR spectra of the sample were recorded at 75 °C

on application of ± 15 volts at 5 kHz repetition rate. The participation of all the segments in the switching process is evident from the intensity variations of the associated modes on the change of polarity of the electric field. As the tilt angle varies with the applied electric field and temperature, the normalized absorbance changes dA_n were calculated for a quantitative comparison of the reorientation rates of molecular segments at different voltages using the relation:

$$dA_n = \frac{|A(t) - A(2)|}{|A(1) - A(2)|} \qquad (5.4)$$

where A(t) is the peak absorbance at time t, A(1) and A(2) are the peak absorbance values at the surface stabilized states I (before the application of electric field) and II (when the reorientation is completed), respectively. These plots also provide information about fractional reorientation of the segments of the molecule at a particular time. Fig. 5.5 shows the plot of dA_n vs. delay time (μs) during the course of switching for selected bands characterizing the mesogen, chiral and alkyl chain segments at 75 °C and 15 V amplitude of the voltage pulse. This figure makes it clear that the reorientation from one state towards other state starts immediately on application of the field and the normalized absorbances of the various modes show a very similar rate of increase till a saturation point is attained. After a certain period (≈ 28 μs), the molecule attains the second surface-stabilized state. A significant point to be noted here is that all the segments of the molecule appear to switch (i.e. attain the second surface stabilized state) at the same time under the present experimental conditions. To quantify the field induced orientations on application of an ac electric field, measurements conducted before, during and after the switching process reveal beyond uncertainty limits that the magnitudes of orientation angles of

the peak absorbances of the different bands are not equal as shown in Fig. 5.6. For example, change in ω for the mesogen bands at 1603 and 1510 cm^{-1} is -18° at 0 μs while it is $+10^{\circ}$ at 80 μs. The net change in the orientation of the dipole moment for the core bands is 28° while that for the alkyl chain bands is 23°. The variation in case of the chiral mode was found to be 21°. This trend is consistent with our static data.

For exploring the response of the different molecular segments to the applied ac electric field, we measured the temporal responses of absorbance changes of the representative bands over a range of polarizer orientation at different time delays at 10 μs time intervals. In Fig. 5.7 we have plotted mean orientation angle $\theta_0(t)$ as a function of delay time for the representative bands of different segments. A significant feature seen here is that the different segments reorient through different angles. The modes related to the mesogen reorient from -20° to $+15^{\circ}$, those related to the chiral part reorient from -15° to $+10^{\circ}$, whereas the alkyl chain modes switch from -15° to $+5^{\circ}$. This figure also shows that there is no induction period for any segment of the molecule within the present experimental conditions. These results are fully consistent with our static data under dc electric field. The non-isotropic rotation of the molecule along its long molecular axis is manifested in the dynamic switching as well as in experiments done under dc electric field. We suggest that the inconsistency in the angular shifts in the peak positions arises as a result of anisotropic interactions among the non-cylindrically distributed dipoles leading to the formation of non-symmetric surface stabilized

states where the average molecular axis may align along two directions at different angles from the normal to the smectic layers.

5.5. Conclusion.

To conclude this chapter we can say that contrary to the existing beliefs, not only the individual segments but the reorientation of the entire molecule along the long molecular axis is biased in this antiferroelectric liquid crystal. It is also observed that the different segments reorient through different angles during dynamic switching as well as under dc electric field. The benzene rings are found to be skewed with respect to each other forming a non-planar structure which results in a distorted packing of the aromatic cores in the smectic layers.

References

1. Lagerwell, S. T., Clark, N. A., Dijon, J., and Clerc, J. F., *Ferroelectrics.*, **94**, 30, 1989.

2. Clark, N. A., and Lagerwell, S. T., *Appl. Phys. Lett.*, **36**, 899, 1980.

3. Clark, N. A., and. Lagerwall, S. T, *Ferroelectrics.*, **59**, 25, 1984.

4. Matsumoto, S., Maruyama, A., Hatho, H., Kinoshita, Y., Harai, H., Ishikawa, M., and Kamagani, S., *Ferroelectrics.*, **85**, 235, 1988.

5. Dijon, J., in *Liquid Crystals, Application and Uses*, ed. by B. Bahadur, World Scientific, Singapore, 1990, **1**, 305, 1992.

6. Goodby, J. W., Blinc, R., Clark, N. A., Lagerwell, S. T., Osipov, M. A., Pikin, S. A., Sakurai, T., Yoshino, K., and Zeks B., *Ferroelectric Liquid Crystals: Principles, Properties and Applications,* Gordon and Breach, Philadelphia, 1991.

7. Kim, K. H., Ishikawa, K,. Takezoe, H, and Fukuda, A., *Phys. Rev. E* **51**, 2166 1995.

8. Jin, B., Ling, Z., Takanishi, Y., Ishikawa, K., Takezoe, H., Fukuda, A., Kakimoto M., and Kitazume, T., *Phys. Rev. E* **53,** R4295, 1996.

9. Chandani, A. D. L., Hagiwara, T., Suzuki, Y., Ouchi Y., Takezoe, H., and Fukuda A., *Jpn. J. Appl. Phys.*, **27**, L729, 1988.

10. Bahr, Ch., Fliegner, D., Booth, C. J., and Goodby, J. W., *Phys. Rev. E.*, **51**, R3823, 1995.

11. Rovsek, B., Cepic, M., and Zeks, B., *Phys. Rev. E.*, **54**, R3113, 1996.

12. Tajari, K., Yamada, N., Orihara, H., Takanishi, I., Terauchi, H., Harada, J., and Ishibashi, Y., *J. Phys. Soc. Jpn.*, **64**, 3157, 1995.

13. Toriumi, H., Yoshida, M., Mikami, M., Takeuchi, M., and Mochizuki, A., *J. Phys. Chem.*, **100**, 15207, 1996.

14. Fukuda, A., Takanishi, Y., Isozaki, T., Ishikawa, K., and Takezoe, H., J., *Mater. Chem.*, **4**, 997, 1994.

15. Katayama, N., Czarnecki, M. A., Satoh, M., Watanabe, T., and Ozaki, Y., *Appl. Spectrosc.* **51**, 487, 1997.

16. Shilov, S. V., Skupin, H., Kremer, F., Gebhard, E., and Zentle, R., *Liq. Cryst.*, **22**, 203, 1997.

17. Shilov, S. V., Okretic, S., Siesler, H. W., and Czarnecki, M. A., *Appl. Spectrosc. Rev.*, **31**, 82, 1996.

18. Shilov, S. V., Skupin, H., Kremer, F., Wittig, T., and Zentle, R., *Phys. Rev. Lett.* **79**, 1686, 1997.

19. Hide, F., Clark, N. A., Nito, K., Yasuda, A., and Walba, D. M., *Phys. Rev. Lett.* **75**, 2344, 1995.

20. Verma, A. L., Zhao, B., Terauchi, H., and Ozaki, Y., *Phys. Rev. E* **59**, 1868, 1999.

21. Verma, A. L., Zhao, B., Ziang, S. M., Shen, J. C., and Ozaki, Y., *Phys. Rev. E* **56**, 3053, 1997.

22. Nagasaki, Y., Masutani, K., Yoshihara, T., and Ozaki, Y., *J. Phys. Chem.*,**104**, 7881, 2000.

23. Nagasaki, Y., Yoshihara, T., and Ozaki, Y., *J. Phys. Chem.* **104**, 2846, 2000.

24. Nagasaki, Y., and Ozaki, Y., *Phys. Chem. Chem. Phys.* **2**, 3037, 2000.

25. Tian, Y., Xu, X., Zhao, Y., Tang, X., Su, F., Zhao, X., and Zhou, E., *Liq. Cryst.* **19**, 295, 1995.

26. Inukai, T., Furukawa. K., Terashima, M., Saito, S., Isogai, M., Kitamura, T., Mukoh, A., *Proc. 12th Jpn. Liq. Cryst. Conf.*, 112, 1986.

27. Michl, J., and Thulstrup, E. W., *Spectroscopy with Polarized Light, Solute Alignment by Photoselection in Polymer, Liquid Crystals and Membranes,* VCH Verlasgsgesellschaft, Weinheim,1986.

28. Kocot, A., Wzralik, R., Orgasingka, B., Perova T., Vij, J. K, and Nguyen, H. T., *Phys. Rev. E* **59**, 551 1999.

29. Hild, E., Kocot, A., Vij, J. K, and Zentel, R., *Liq. Cryst*, **16**, 783, 1994.

30. Vij, J. K., Kocot, A., Kruk, G., Wrzalik, R., and. Zentel, R., *Mol. Cryst. Liq. Cryst*, Sci. Technol., Sect.A, **237**, 337, 1993.

31. Tishiro, K., Hao, J., Kobayashi, M., and Inone, T., *J. Am. Chem. Soc.* **112**, 8273, 1990.

32. Centore, R., and. Tuzi, A, *Acta Crystallogr., Sect. C: Cryst. Struct. Commun.* **45**, 107, 1998.

Table.5.1. Dichroic ratio (D) and vibrational band assignment for the relevant peaks in the infrared spectra of Chisso-2061 liquid crystal in the Sm-C_A* phase at 75 ^{0}C.

Wavenumber (cm^{-1})	$D(A_{\parallel}/A_{\perp})$	Assignment
2958	1.17	CH_3 asym st.
2930	0.50	CH_2 antisym st.
2871	1.17	CH_3 sym st.
2859	0.85	CH_2 sym st.
1741	0.57	C=O st. (Ph-COO-Ph) (core)
1720	0.66	C=O st. (Ph-COO-R) (chiral)
1603	7.66	C=C (phenyl) st.
1578	2.70	C=C (phenyl) st.
1510	3.36	C=C (phenyl) st.
1504	3.42	C=C (phenyl) st.
1467	1.07	CH_2 scissoring mode
1457	0.81	CH_2 scissoring mode
1421	2.08	CH_2 scissoring mode
1413	2.06	CH_2 scissoring mode
1379	0.10	CH_3 in-plane deformation
1324	1.67	Phenyl C=C in plane
1305	5.67	Phenyl C=C in plane
1265	4.11	C-O st.
1237	4.63	C-O st.
1203	4.58	C-O st. ?
1160	7.32	phenyl C-H in plane deformation
1113	2.37	C-C-C in plane stretch and CH_3 rock
1097		phenyl C-H in plane deformation
1057	4.28	phenyl C-H in plane deformation
1015	6.67	phenyl C-H in plane deformation
888	0.12	C-C-C in plane stretch and CH_3 rock
846	0.37	Skeleton

Table. 5.2. Values of angular shift ω of peak profiles and total angular variation Δω with applied electric field in the Sm-*C** phase of Chisso-2061 at 75 ^{0}C.

Band position ⇒	1160 cm^{-1}	1203 cm^{-1}	1510 cm^{-1}	1602 cm^{-1}	1720 cm^{-1}	1741 cm^{-1}	2930 cm^{-1}
-15 V	10^0	7^0	10^0	10^0	7^0	10^0	9^0
15 V	-18^0	-14^0	-18^0	-18^0	-14^0	-18^0	-14^0
Δω	28^0	21^0	28^0	28^0	21^0	28^0	23^0

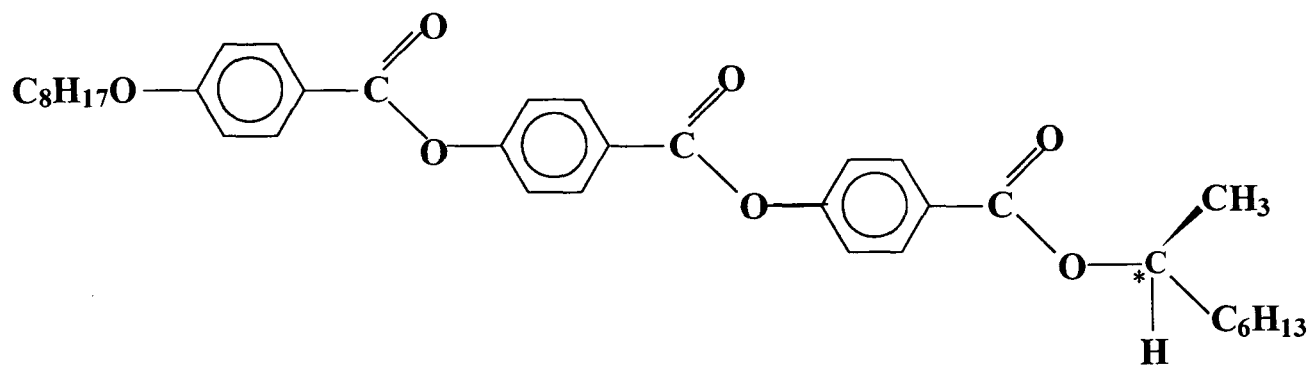

$$Cr \xrightleftharpoons{52.0} S_{IA}^{*} \xrightleftharpoons{68.4} S_{CA}^{*} \xrightleftharpoons{88.2} S_{A} \xrightleftharpoons{142.3^{o}C} Iso$$

Fig. 5.1. Structure of the Chisso-2061 chiral antiferroelectric liquid crystal and its phase transition temperatures.

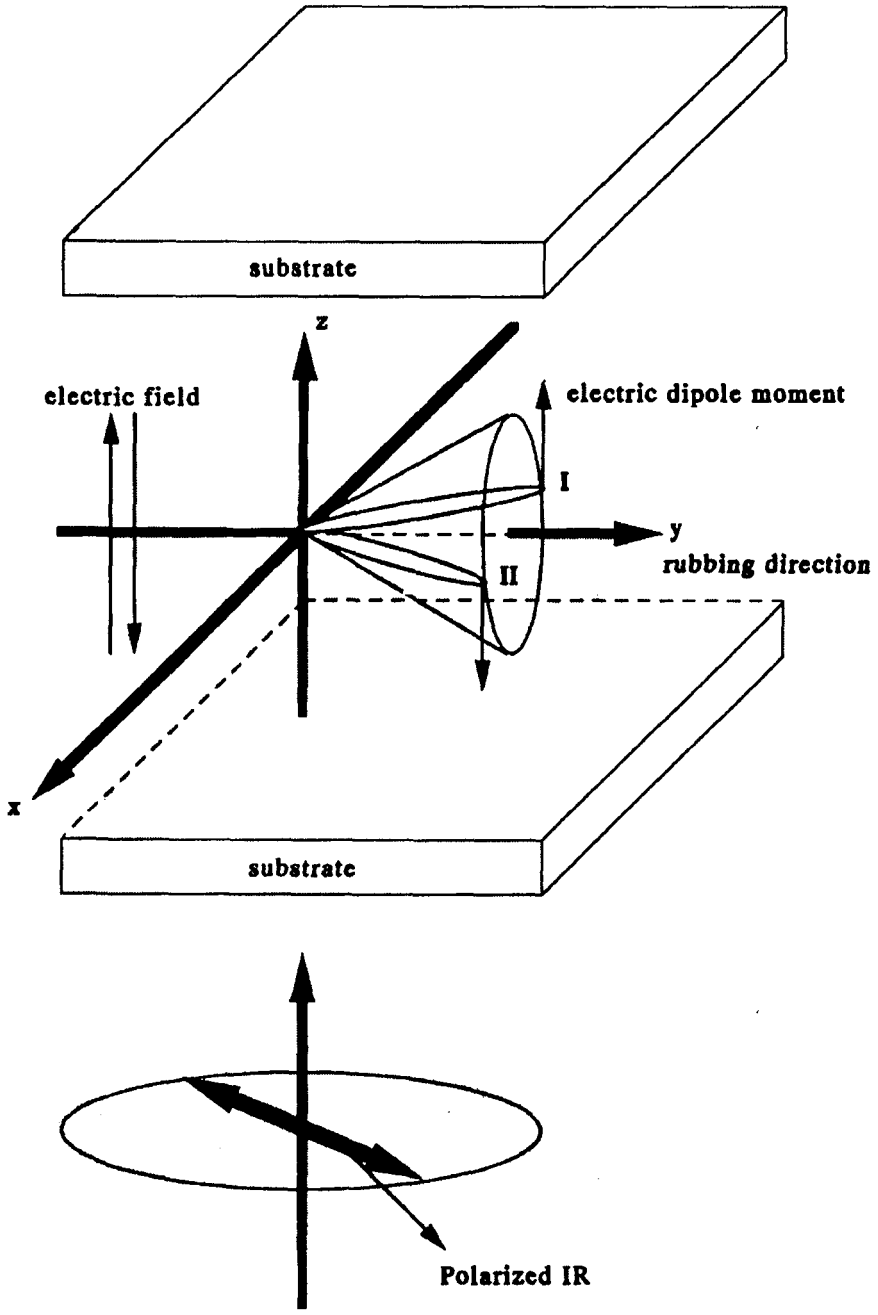

Fig 5.2 Schematic arrangement for the time resolved infrared measurements. I and II are the projections of the directions of the long molecular axis in the plane of the cell window, YZ (surface stabilized states of the ferroelectric liquid crystal), θ is the angle between the projection of the long molecular axis and the projection of the smectic layer normal in the plane of the cell windows (broken line parallel to the rubbing direction, Z). E is the direction of the applied electric field, X is the direction of the infrared light, $P_{\perp}$ and $P_{\parallel}$ represent the horizontal and vertical polarizations of the light respectively.

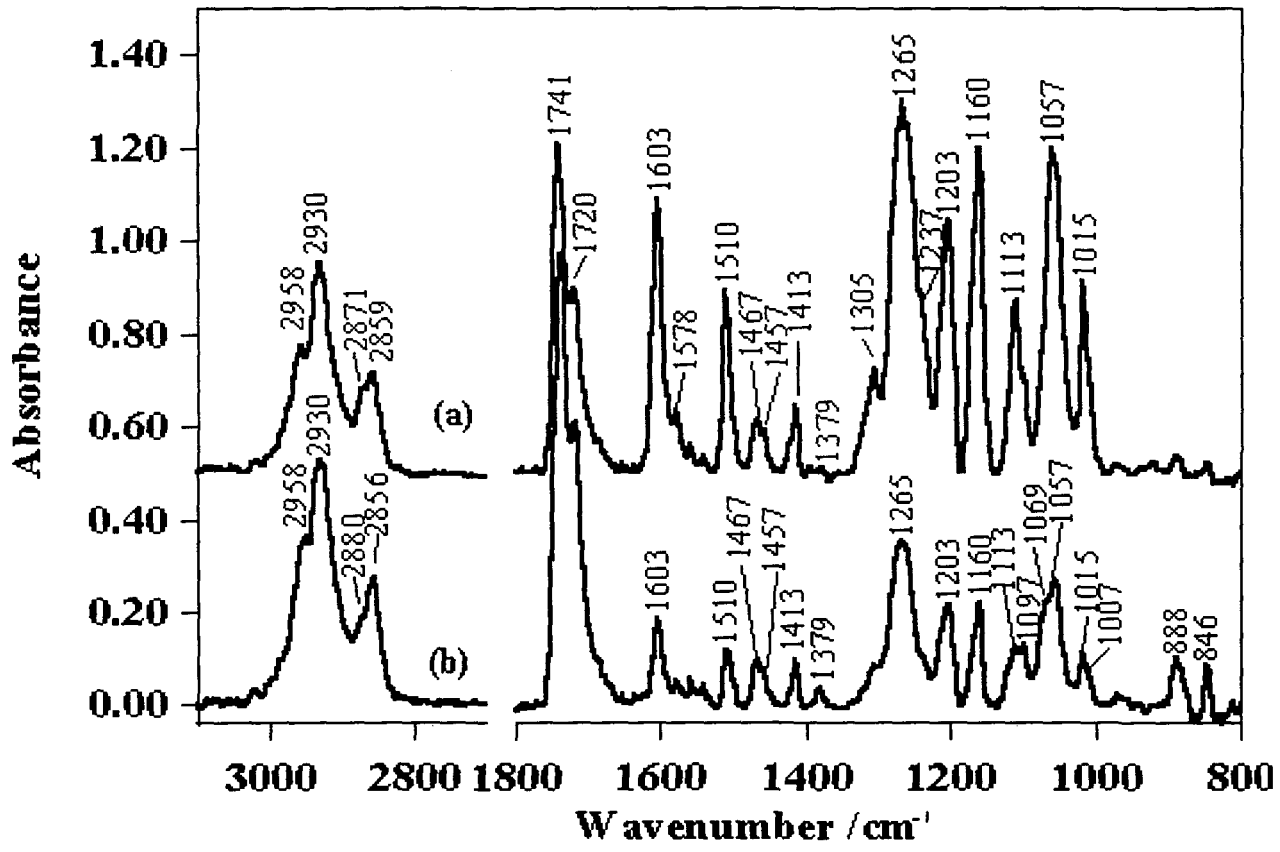

Fig. 5.3. Polarized FT-IR spectra of Chisso 2061 at 75 °C in the (a) parallel and (b) perpendicular polarization geometries. Resolution, 4 cm^{-1}, 100 accumulations.

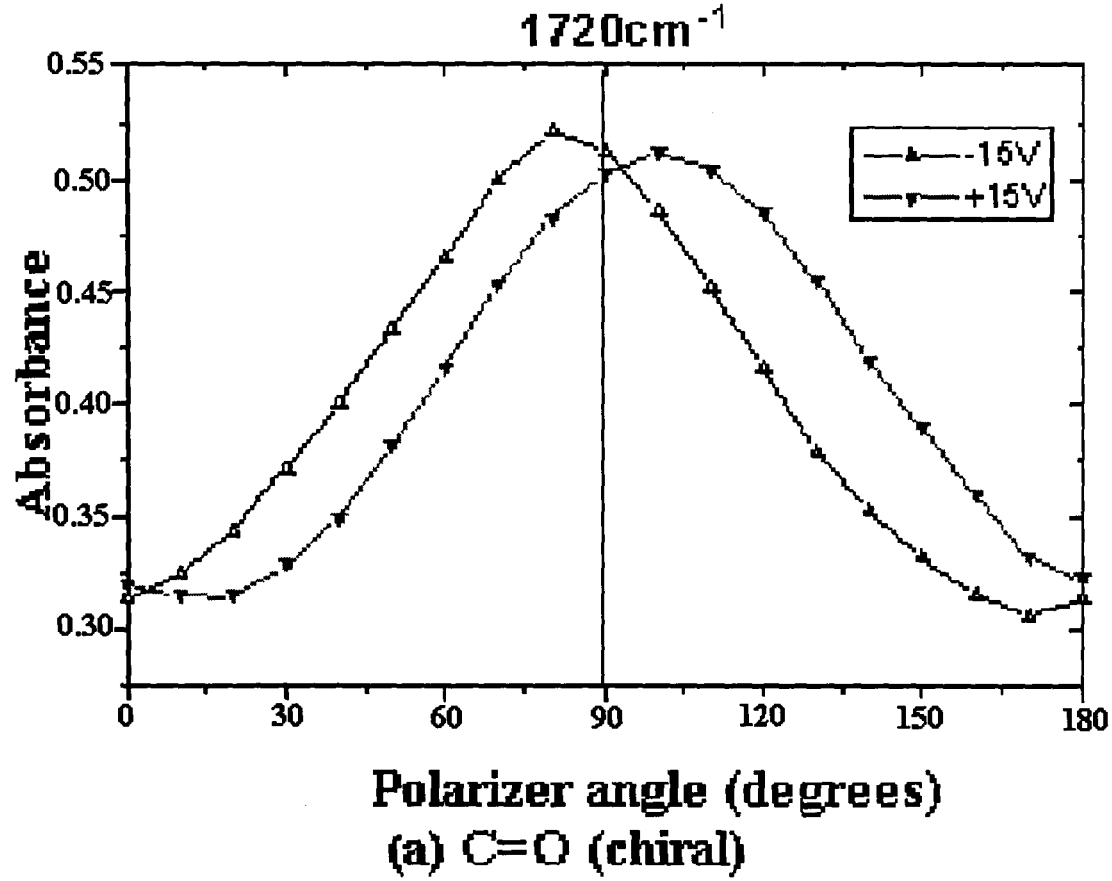

Fig. 5.4a. Plots representing the absorbance (arbitrary units) as a function of polarizer angles ω at 75 °C for C=O stretch (chiral) of Chisso-2061 in the S_C* phase on application of ±15 V dc electric field .

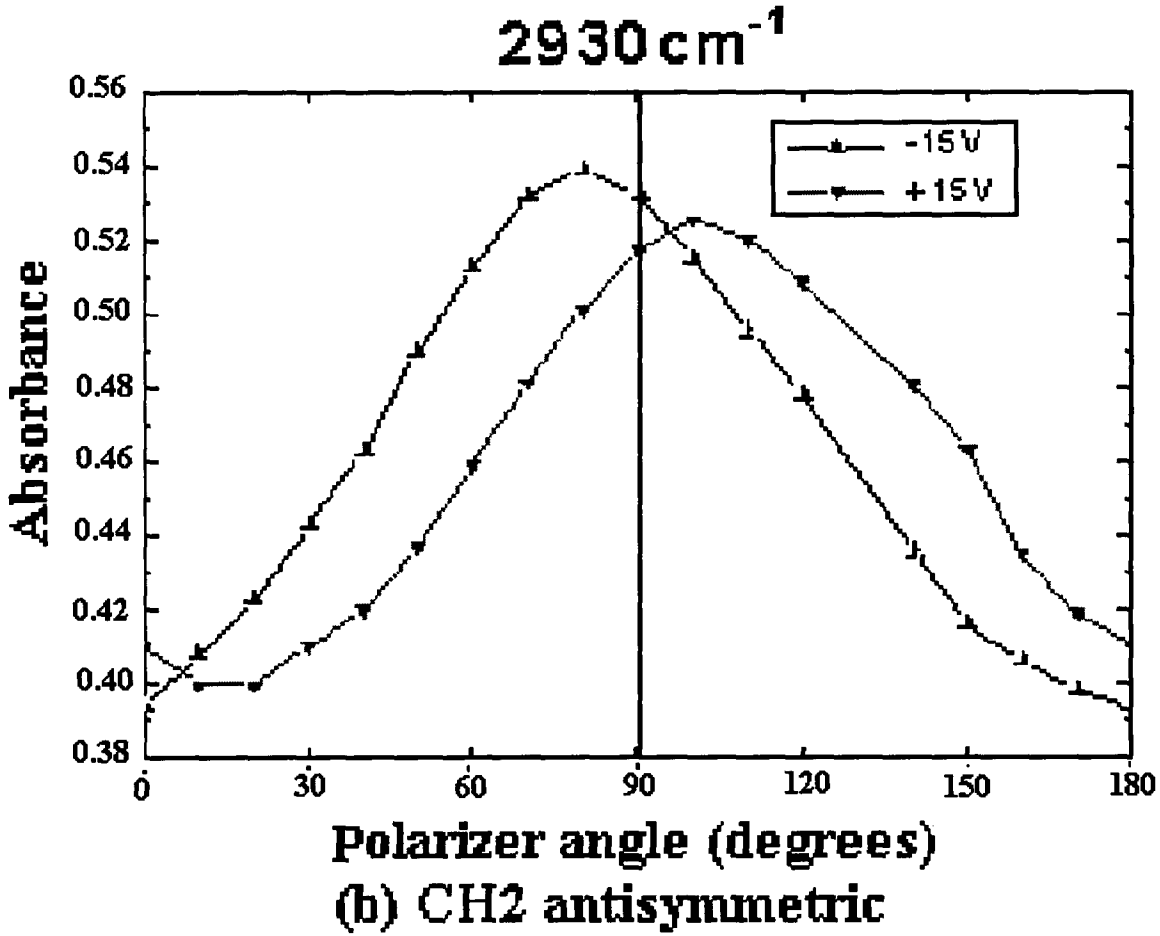

Fig. 5.4b. Plots representing the absorbance (arbitrary units) as a function of polarizer angles ω at 75 ^{0}C for CH_2 antisymmetric stretch of Chisso-2061 in the S_C* phase on application of ±15 V dc electric field .

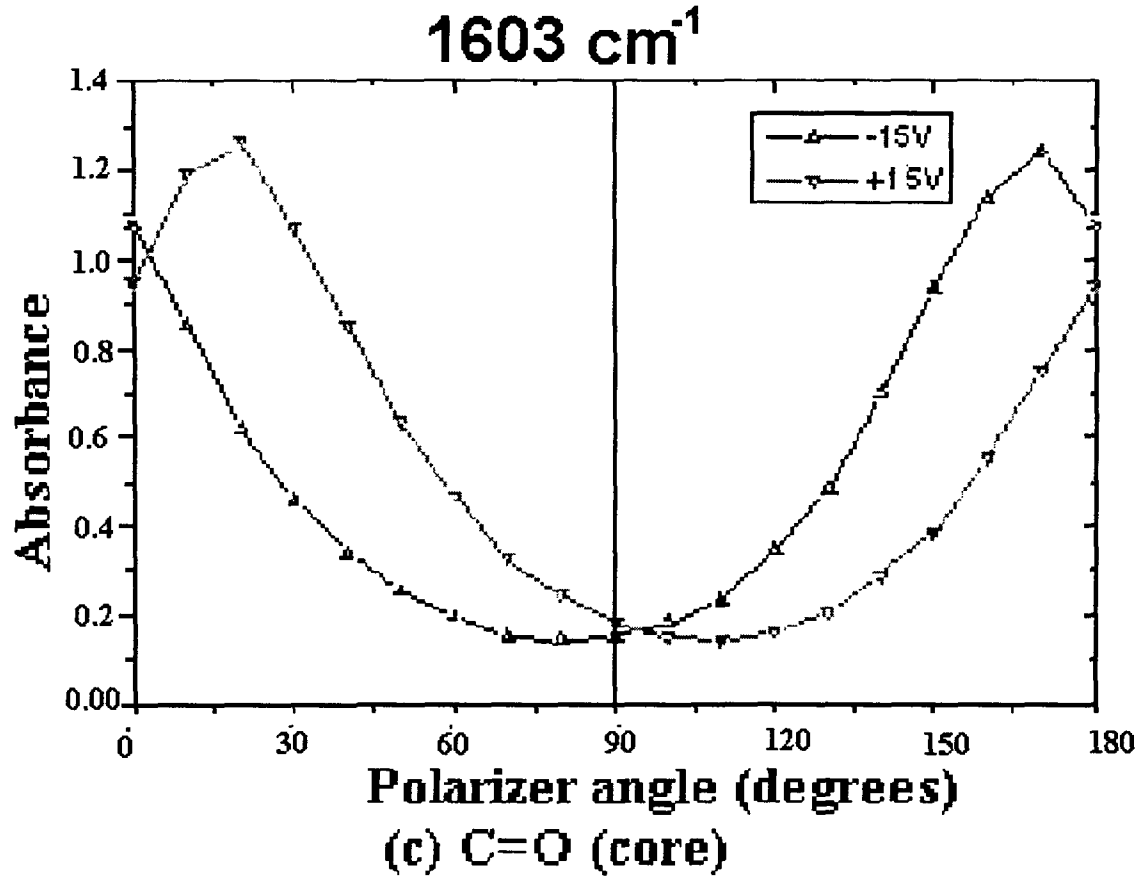

Fig. 5.4c. Plots representing the absorbance (arbitrary units) as a function of polarizer angles ω at 75 ^{0}C for the C=O stretch (core) of Chisso-2061 in the S_C* phase on application of ±15 V dc electric field.

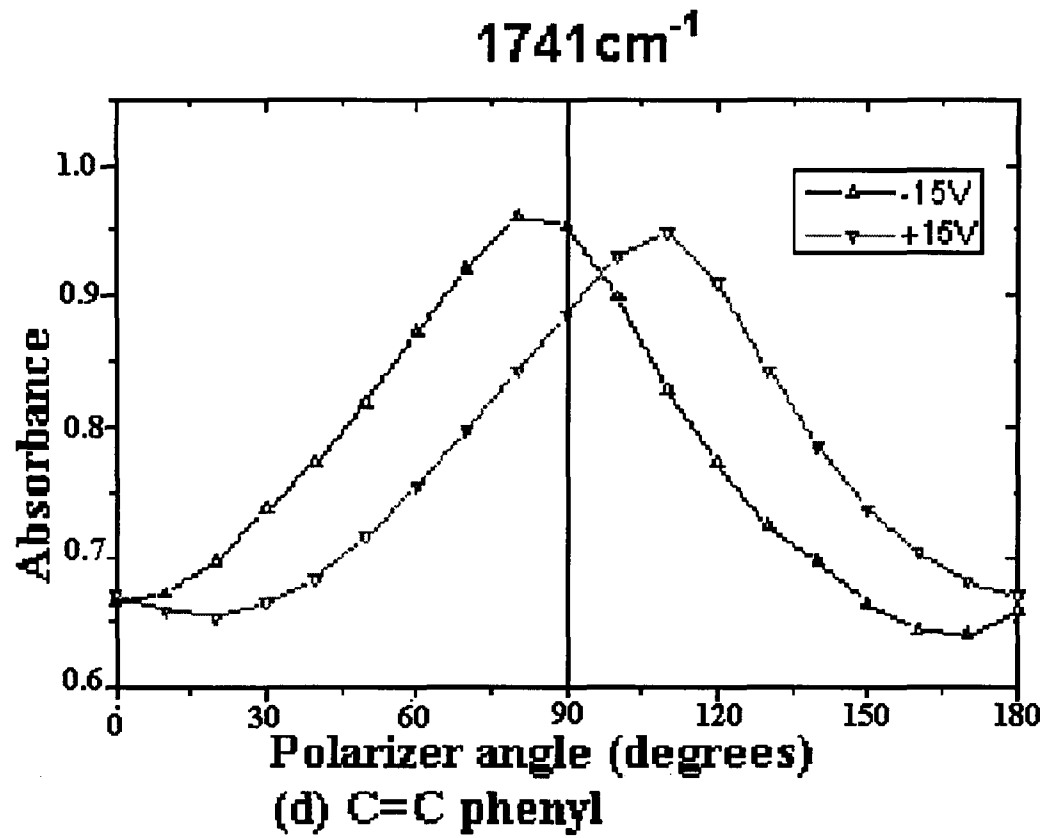

Fig. 5.4d. Plots representing the absorbance (arbitrary units) as a function of polarizer angles ω at 75 ^{0}C for the C=C stretch (phenyl) of Chisso-2061 in the S_C* phase on application of ±15 V dc electric field.

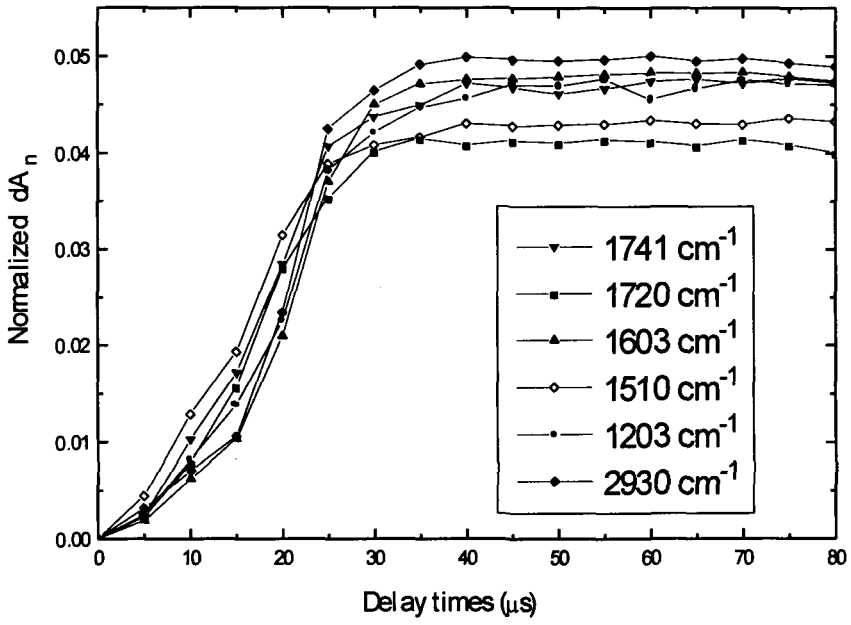

Fig. 5.5 Time dependence of the normalized intensity changes dA_n vs. the delay time for the representative IR bands for the chiral, the alkyl chains and the mesogen segments of Chisso2061 molecule at 75 ^{0}C on application of square wave electric field of ±15 V and 5 kHz repetition rate

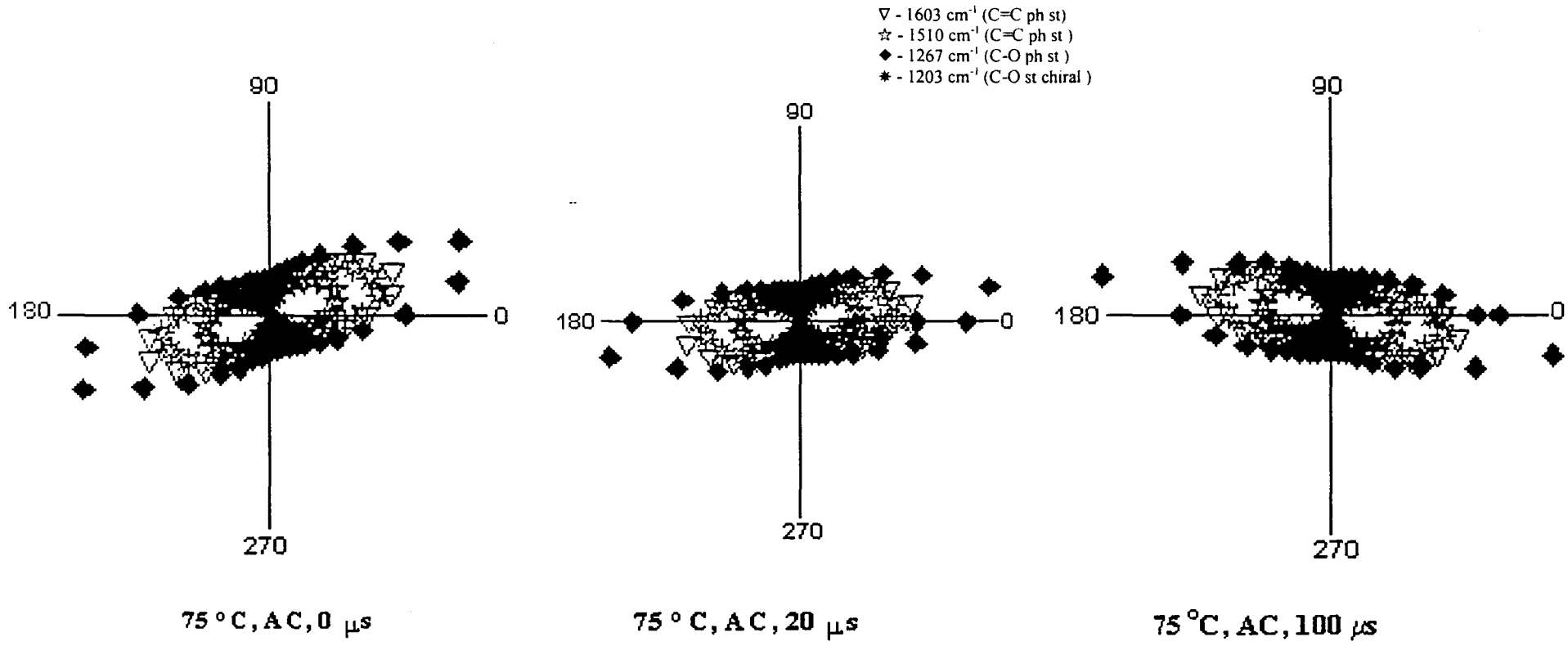

Fig. 5.6a. Polar plots of the peak absorbance A (ω) vs. the polarization angle ω before and during the dynamical switching of the Chisso-2061 in the Sm-C_A* phase at 0, 20, and 100 μs at 75 °C and applied voltage pulse of ±15 V and 5 kHz repetition rate for the selected bands characterizing, the alkyl chains, mesogen and the chiral segments.

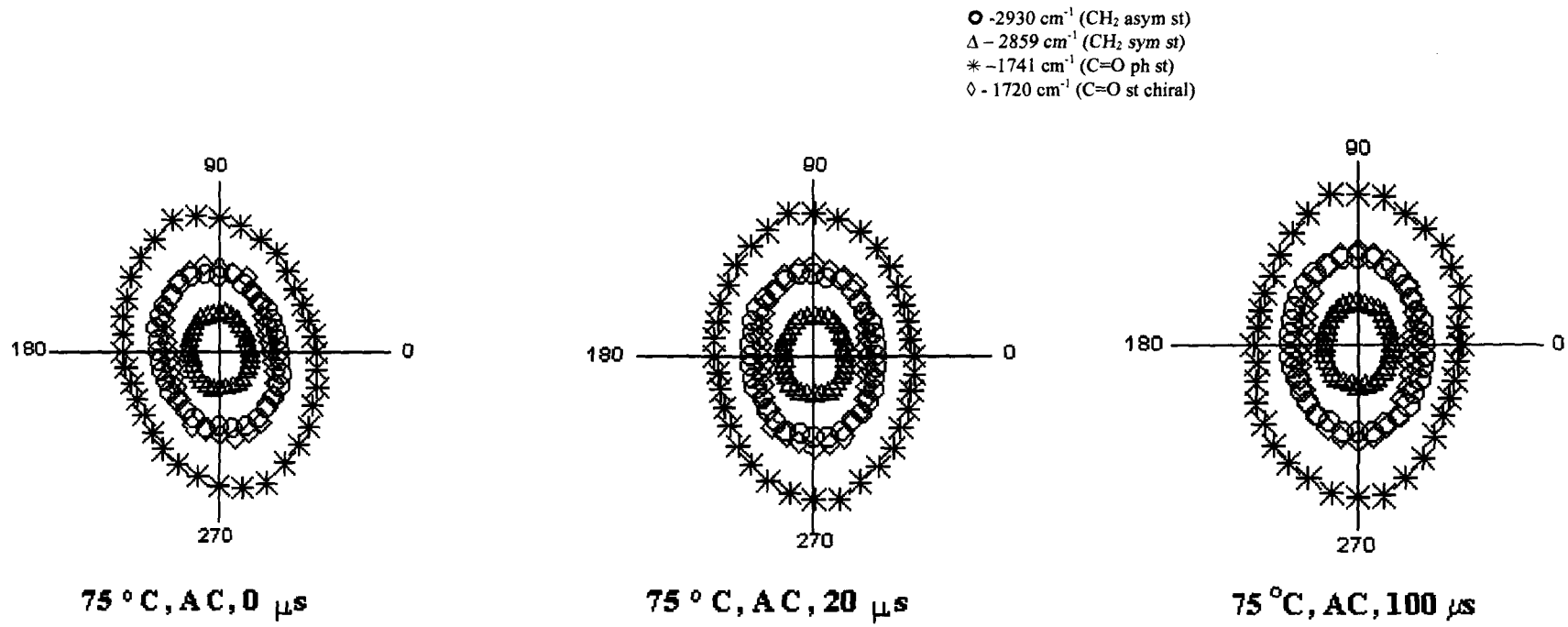

Fig. 5.6b. Polar plots of the peak absorbance A (ω) vs. the polarization angle ω before and during the dynamical switching of the Chisso-2061 in the Sm-C_A* phase at 0, 20, and 100 μs at 75 °C and applied voltage pulse of ±15 V and 5 kHz repetition rate for the selected bands characterizing, the alkyl chains, mesogen and the chiral segments.

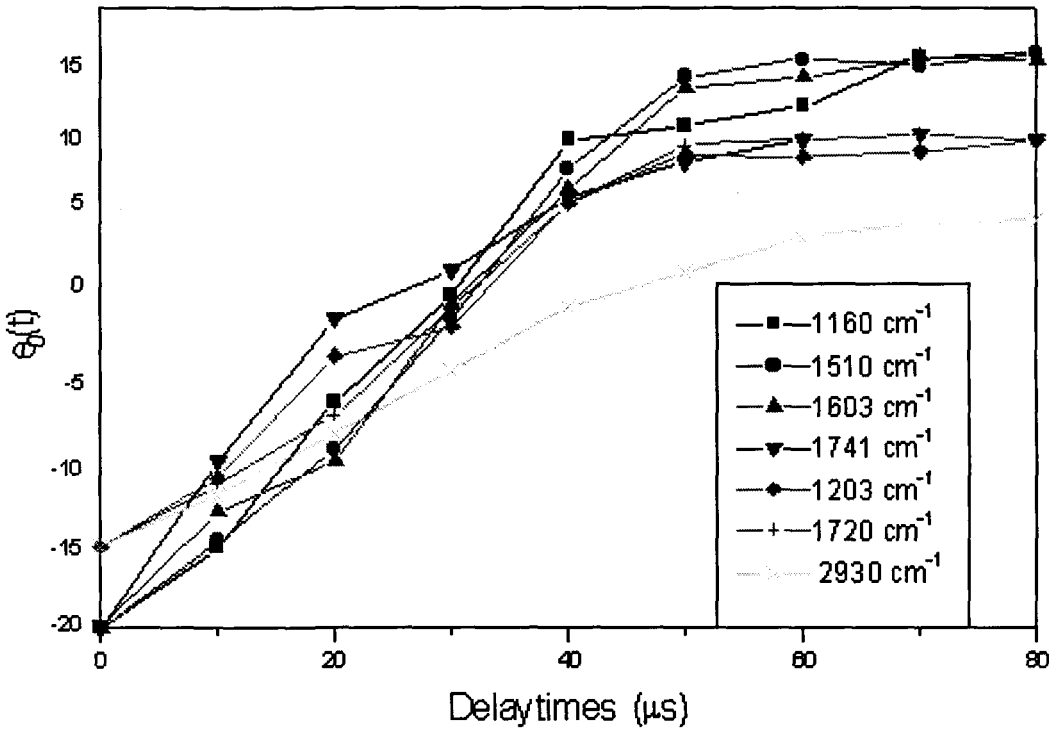

Fig. 5.7. Time dependence of the mean orientation angle $\theta_0(t)$ as a function of delay time for the representative bands of Chisso-2061, at 75^{0}C on application of square wave electric field of ±15 V and 5 kHz frequency.

Chapter 6

~~SUMMARY AND~~ CONCLUSIONS.

The main aim of this chapter is to summarize the discussion in the previous chapters and to highlight the major conclusions drawn on each chapter. As realized from the discussions in previous chapters, in this thesis two different kinds of liquid crystals have been exhaustively studied. Two thermotropic liquid crystals of the N(p-n-alkyloxy benzylidene) p-n alkylaniline, (nO.m) homologous series, viz., 5O.5 and 5O.6 have been studied using Raman spectroscopy, whereas, a chiral antiferroelectric liquid crystal 4-(1-methylheptyloxy carbonyl) phenyl 4-(4'-octyloxy benzoyloxy) benzoate, named as Chisso 2061, has been studied by the technique of time-resolved Fourier transform infrared spectroscopy. In these studies, we have used the advantages of vibrational spectroscopy to obtain information about specifically selected groups/ regions of the molecules. Some important conclusions drawn in our study of the nO.m compounds 5O.5 and 5O.6 include the evidence for existence of a lateral dipole moment in these compounds due to the presence of oxygen atom and also some important information regarding orientational and vibrational dynamics of the core related molecular segments during various phase transitions. The major conclusion from the FTIR study of antiferroelectric liquid crystalline compound Chisso 2061 is related to the hindered rotation of the entire molecule along the long molecular axis, which has been observed for the first time in antiferroelectric liquid crystals. The major conclusions drawn from the different chapters are explained briefly in the following sections:

In chapter 1 a brief introduction to liquid crystals is given. In this chapter the various basic requirements of liquid crystalline molecules along with their important properties have been explained briefly. A description of the different liquid crystalline phases based on their structural characteristics and optical textures observed under polarizing microscope are given. Some theoretical aspects of liquid crystals like the various order parameters have been briefly discussed to facilitate the understanding of their classification. A section has also been dedicated to explain the importance and significance, with respect to contemporary research and applications, on the study of nO.m compounds and the chiral antiferroelectric liquid crystals. The origin of ferroelectricity has been explained in brief. Some earlier work on liquid crystals have also been described with an emphasis on the spectroscopic techniques, especially time-resolved FTIR spectroscopy in case of ferroelectric liquid crystals.

Chapter 2 can broadly be divided into two sections. The first part deals with the theory of the experimental techniques used. Here basic principles and the theoretical background of Raman and time-resolved FTIR spectroscopy has been described. The second part of this chapter is dedicated to the explanation of the actual experimental techniques used in the present study. This portion includes sections on synthesis of the liquid crystalline compounds 5O.5 and 5O.6, their characterization and brief discussion on the phase transition sequence of the nO.m compounds. The construction details of high temperature cells fabricated by us for recording the Raman spectra of the liquid crystals in bulk and in free-standing thin films have

been described. The sample preparation for Raman and FTIR studies as a function of temperature and the commercial high temperature cells used to record the spectra are also discussed. Another section of this chapter deals extensively with the instrumentation used for Raman and asynchronous time-resolved Fourier transform infrared spectroscopies.

In chapter 3, experimental results on the bulk samples of liquid crystalline compound 5O.5 obtained from Raman spectroscopy are discussed. By carefully studying the temperature dependent Raman spectra, changes in the spectral parameters at the various phase transitions were analyzed. Our results indicate that the crystal—G phase transition in 5O.5 is a first order transition between two well defined three dimensional structures. At the transition, the alkyl chains attain a higher degree of orientational and vibrational freedom whereas the core portion remains almost rigid. The lateral gap among the pseudo- hexagonal clusters enable the alkyl chains to move freely, putting strain on the core part of the molecule and resulting in softening of the -ϕ-N= bond. The G—S_F transition is characterized by a subtle increase in the peak positions and the linewidths indicating higher freedom of molecule in the S_F phase. The observation that the integrated intensity remains almost constant indicates that there is only a loss of intermolecular ordering at this transition. The S_F—S_C phase transition shows sharp changes in all the spectral parameters indicating the first order nature of this transition. There is also a high degree of positional and orientational freedom of the molecules in the S_C phase. The S_A—N phase transition is a second order transition marked by gradual changes in

peak positions, linewidths and integrated intensities. Some pre-transitional effects are also observed which are attributed to the formation of cybotactic clusters.

The studies in chapter 4 can be divided into three parts. Firstly, comparative studies of the Raman spectra of 5O.5 and 5O.6 in bulk forms are discussed. Secondly, comparative analysis of Raman spectra of 5O.6 in bulk, solution and thin film forms are described. Finally, changes in spectral parameters at the S_F—S_B phase transition are correlated with the molecular dynamics at this transition. From these studies following conclusions have been drawn. Comparative analysis of Raman spectra of 5O.5 and 5O.6 compounds suggest that the strain on the various molecular segments increases with increase in end chain length of the molecule (i.e., the alkyl chain) as is evident from the shift of the peak positions to lower wavenumber in case of the higher homologue 5O.6. In the solution state, though the strain on the molecule due to the lattice is reduced, there is a tendency towards the straightening of the molecule resulting in the increase in strength of all bonds except for the C=N bond which weakens. In the thin film form, the molecules are aligned perpendicular to the layers in a random bipolar orientation without affecting the core much.

Chapter 5 deals with polarization dependent and time-resolved Fourier transform infrared (FTIR) studies on the electric field induced ferroelectric phase (S_C*) of a chiral, anti-ferroelectric liquid crystal. An important conclusion from the FTIR studies in this chapter is that, contrary to existing beliefs, there is biased orientation and hindered rotation of almost all the molecular segments around the

average molecular long axis, and also the hindered rotation of the whole molecule around its average long molecular axis in this antiferroelectric liquid crystal. It is also observed that the different segments reorient through different angles during dynamic switching as well as under dc electric field. The benzene rings are found to be skewed with respect to each other forming a non-planar structure which results in a distorted packing of the aromatic cores in the smectic layers.

Future Scope and Applications.

Our studies on nO.m compounds 5O.5 and 5O.6 established the usefulness of Raman spectroscopy in understanding the molecular dynamics, especially at phase transitions. An elaborate study of the other homologues of the 5O.m and other groups such as 9O.m series, etc, using Raman spectroscopy is likely to provide ample information to understand the structure-property relationship of these systems at molecular level. The preliminary studies on comparison of Raman spectra of 5O.6 in bulk form and free-standing thin film form have shown drastic differences in spectral features in the same phase. Therefore, a careful study of the free-standing films of these compounds using Laser Raman spectroscopy may reveal important information regarding these systems. Liquid crystal dimers may be formed by joining these monomers (5O.5 and 5O.6) through flexible alkyl chains. A spectroscopic study of such compounds may also provide vital information regarding the molecular dynamics in these model compounds for main chain polymeric liquid crystals which is of basic research importance.

The studies conducted on the antiferroelectric liquid crystal Chisso2061, revealed biased orientation and hindered rotation of almost all the molecular

segments around the average molecular long axis, and also the hindered rotation of the whole molecule around its long molecular axis. The detailed molecular dynamics and switching behaviour of the antiferroelectric liquid crystals is however, not yet fully understood. Further investigations on more antiferroelectric liquid crystals of similar nature using various experimental techniques may provide further evidence on the dynamical aspects of electric field induced switching. In the field of technological applications, fast display devices and high definition flat panel displays based on antiferroelectric liquid crystals have been constructed. Further time-resolved spectroscopic studies may provide better understanding of the segmental mobility and reorientational dynamics paving the way for their use in fast switching display devices (in sub-microsecond range).

Biodata of the candidate

Name: **Ayon Bhattacharjee**

Father's name: **Shri. A. S. Bhattacharjee**

Date of Birth: **6th Dec, 1974**

Educational Qualifications:

Degree	Year	Institution	Board /University	Subjects	Division	Remarks
Class X (AISSE)	1990	B. K. Bajoria School.	CBSE	Eng, Science, Soc Sc, Hin, Maths.	1st div (79.4%)	All India merit certificate for English course A
Pre. University (Sc.)	1992	St. Edmund's College	North Eastern Hill University	Eng, Hin, Maths, Phys, Chem, Bio.	1st div (75%)	
B. Sc (Pass)	1994	St. Edmund's College	North Eastern Hill University	Eng, Maths, Phys, Chem.	1st div (63%)	
B. Sc (Hons)	1995	St. Edmund's College	North Eastern Hill University	Physics	1st div (72%)	2nd rank in the University.
M. Sc	1997	North Eastern Hill University	North Eastern Hill University	Physics (Laser Physics)	1st div (69.44%)	2nd rank in the University.

Address for correspondence: **Ayon Bhattacharjee, (Research Scholar)**
Department of Physics
North Eastern Hill University
Shillong- 793022

Email: **mrphysics@rediffmail.com**

Permanent address: **C/o Ardhendu S Bhattacharjee**
Bipul Bhawan, Jailroad Bazar
Shillong -793001
Phone 0364-228026

Research experience: Worked in the field of Laser Raman Spectroscopy and Liquid Crystals for five years.

Computer exposure: Knowledge in C, Unix, LINUX, Fortran etc.